

2012

Modeling, Simulation, And Optimization Of Diamond Disc Pad Conditioning In Chemical Mechanical Polishing

Emmanuel Ayensu Baisie
North Carolina Agricultural and Technical State University

Follow this and additional works at: <https://digital.library.ncat.edu/dissertations>

Recommended Citation

Baisie, Emmanuel Ayensu, "Modeling, Simulation, And Optimization Of Diamond Disc Pad Conditioning In Chemical Mechanical Polishing" (2012). *Dissertations*. 37.
<https://digital.library.ncat.edu/dissertations/37>

This Dissertation is brought to you for free and open access by the Electronic Theses and Dissertations at Aggie Digital Collections and Scholarship. It has been accepted for inclusion in Dissertations by an authorized administrator of Aggie Digital Collections and Scholarship. For more information, please contact iyanna@ncat.edu.

MODELING, SIMULATION, AND OPTIMIZATION OF
DIAMOND DISC PAD CONDITIONING IN
CHEMICAL MECHANICAL POLISHING

by

Emmanuel Ayensu Baisie

A dissertation submitted to the graduate faculty
in partial fulfillment of the requirements for the degree of
DOCTOR OF PHILOSOPHY

Department: Industrial and Systems Engineering
Major: Industrial and Systems Engineering
Major Professor: Dr. Zhichao Li

North Carolina A&T State University
Greensboro, North Carolina
2012

ABSTRACT

Baisie, Emmanuel Ayensu. MODELING, SIMULATION, AND OPTIMIZATION OF DIAMOND DISC PAD CONDITIONING IN CHEMICAL MECHANICAL POLISHING. (**Major Professor: Dr. Zhichao Li**), North Carolina Agricultural and Technical State University.

Chemical Mechanical Polishing (CMP) is a major manufacturing step extensively used to planarize and smooth silicon wafers upon which semiconductor devices are built. In CMP, the polishing pad surface is glazed by residues as the process progresses. Typically, a diamond disc conditioner is used to dress the pad to regenerate newer pad asperity and a desired surface profile in order to maintain favorable process conditions.

Conditioner selection and the determination of the optimal conditioning parameter values to yield a desired pad surface still remain difficult problems. Various analytical process models have been proposed to predict the pad surface profile. However, not much work has been done concerning the incorporation of conditioner and pad design features in these analytical models. This research sought to address the concern about the lack of models that are reliable enough to be used for verification and optimization of the process.

In this research, two kinematic models were developed to predict the pad surface profile due to conditioning. One model was developed using a surface element approach and the other by characterizing the diamond disc conditioning density distribution. Three metrics; Total Thickness Variation, Bow, and Non-Uniformity, were defined and utilized to evaluate the resulting pad surface profile characteristics. Experimental data confirmed that both models were able to simulate the kinematics of diamond disc pad conditioning

and accurately predict the pad surface profile. However, a slightly skewed deviation of the simulation results corroborated the suspicion that, deformation of the microporous pad could affect the pad surface profile.

Thus, a 2-D image processing procedure was developed to characterize the morphological and mechanical properties of microporous Class-III CMP pads. Pad characterization data was incorporated into a 2-D axisymmetric quasi-static finite element model to investigate effects of process parameters such as stack height, pad stiffness, and conditioning pressure on the pad deformation with enhanced fidelity. Simulation results were consistent with literature and showed that the pad profile was affected by deformation due to conditioning.

Since the conditioner design also has a significant effect on the pad conditioning process, a new metric to evaluate the pad surface texture generated by a specific conditioner design was developed. The metric was applied in a genetic algorithm (GA) to optimize conditioner design parameters including geometric arrangement of diamonds, grit density and disc size. The GA model was able to find design parameter values that produced better CMP pad surface textures.

School of Graduate Studies
North Carolina Agricultural and Technical State University

This is to certify that the Doctoral Dissertation of

Emmanuel Ayensu Baisie

has met the dissertation requirements of
North Carolina Agricultural and Technical State University

Greensboro, North Carolina
2012

Approved by:

Dr. Zhichao Li
Major Professor

Dr. Salil Desai
Committee Member

Dr. Samuel Owusu-Ofori
Committee Member

Dr. Paul Stanfield
Committee Member/Dept. Chairperson

Dr. Sanjiv Sarin
Associate Vice Chancellor for Research and Dean, School of Graduate Studies

BIOGRAPHICAL SKETCH

Emmanuel Ayensu Baisie was born on July 4, 1984 in Takoradi, Ghana. He completed his senior secondary school education at Mfantsipim School, Ghana. His ever-growing interest in engineering led him to pursue an undergraduate degree in Mechanical Engineering at Kwame Nkrumah University of Science and Technology (KNUST). After graduating with a First Class honors in 2007, he continued his academic journey as a teaching/research assistant at the Mechanical Engineering Department and The Energy Center of KNUST. Following this, he enrolled in a straight PhD program at the Industrial and Systems Engineering Department of North Carolina Agricultural & Technical State University (NCA&T).

Emmanuel's research achievements at NCA&T include: the publication of 14 research papers (2 journal papers, 12 refereed conference papers, and 4 journal papers under review); ASME Manufacturing Engineering Division 2011 Best Paper 1st Runner-Up Award (out of 150+ research papers); the NCA&T Industrial and Systems Engineering Department 2011 Outstanding Graduate Research Assistant Award; and the E. Wayne Kay Graduate Scholarship from the SME Education Foundation.

Following his doctoral studies, Emmanuel will move on to pursue a post-doctoral position with Cabot Microelectronics Corporation, a leading manufacturer of CMP consumables.

ACKNOWLEDGMENT

My utmost gratitude goes to our Omnipotent God for granting me the ability to learn and discern, and for the undeserved favor and numerous opportunities that come my way.

I am extremely thankful for my advisor, Dr. Zhichao Li, for all his candid comments, keen attention, direction, grooming, and unyielding financial support throughout my PhD studies. Without his guidance, I could not have completed this work within four years.

My sincere gratitude goes to Professor Owusu-Ofori for his expert advice and for mentoring me throughout my doctoral studies. I thank Dr. Paul Stanfield for his financial support, opportunities that were opened to me, and his acknowledgement of my successes. My sincere gratitude also goes to Dr. Salil Desai for his insight, career advice, sharing his experience, and especially, his confidence in me. Many thanks go to Dr. Xiaohong Zhang of Seagate Technology for her industrial collaboration and for reviewing my publications. I appreciate the international collaboration provided by Dr. Bin Lin of Tianjin University, China. I am also grateful for the support from my lab mates Anweshana Vaizasatya, Matthew Stanco, Alexander Martin, and Brittany Lassiter.

May the Lord continue to bless my parents and my siblings for their prayers, support, moral upbringing, and the patience they had for me when I was preoccupied with my studies. Finally, I appreciate the company, motivation and moral support from all my friends and loved ones who embraced me with a social life.

TABLE OF CONTENTS

LIST OF FIGURES	x
LIST OF TABLES	xiii
LIST OF SYMBOLS	xiv
CHAPTER 1. INTRODUCTION	1
1.1 Semiconductor Industry Trends and Challenges.....	1
1.2 Research Scope	2
1.3 Chemical Mechanical Polishing.....	3
1.4 Research Motivation	5
1.5 Technological Trends/Challenges	7
1.6 Research Gaps	8
1.7 Research Objectives	10
1.8 Research Approach	10
1.9 Outline.....	11
CHAPTER 2. LITERATURE REVIEW.....	13
2.1 Introduction	13
2.2 Diamond Disc Pad Conditioning.....	13
2.3 Development of Diamond Disc Conditioner.....	16
2.3.1 Evolution	16
2.3.2 Disc Design.....	19
2.3.3 Manufacture.....	19
2.4 Process Control	22

2.4.1	Diamond Disc Conditioning Process Control	22
2.4.2	Measurement and Evaluation of Pad Characteristics	25
2.5	Process Modeling	25
2.6	Review Summary	30
CHAPTER 3. SURFACE ELEMENT MODEL		32
3.1	Introduction	32
3.2	Model Development.....	33
3.2.1	Assumptions	33
3.2.2	Model Derivations	35
3.2.3	Simulation.....	43
3.3	Simulation Results and Experimental Validation	44
3.3.1	Simulation Conditions	44
3.3.2	Simulation Results and Discussion.....	45
3.4	Effect of Conditioning Parameters on Pad Surface Profile.....	49
3.4.1	Metrics for Pad Surface Profile Evaluation.....	49
3.4.2	Effect of Section Sweeping Time t_i	53
3.4.3	Effect of Sweeping Profile $\{t_i\}$	53
3.4.4	Effect of Pad Rotating Speed.....	55
3.4.5	Effect of Conditioner Rotating Speed	57
3.4.6	Effect of Conditioner Diameter	57
3.5	Conclusions	59
CHAPTER 4. CONDITIONING DENSITY MODEL.....		61
4.1	Introduction	61
4.2	Model Development.....	62

4.2.1	Assumptions	62
4.2.2	Model Derivation.....	63
4.3	Simulation and Experimental Validation	73
4.3.1	Simulation Conditions	73
4.3.2	Simulation Results and Discussion.....	73
4.4	Conclusions	77
CHAPTER 5. 2-D MORPHOLOGY AND FINITE ELEMENT ANALYSIS OF PAD		79
5.1	Introduction	79
5.2	Image Processing.....	81
5.3	Characterization Results.....	86
5.4	FE Model Development	87
5.4.1	Assumptions	87
5.4.2	Model Parameters	88
5.4.3	Finite Element Model	90
5.5	Results and Discussion.....	91
5.6	Conclusions	95
CHAPTER 6. CONDITIONER DESIGN OPTIMIZATION.....		97
6.1	Introduction	97
6.2	Disc Design	99
6.3	Genetic Algorithms in Design Optimization.....	101
6.4	Problem Representation	102
6.4.1	Solution Representation.....	102
6.4.2	Design Evaluation.....	104
6.4.3	Selection	106

6.4.4	Reproduction	107
6.5	Results and Discussion.....	109
6.5.1	Simulation Parameters.....	109
6.5.2	Search Results.....	110
6.5.2.1	Performance of Design Optimization.....	110
6.5.2.2	Evolution of Size.....	111
6.5.2.3	Evolution of Grit Density.....	111
6.5.2.4	Evolution of Geometric Arrangement.....	113
6.6	Conclusions	115
CHAPTER 7. CONCLUSIONS AND FUTURE WORK.....		117
7.1	Research Overview	117
7.1.1	Findings from Literature Review	117
7.1.2	Modeling and Prediction of Pad Surface Profile	118
7.1.3	2-D Morphology and Finite Element Analysis of Pad	119
7.1.4	Conditioner Design Optimization.....	119
7.2	Future Work	120
7.2.1	Control of Pad Profile.....	120
7.2.2	Finite Element Analysis.....	120
7.2.3	Understanding and Characterizing the Preston Coefficient K in Pad Conditioning	121
7.2.4	Conditioner Design Optimization.....	122
7.2.5	Process Model Integration	122
REFERENCES		123
APPENDIX I. SELECTED PAD CONDITIONING ANALYTICAL MODELS		134

APPENDIX II. PUBLISHED EXPERIMENTAL DATA:	144
APPENDIX III. LIST OF PUBLICATION OUTCOMES FROM Ph.D. STUDY.....	148

LIST OF FIGURES

FIGURES	PAGE
1.1. Chemical mechanical polishing process	5
1.2. Need for pad conditioning in CMP	6
2.1. Typical diamond disc conditioners	14
2.2. Illustration of (a) diamond disc conditioner face, and (b) interaction between the conditioner and the pad	15
2.3. Conditioning unit assembly	16
2.4. Conditioner evolution	18
2.5. Conditioner disc assembly	21
2.6. Common diamond bonding methods	22
3.1. Illustration of a diamond disc conditioning cycle.....	33
3.2. Schematic of pad conditioning kinematics	36
3.3. Model to calculate the pad area swept by the conditioner	38
3.4. Illustration of cumulative wear thickness	42
3.5. Simulation results for sweeping profile FLAT 1.....	46
3.6. Simulation results for sweeping profile FLAT 2.....	46
3.7. Simulation results for sweeping profile BELL	47
3.8. Simulation results vs. experimental data showing 3-D views of pad surface profiles	48
3.9. Metrics to evaluate the pad surface profile	51
3.10. Effect of section sweeping time t_i showing (a) pad profile comparison and (b) flatness evaluation	52

3.11. Effect of sweeping profile $\{t_i\}$ showing (a) pad profile comparison and (b) flatness evaluation at $R_p=12''$, $R_c=1''$, $N_p=45\text{ rpm}$, $N_c=30\text{ rpm}$	54
3.12. Effect of pad rotating speed showing (a) pad profile comparison and (b) flatness evaluation	55
3.13. Effect of conditioner rotating speed showing (a) pad profile comparison and (b) flatness evaluation	56
3.14. Effect of conditioner diameter showing (a) pad profile comparison and (b) flatness evaluation	58
4.1. Position of diamond grit relative to the pad x-y coordinates	64
4.2. Trajectory on pad created by 2" conditioner with single diamond	66
4.3. Trajectories on pad created by 5 grit/2" conditioner with radial diamond arrangement	66
4.4. Trajectories on pad created by 12 grit/2" conditioner with annular diamond arrangement	67
4.5. Trajectories on pad created by 49 grit/2" conditioner with combined (radial x annular) diamond arrangement	67
4.6. Development of surface map from trajectory length per unit area	69
4.7. Development of pad profile from trajectory length	70
4.8. Simulation results for typical conditioning case (UNIFORM).....	72
4.9. Simulation results vs. experimental results of three sweeping profiles	76
5.1. Image processing procedure	82
5.2. Geometric model of IC1400 (a) top-pad and (b) sub-pad cross sections overlain with corresponding Delaunay triangulations	87
5.3 Relationship between the porosity and elastic modulus	90
5.4 Boundary conditions of 2-D FEA model	91
5.5. (a) FEA model and (b) variation of average pad deformation at $E_0=130\text{ Mpa}$ and $P=70\text{ N}$	93
5.6. Effect of conditioner pressure (P) on deformation ($E_0=177\text{ Mpa}$).....	94

5.7.	Effect of pad stiffness (E_0) on deformation at $P = 70$ N for top-pad.....	94
5.8.	Effect of pad stiffness (E_0) on deformation at $P = 70$ N for sub-pad	95
6.1.	Types of (a) diamond geometric arrangements and (b) disc shape	100
6.2.	Genetic Algorithm (GA) process	102
6.3.	Binarized trajectories generated by a specified conditioner design.....	106
6.4.	(a) Traditional crossover and (b) random linear crossover operations	108
6.5.	Effect of population size on run performance.....	109
6.6.	Evolution of (a) fitness, (b) disc size, (c) grit density, and (d) geometric arrangement	112
6.7.	Solution space	113
6.8.	Best design in last generation showing (a) (3, 42.14, 3.69, 0) design displayed on polar grid and (b) its corresponding $CD' = 0.75$	114

LIST OF TABLES

TABLES	PAGE
1.1. Scope of research work within ITRS	3
2.1. Design considerations in conditioner design	20
2.2. Process control factors (Conditioning kinematics).....	23
2.3. Process control factors (Consumables).....	24
2.4. Classification of pad conditioning analytical models	28
3.1. Experimental conditions	44
3.2. Sweeping profiles used for pad surface profile simulation.....	45
3.3. Sweeping profiles used for pad surface profile simulation.....	53
4.1. Sweeping profiles used for model verification	74
5.1. Pad morphological parameters.....	83
5.2. Image processing results	85
5.3. Parameters used for simulation.....	92
6.1. Constraints on conditioner design parameters	103
7.1. Relationship of chosen parameters with K	121

LIST OF SYMBOLS

$\Delta H(r_p)$	Actual pad wear at radius r_p on pad
Δh_i	Pad wear for section i
\vec{s}_c	Horizontal displacement vector
$A_{swept(i)}$	Pad area swept for section i
O_{ij}^{AB}	Allele of offspring and O_{ij}^{BA} of conditioner disc j in generation i
P_{ij}^A	Alleles of parent gene of conditioner disc j in generation i
\vec{Z}	Total displacement vector
a_i	Area of image component i
d_i	Equivalent diameter of image component i
o_i	Centroid of image component i
p_i	Perimeter of image component i
μ_d	Mean pore diameter
μ_{grit}	Average diamond grit size
ΔH	Pad wear thickness
Ac_{ij}	Area covered by trajectories
A_p	Total pad surface area
$a.u$	Auxiliary unit
CD'	Modified conditioning density
CD_j	Conditioning density for segment j
d	Radial distance travelled by conditioner

dA	Small area swept by conditioner on pad surface
dh	Small pad wear thickness
D_{ij}	Grit density of conditioner disc j in generation i
dl	Small distance swept by diamond abrasive on pad surface
E	Young's modulus
E_0	Young's modulus of pad polymer matrix
G_{ij}	Index of geometric arrangement of conditioner disc j in generation i
H	Pad thickness
H_0	Initial pad thickness
k	A coefficient determined by pad/conditioner properties
K_p	Preston coefficient
L	Initial distance of conditioner center from pad center
L_i	Distance between the i^{th} position and the initial conditioner position
m	Number of segments
N	Number of cycles
n	Number of image components
N_c	Conditioner rotational speed in rpm
N_d	Number of diamond grits on conditioner
N_p	Pad rotational speed in rpm
NU	Non-uniformity
O_c	Conditioner center
O_p	Pad center

P	Conditioning pressure
q	Number of divisions of sweeping range
R_c	Radius of conditioner
r_i	Radial position of diamond grit i
R_{ij}	Number of rays of conditioner disc j in generation i
r_j	Inner radius of segment j
R_j	Outer radius of segment j
R_p	Radius of pad
r_{pj}	Pad radius that falls within segment j
S	Image scale
S_A	Shore A hardness and
S_D	Shore D hardness
S_{ij}	Length of trajectory i within segment j
S_{ij}	Size of conditioner disc j in generation i
S_j	Total length of all trajectories within segment j
T	Total time period for conditioning session
t	Time
t'	Conditioning time within a cycle
t_1	Thickness of top-pad
t_2	Thickness of sub-pad
t_{cycle}	Total time period for one conditioning cycle
t_i	Time period for conditioner center to traverse a random segment

t_k	Time period for conditioner to traverse section k of sweeping range
t_{rj}	Time diamond grit enters segment j
t_{Rrj}	Time diamond grit leaves segment j
TTV	Total thickness variation
V	Velocity
V_c	Conditioner velocity
$V_{p/c}$	Relative velocity between conditioner and pad
w	Width of one division of sweeping range
X_{pad}	x coordinate axis relative to pad center
Y_{pad}	y coordinate axis relative to pad center
θ_i	Angular position of diamond grit i
ξ	Pad material removal
ν	Poisson ratio
ω_c	Angular speed of conditioner
ω_p	Angular speed of pad
$r(t)$	Linear component of displacement vector in polar form
δ	Diamond pitch factor
$\varphi(t)$	Angular component of displacement vector in polar form
ϕ	Ratio of the area of pores to the total or bulk area of the pad

CHAPTER 1

INTRODUCTION

1.1 Semiconductor Industry Trends and Challenges

Today, semiconductor devices are pervasive in a wide range of industries including computers, communications, aerospace, manufacturing, agriculture, and healthcare. Semiconductor manufacturing technologies are essential to the success in the production of next-generation integrated circuits (IC) (Texas Semiconductor Industry Report, 2007). These enable harnessing of information technology by creating improved components for computing systems and also better interface devices for human-computer interactions. From its inception around 40 years ago, the industry has grown to become very large, with billions of dollars (over \$20 billion in 2010 (Wilson, 2011)) invested in only its research and development (Ballhaus et al., 2009). The importance of the semiconductor industry today lies in the fact that it is so intensively present in everyone's life.

Microfabrication (originally based on structuring the surface of silicon) remains the basic manufacturing technology of the semiconductor industry. The semiconductor business model has been driven by "Moore's Law" which predicts that the number of transistors the industry would be able to place on a computer chip would double every two years. While originally intended as a rule of thumb in 1965, it has become the guiding principle for the industry to deliver ever-more-powerful semiconductor chips at

proportionate decreases in cost. A report by Price Waterhouse Coopers (Ballhaus et al., 2009) states that companies would continue to carry out R&D focusing on even smaller feature sizes, more functionality per chip, lower power consumption and less expensive production .

The International Technology Roadmap for Semiconductors (ITRS) provides further details on perspectives and challenges for the future (ITRS Roadmap Committee, 2010). Currently, system solutions are sought to develop new industries and applications, and increase productivity in existing ones (Daane, 2010).

1.2 Research Scope

The manufacturing process for semiconductors is typically divided into two parts: front-end and back-end (Li, 2008). The front-end manufacturing stage of the process is responsible for creating the finished die. The progressively decreasing feature size of circuit components has tremendously increased the need for global surface planarization of the various thin film layers that constitute the integrated circuit (IC). Chemical mechanical polishing (CMP) is the planarization method that has been selected by the semiconductor industry today (Zantye et al., 2004). Presently, CMP provides a technological advantage in front-end process modules such as shallow trench isolation and polysilicon polish as well as back-end-offline (BEOL) processing. CMP's ability to planarize, smooth surfaces and achieve high selectivity provides a significant advantage over competing technologies (Li, 2008). There are sixteen active International Technical

Working Groups (ITWGs) as part the ITRS effort to define the near and long term technology requirements for the semiconductor industry as well as the description of potential technical solutions to meet these needs. As shown in Table 1.1, out of the sixteen, this research work falls in the area of modeling and simulation of front-end manufacturing processes, specifically CMP.

Table 1.1. Scope of research work within ITRS (Adapted from Wolfgang, 2002)

		← Crosscut ITWGs →				
		Environment & Safety	Metrology	Yield Improvement	Modeling & Simulation	
Focus ITWGs	↑	System Drivers				
		Design				
		Test & Test Equipment				
		Process Integration				
		RF & A/MS Technologies				
		Emerging Research Devices				
		Emerging Research Materials				
		Front-End Processes				CMP
	↓	Lithography				
		Process Integration				
		Assembly and Packaging				
		Factory Integration				

1.3 Chemical Mechanical Polishing

Chemical Mechanical Polishing (CMP) is a final major manufacturing step extensively used in semiconductor fabrication for flattening semiconductor wafers to obtain mirror surface finish. In 2011, the CMP pad market yielded \$626 million while the

slurry market totaled \$1.0 billion, and is forecasted to grow 7.0% in 2012 and exceed \$1.3 billion by 2016 (Shon-Roy, 2012). CMP is still considered the leading planarization technology for current and future manufacturing (Dornfeld, 2010).

There are various types of CMP machine configurations. A basic design of CMP machine consists of a single or multiple wafer carriers with a retaining ring and a rotating polishing pad mounted on a rotatable platen. The wafer is held in the rotating carrier and a down force is applied to press the wafer against the pad as shown in Figure 1.1.

The CMP material removal mechanism involves a special combination of chemical and mechanical forces (Hooper et al., 2002). First, corrosive slurry containing fine abrasive particles is released onto the porous pad and attacks the wafer to chemically weaken it. This step allows the mechanical action involving a three-body contact motion of pad, abrasive and wafer under an applied pressure to easily facilitate material removal. (Zantye et al., 2004, Philipossian and Olsen, 2003, Bozkaya, 2009). For further reading on CMP, Zantye (2004) presents an overview of the CMP process in general and Li (2008) summarizes the state-of-the-art research advances in CMP technology in his book “Microelectronic Applications Of Chemical Mechanical Planarization”. Another review by Krishnan (2009) focuses mainly on the physicochemical processes that are associated with CMP.

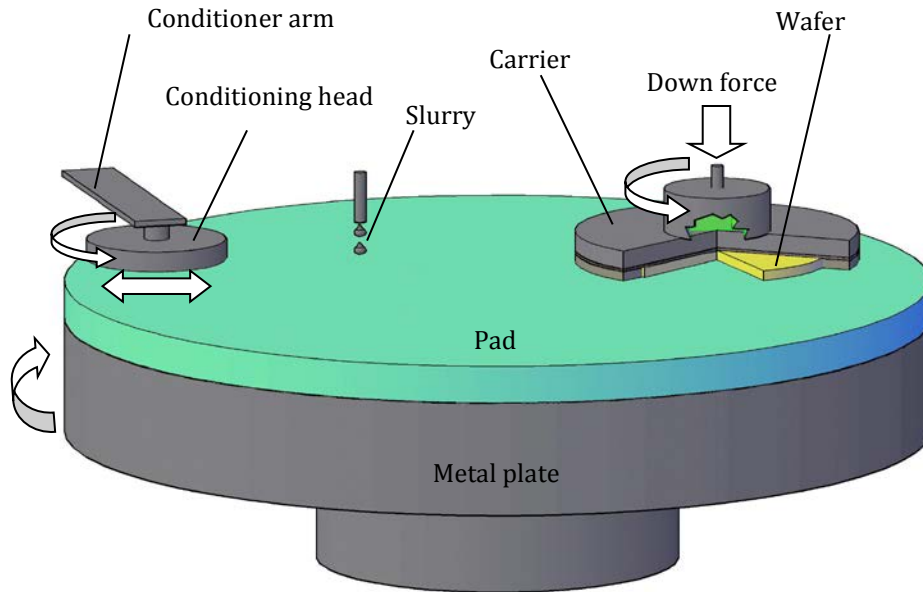


Figure 1.1. Chemical mechanical polishing process

1.4 Research Motivation

During the CMP process, slurry and debris removed from the wafer and the pad “glaze” the surface of the polishing pad and make the pad surface slick. In the absence of a pad regeneration process, it will lead to degradation of the pad surface. Therefore, conditioning is used to regenerate the pad surface by breaking up the glazed areas. A diamond disc conditioner is often used to “condition” the pad to regenerate new pad asperity and desired surface profile in order to maintain favorable process conditions (Zantye et al., 2004). As shown in Figure 1.2, diamond disc conditioning plays a key role in maintaining removal rates (Lee and Yoon, 2008), within-wafer non-uniformity

(WIWNU) and extending the life of the pad (Pei-Lum et al., 2009, Charm and Tam, 2006, Dyer and Schlueter, 2002). Zhou et al. (2008) reported that material removal rate (MRR) can be maintained at the same level and WIWNU can be improved with proper pad conditioning.

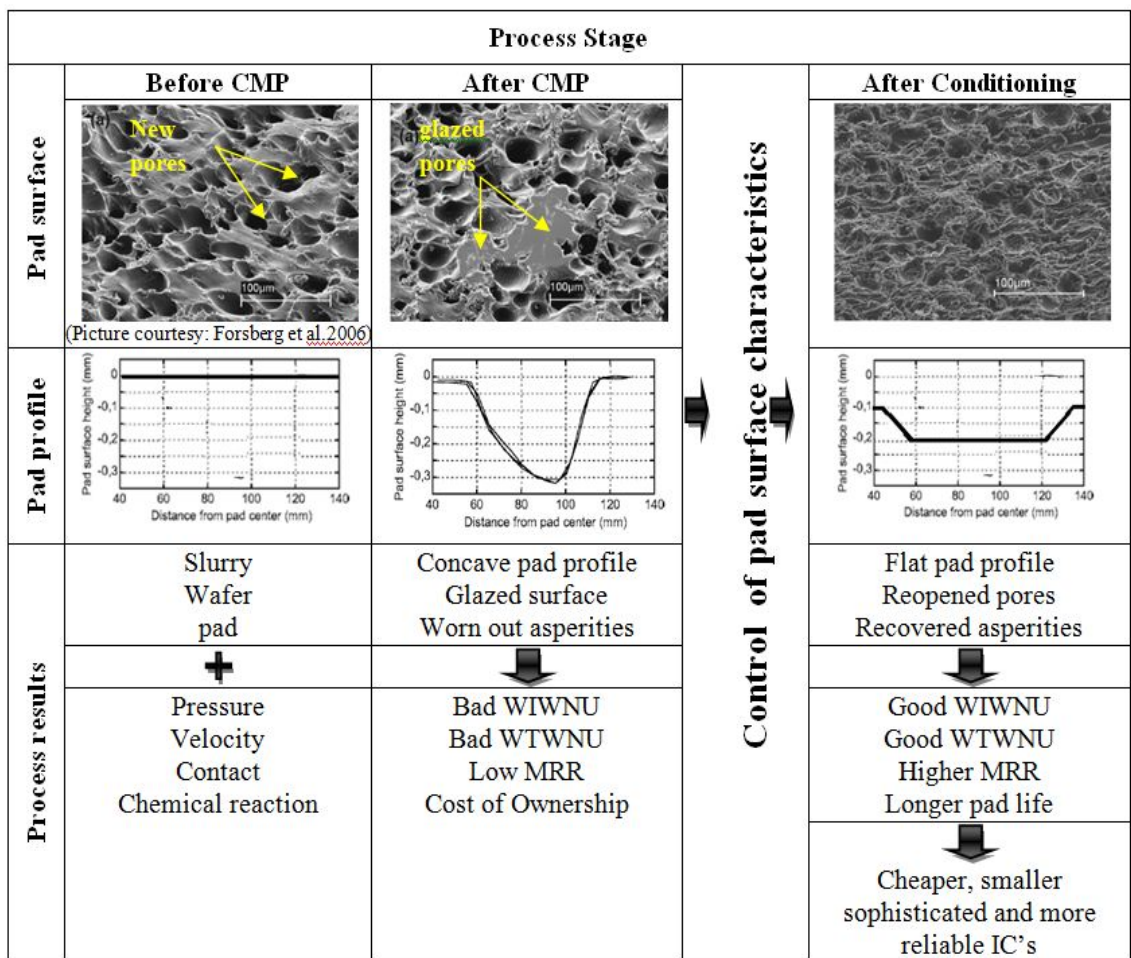


Figure 1.2. Need for pad conditioning in CMP

Many researchers have studied the relationship between the diamond disc pad conditioning and the CMP process in several aspects and various useful analytical models have been developed and validated. Pad conditioning models are functional in describing the evolution of pad surface characteristics such as roughness, MRR, profile/wear distribution and the effect of conditioning on the pad properties, and pad life. These models can be used to provide guidance for matching consumables to obtain desired polishing objectives, CMP process control, and improving process reliability and yields .

1.5 Technological Trends/Challenges

Based upon a comprehensive literature review, conditioning process has developed to an advanced stage where all dimensions are highly controlled (Baisie et al., 2009). Currently, pad conditioning faces constant challenges in the design, characterization, and evaluation of consumables towards meeting the demands of the ever-competitive global semiconductor manufacturing environment. Singh et al. (2011) have discussed succinctly the next generation CMP pad conditioning challenges and objectives. Their remarks are explained as follows.

1. The increasing intensity, complexity and changing requirements of next-generation CMP processes (recently 15 CMP steps in 180 nm Logic device and 32 steps in a 32 nm Logic device) demands more stringent specifications, smaller technology nodes and thinner wafers. Its emerging applications also call for new and tunable consumables and unique metrology requirements.

2. Currently, CMP consumables/system suppliers and end users are more interested in collaboration in the form of joint development and evaluation of new consumables. This collaboration is geared towards reducing CMP Cost of Ownership (CoO) through extended pad and conditioner lifetime and minimizing development/optimization time and repetition of efforts.
3. The pad conditioner's performance must be optimized not only for maintaining desired pad morphology but also for preserving device yield, reducing defectivity and enhancing process stability throughout pad's lifetime. This calls for significant cleanliness (extractables and particulate) improvements, and more stringent control of abrasive features/contacts size and shape distributions and diamond bond.

1.6 Research Gaps

Despite the fact that many researchers have investigated the diamond disc conditioning process with emphases on pad surface asperities, deformation, conditioning rate, conditioner life, and others, the determination of the necessary parameter values to yield an efficient pad dressing has not been investigated extensively. From a practical view-point, it has become more evident that, the individual models alone provide limited information to provide advice on maintaining high process efficiency. There is a school of thought that, as of now, most of the available models are not reliable enough to be used for verification of current processes or optimization of future processes (Dornfeld, 2010). The research gaps are discussed below.

- *Conditioner Design*: Because requirements for the performance of CMP conditioners have diversified it is important to select conditioner design to match applications based on factors such as the CMP pad type and wafer size. Diamond disc design parameters impact conditioner performance in CMP. However, not much work has been done concerning the incorporation of relevant conditioner design features in the mathematical models. Opportunities exist to advance this knowledge.
- *Finite Element Modeling*: A set of investigators have used the Finite Element Analysis (FEA) approach to model the interactions between the pad, wafer and abrasive particles to predict CMP performance. This powerful computational approach allows for 3-D geometries and more detailed representation of physical characteristics and mechanics of the process elements in the model. However, none of the available FEA modeling reports considers the conditioning aspects and its effects on the process. Future work could concern FEA of the conditioning process, further improving conditioner disc design, and advancing process optimization at a scale consistent with current requirements.
- *Multi-scale Model Integration*: Currently, there is a call for models to be able to address wafer, die, and feature scale issues in a more integrated fashion and provide feedback to designers so that circuits can be designed for easy manufacturability and high yield. From the review of literature on conditioning, many avenues exist for the optimization for a stable and efficient process at current scales. A more comprehensive analytical model that integrates all the key operational factors needs

to be developed. Models should be linked to both up-stream as well as down-stream processes to allow series process improvement.

1.7 Research Objectives

The aim of this research is to improve the current understanding of the diamond disc pad conditioning process in CMP to ensure more reliable verification of current processes and optimization of future processes.

The following objectives are intended to capture this overall aim: (1) to develop analytical models to simulate and predict the pad surface profile resulting from diamond disc conditioning; (2) to characterize the pad structure geometrically and develop a finite element model to simulate the pad's mechanical response to conditioning forces; (3) to evaluate effects of pad conditioning parameters on pad surface characteristics and conditioning uniformity; (4) to develop a set of metrics to adequately measure conditioning performance and optimize conditioning uniformity; and (5) to develop a model to optimize the conditioner design.

1.8 Research Approach

An initial step was to research, develop, and validate mathematical models that captured the relevant process parameters involved in the diamond disc pad conditioning process. One hypothesis was to ascertain if a set of process input variables had a

significant effect on performance variables. This allowed a systems engineering approach to be used to optimize the conditioning process. Here, the question that was addressed was: at what levels are parameters - identified to be significant - more relevant to the performance attributes?

One major roadblock to completing the proposed study was access to equipment for an experimental setup to validate developed models. The approach proposed to overcome this was to consider using equipment of another institution or company that is involved in CMP. However, this was accompanied by many difficulties. Alternatively, data was obtained from available peer reviewed publications about experimental work on pad conditioning in CMP.

1.9 Outline

Following Chapter 1, Chapter 2 presents a thorough literature review on diamond disc pad conditioning in CMP which discusses technical challenges and perspectives. The review yields a classification of conditioner design features, process control and analytical models of diamond disc pad conditioning.

In Chapter 3, a surface element method is proposed to develop a mathematic model to predict the pad surface profile resulted from diamond disc conditioning. The mathematic model is validated by published experimental data and utilized to investigate the effect of conditioning parameters on pad surface profile.

A different approach based on conditioning density distribution is developed in Chapter 4 to predict the pad surface profile resulted from the diamond disc conditioning in CMP. Here, conditioner design is considered and the resulting conditioning density distribution is correlated with the wear of the polishing pad and compared with experimental data.

In Chapter 5, a 2-D image processing procedure is developed for the characterization of the morphological and mechanical properties of CMP pads. A sample pad is characterized and incorporated into a 2-D axisymmetric quasi-static FEA model to investigate effects of process parameters (pad stiffness, and conditioning pressure) on the pad deformation.

Chapter 6 describes how the conditioning density model developed in Chapter 4 is further applied in a genetic algorithm to optimize the conditioner design parameters (including geometric arrangement of diamonds, grit density and disc size) towards optimization of the pad conditioning process.

In Chapter 7, a recap of the major findings of the research is provided and recommendations for future research are made.

CHAPTER 2

LITERATURE REVIEW

2.1 Introduction

This chapter contains a thorough literature review of recent research work on diamond disc conditioning in CMP. Various analytical models developed for diamond disc pad conditioning in CMP are summarized and compared in a format suitable for quick reference. Section 2.2 briefly introduces a technical background about the diamond disc conditioning process. Diamond disc conditioner development (including design and manufacture) is introduced in Section 2.3. Conditioning process control and pad surface measurement and evaluation are acknowledged in section 2.4. Section 2.5 describes the theories of the process mechanism and presents a review of various analytical models. Technical challenges are discussed and the objectives and research plan of this research are proposed in sections 2.6, 2.7 and 2.8 respectively.

2.2 Diamond Disc Pad Conditioning

During CMP, the pad surface pores can be clogged by removed wafer material, abrasive grits, and chippings from the pad itself (Zhou et al., 2008). At the same time, the pad surface asperities needed to hold the abrasive grits are diminished. This leads to a deterioration of removed material transportation, poor chemical-mechanical action and

eventually, to low MRR, high WIWNU, high wafer-to-wafer non-uniformity (WTWNU) (Zhou et al., 2008), and high cost of ownership (Tso and Ho, 2004). Pad conditioning is introduced to regenerate new pad asperity and maintain desired surface characteristics. Established conditioning methods include the utilization of high pressure water jet (Seike et al., 2005, Seike et al., 2006), wire brush (Jeong, 1999), vacuum (Breivogel et al., 1993), and ultrasonic vibration (Seo et al., 1999). The choice of each method depends upon the nature of pad being conditioned (Li, 2008). Today, diamond disc conditioning is the most widely used method for pad conditioning in wafer fabrication facilities (Lujan, 2006). Figure 2.1 shows a display of industrial diamond disc conditioners.



Figure 2.1. Typical diamond disc conditioners (Photo: Courtesy of Abrasive Technology)

During the conditioning process, the conditioner rotates and sweeps back and forth radially or in a semi-circular manner (Lee et al., 2009)) across the pad as was shown in Figure 1.1. Conditioning takes place either during polishing termed “in-situ” (Sung and

Kan, 2006) or between polishing operations termed “ex-situ”(Fukushima et al., 2001). A study by Fukushima et al (2001) has shown that higher removal rates and better planarity can be expected for in-situ conditioning. In-situ conditioning also allows better throughput and real-time process control with respect to maintaining stable pad surface properties(Fukushima et al., 2001). The governing principle of pad conditioning is to introduce friction between the polishing pad and the diamond disk, which characterizes a two-body abrasive wear mechanism. As illustrated in Figure 2.2, the diamond abrasives embedded on the disk create microscopic cuts or furrows on the pad surface to continually regenerate new pad surface and asperities. At the same time, they remove the glazed or accumulated particles on the polishing pad surface.

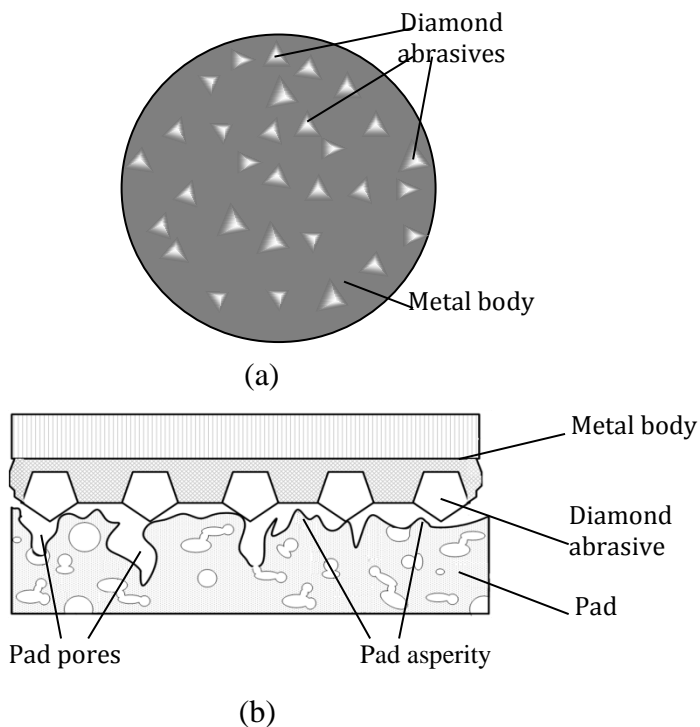


Figure 2.2. Illustration of (a) diamond disc conditioner face, and (b) interaction between the conditioner and the pad

The conditioning unit assembly, which is attached to the CMP machine, typically consists of a conditioner, a conditioner head, a directional arm, a connecting arm, and an arm drive mechanism as shown in Figure 2.3 (Skocypec et al., 2007). During operation, the conditioning assembly moves over the pad surface whilst maintaining a desired contact force between the conditioner and the pad surface. A computer may be programmed to generate a unique movement of the conditioner such that its velocity varies to compensate for locations of interest on the polishing surface (Jackson et al., 1995).

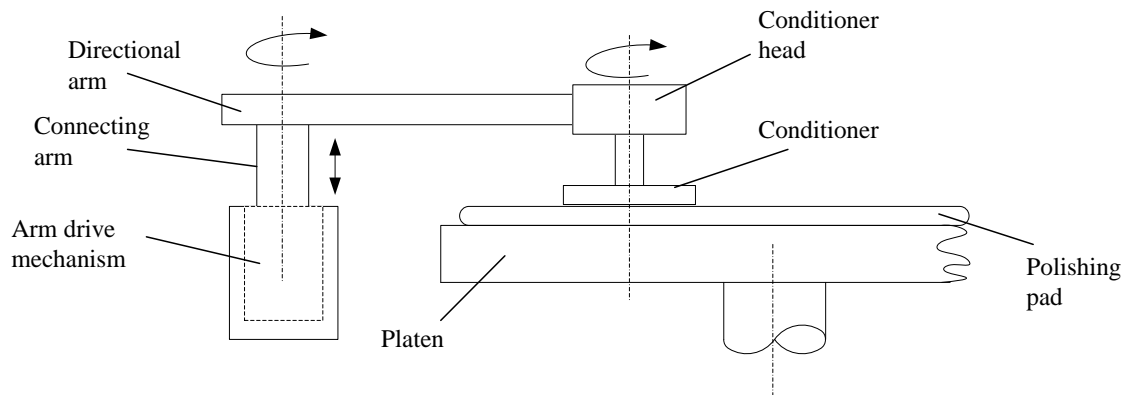


Figure 2.3. Conditioning unit assembly (Adapted from Skocypec, 2007)

2.3 Development of Diamond Disc Conditioner

2.3.1 Evolution

Over the last two decades, the geometry, material, and manufacture of diamond disc conditioners have evolved significantly. Notable stages of this transition are

presented in Figure 2.4. Breivogel et al. (Breivogel et al., 1993) invented an initial pad conditioning device in which a flat block holds several diamond tipped stainless steel rods. The rods are threaded into a block and can be manually adjusted to a desired position. This device introduces local compression on the pad and since there are only a few diamond tips, the effective conditioning area is limited (Benner et al., 2003). Furthermore, it has neither an effect on the removal of process fluid streams nor on active cleaning of pad (Benner et al., 2003). In later developments such as the abrasive disc described by Jackson et al.(Jackson et al., 1995), diamond grits were more often used as the abrasive particles because of its wear resistance, chemical inertness and reduced propensity to contaminate the pad or wafer (Benner et al., 2003). To overcome the initial shortcomings, another device was proposed to employ a larger diameter metal disc on which diamond abrasives are uniformly arranged and coated (Skocypec et al., 2007). In this case, pressure applied to the diamond disc controls the depth of grooves in the pad.

In more recent developments, diamond abrasives are encapsulated by chemical vapor deposition (CVD) to improve wear resistance among other advantages (Ohi, 2004, Thear and Kimock, 2004a). Other advanced designs proposed by Sung et al. (Sung, 2006, Sung, 2005, Sung et al., 2008, Sung et al., 2009), Tsai et al. (Tsai and Sung, 2009, Tsai et al., 2009, Tsai, 2010a) and Forsberg et al.(2006) include electro discharging of polycrystalline diamond (PCD) abrasives for what has been termed “Advanced Diamond Discs” and using polymers as diamond disc base for “Organic Diamond Discs”. These designs are characterized by high regularity of diamond shape and the promise of highly uniform regeneration of pad asperities.

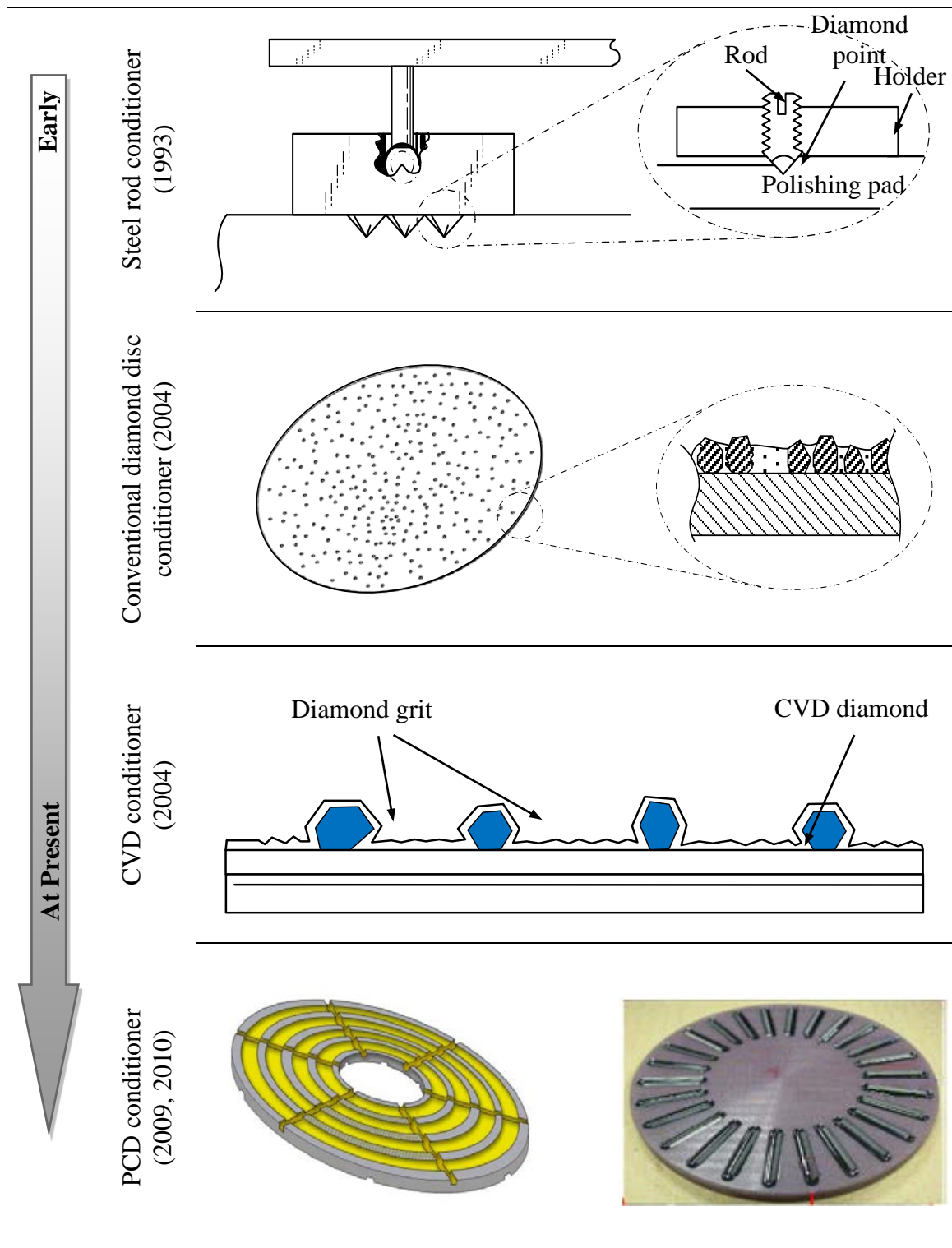


Figure 2.4. Conditioner evolution (Adapted from Breivogel et al, 1993, Myoung et al, 2004, Thear and Kimock, 2004, Sung, 2009, and Tsai et al., 2010)

2.3.2 *Disc Design*

The main considerations that drive disc design are the need for excellent and stable conditioning performance while obtaining the maximum pad and conditioning disc life. The performance of CMP conditioners is characterized by diamond grit pop out, wafer removal rate, conditioner life, and consistency of conditioners among batches (Ohi, 2004). A number of design parameters can impact conditioner performance (Li et al., 2006, Thear and Kimock, Garretson et al., 2000). Typically, diamond size (Manocha et al., 2010, Tsai and Sung, 2009, Sun et al., 2010, Yang et al., 2010, Thear and Kimock, 2004b), shape (Bubnick et al.), density (Hua et al., 2009), and exposure (Liao and Yang, 2009, Borucki et al., 2009, Tsai, 2010b, Andersson et al., 2005) will determine the conditioning outcome. Table 2.1 summarizes parameters considered in disc design. Ohi, in his discussion of trends and developments of diamond CMP pad conditioners (Ohi, 2004), suggests to select conditioner design based on the CMP pad type and the wafer size because requirements for the performance of CMP conditioners have diversified.

2.3.3 *Manufacture*

Many different ways to manufacture diamond disc conditioners have been reported (Skocypec et al., 2007, Myoung and Yu, 2004, Huang et al., 2008, Wielonski and Peterman Jr., 2007). In one description by Wielonski (Wielonski and Peterman Jr., 2007), diamond disc fabrication typically begins with forming a disc shaped metallic substrate of material such as stainless steel. The stainless steel disc is then coated with a monolayer of abrasive particles.

Table 2.1. Design considerations in conditioner design

Design Feature	Design Considerations
<i>Diamond Size</i>	Based on relatively small changes in the tail of the grit size distribution, extreme variations in conditioner performance can result if the average penetration of grit into pad is less than one or two standard deviations at standard conditions.
<i>Diamond shape</i>	Diamond grits (both regular and irregular) have been characterized according to their shape parameters such as aspect ratio, convexity, and sharpness (Hwang et al., 2007). The shape of diamond (jagged, cubic, octahedral, etc) has an effect on uniformity and thoroughness of conditioning. Good diamond shape also allows for optimal revolutions per minute, distribution of diamonds, protrusion and generation of force onto the polishing pad.
<i>Diamond Exposure</i>	Protrusion distance relates to optimal depth of grooves generated into polishing pad.
<i>Diamond Orientation</i>	This relates to the tip angle and positioning of the grit. Lack of diamond orientation results in different heights and has an effect on front side flatness which negatively affects polishing uniformity.
<i>Geometric Arrangement</i>	Grits may be distributed in a random or uniform manner. In more recent designs, a set of grits may be arranged in a grid, annular, radial or involute shaped array for enhanced performance in peculiar applications.
<i>Diamond density</i>	“Working Grit Density” is the ratio of number of grits in contact with the pad to the total conditioner area. Lower density results in fewer grooves. Substantial grit distribution density variation in different regions of the conditioner causes regions of higher density to have much lower working densities. This is due to a more global effect on pad distortion caused by smaller inactive grits adjacent to larger active grits which create larger grooves ahead of smaller grits.
<i>Disc size</i>	Disc size affects disc-to-pad size ratio. Higher ratios culminate in decrease of diamond fracture rate and more effective conditioning. Conditioners with a relatively small disc-to-pad size ratio are classified as scan type (usually used to condition the surface covered by wafers) (Li, 2007) .
<i>Disc front-side flatness</i>	If the conditioner substrate surface is not flat then working densities are affected in a global fashion. As little as 40 microns of bow in a two inch conditioner can alter the working density by as much as 50% (Thear and Kimock, 2004b, Thear and Kimock, 2004a). Other discs (Shimizu, 2010, Sung, 2007) have convex or contoured cross section aimed at reducing the friction between the pad and conditioner for extended life and to allow slurry to reach the center of the conditioner.
<i>Manuf. methods</i>	The diamond grits may be bonded to a metal substrate by electroplating, brazing and metal sintering. In more recent developments, diamond abrasives are encapsulated by chemical vapor deposition (CVD) and electro discharging of polycrystalline diamond (PCD).
<i>Bond thickness</i>	The thickness of the bond relates to diamond retention ability and tool life.

Typically, natural diamond particles or synthetic diamonds such as cubic boron nitride particles are preferred. These particles are distributed in a random or structured pattern using conventional techniques. A bonding metal such as nickel is often deposited on the diamonds to secure them to the substrate. A typical assembly of a conditioner disc is illustrated in Figure 2.5.

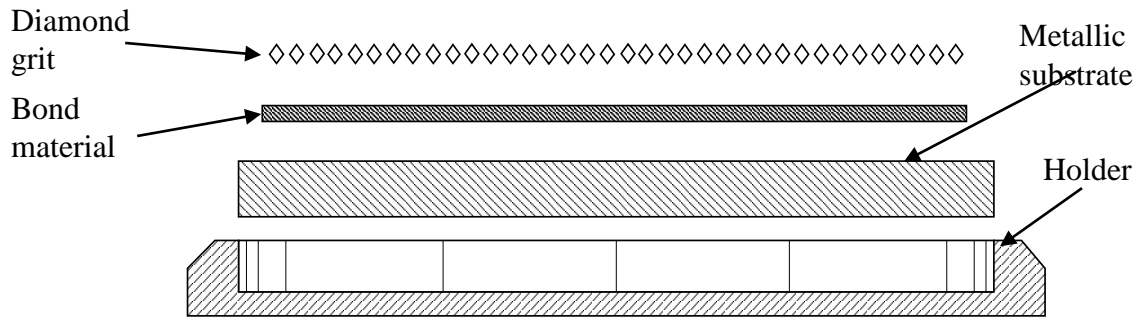


Figure 2.5. Conditioner disc assembly (Adapted from Wielonski, 2007)

The super-abrasive particles may be bonded to the substrate by electroplating, brazing, metal sintering, and CVD diamond bonding. Features of common diamond bonding methods (Park, 2005) are described in Figure 2.6. The brazing bond has become more preferred since it forms a stronger bond between the diamond particles and substrate. In this way, the diamond particles are less likely to loosen and fall free (pop out) compared to electroplated conditioning discs (Wielonski and Peterman Jr., 2007). After deposition of the particles, a holder for the substrate disc is adapted to fit the CMP polishing machine in a conventional manner.

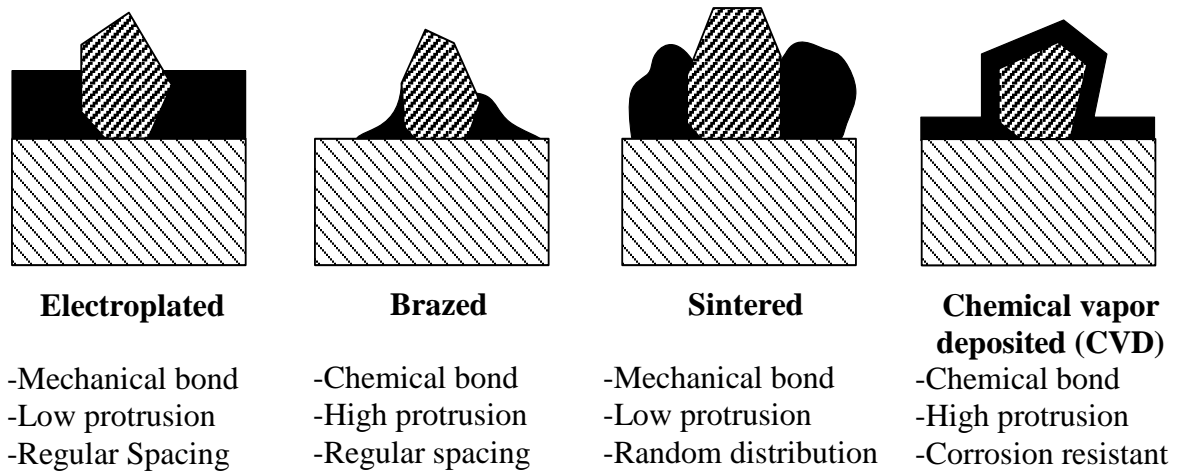


Figure 2.6. Common diamond bonding methods (Adapted from Park, 2005)

2.4 Process Control

2.4.1 Diamond Disc Conditioning Process Control

Previously, the method of monitoring the CMP pad conditioning processes was by trial-and-error. Different control parameters were changed manually by an operator to achieve optimal conditioning (Lim and Lee, 2007). The manual operator adjustments were based solely on operator experience. It is especially difficult to achieve good repeatability for the conditioning process if the manual adjustment is performed by different operators (Lim and Lee, 2007). To improve the control of the conditioning process, studies have been performed to develop models which describe the relationship between the control parameters and the conditioning process. These models are reviewed and summarized in Section 5.

Table 2.2. Process control factors (Conditioning kinematics)

Pressure	Conditioning pressure is related to downforce applied to the conditioner disc. Pad wear rate increases with the conditioning contact pressure between the diamond disk and the polishing pad.
Velocity	This is the combination of all the planar motions of the pad and the conditioner. Pad wear rate increases with conditioning velocity. On the other hand, surface roughness would be more rugged due to higher conditioning velocity. Wafer MRR increases with pad speed.
Time	This is the time spent at each region that the disc conditions. Chen [17] stated that the actual conditioning time is the main determinant of the amount of pad wear. Also, when the conditioner stays at one region for a longer time, local pad thickness would reduce and local conditioner contact pressure also reduces. As a result, MRR gradually reduces with longer conditioning time.
Sweeping pattern	This is described by the direction or trajectory in which the disc moves usually in allocated regions on the pad and the frequency of sweeping oscillation. The trajectory may be linear or semi-circular.

Pad conditioning is primarily a highly mechanical process. Its effects on the polishing process are dictated by the conditioning kinematics (Table 2.2) and other parameters such as pad temperature (Hua et al., 2009, Kim et al., 2006, Mudhivarthi et al., 2006) and pad properties (Tso and Ho, 2004) listed in Table 2.3. It is worth mentioning that automatic control of the process has been achieved through controllers which adjust the settings of the equipment during operation (Karupiah et al., 2006, Fukuzawa, 2002). For a reciprocating diamond disk moving along a radial or semi-circular trajectory within the polishing area of the polishing pad, a variation of the conditioning parameters may be adapted for optimal conditioning of the pad. As described by Lim and Lee (2007), the trajectory of the diamond disk may be divided into a number of sections, and its movement speed may be varied at each section. The diamond disk may move through the edge area of the polishing pad at a highest speed, an intermediate area at a lowest speed, and the center area at a medium speed (Lim and Lee,

2007). A contact pressure between the diamond disk and the polishing pad may also be varied at each section where it may have a highest contact pressure at the edge part of the polishing pad, a lowest contact pressure at an intermediate part, and a medium contact pressure at the center part.

Table 2.3. Process control factors (Consumables)

	Temperature	Elevated pad temperatures result in improved removal rates due expanded pad pores and better slurry transport and also good planarity and smooth surface morphology of the pad (Hua et al., 2009, Kim et al., 2006). However it lengthens the time to achieve steady-state, and also plays a major role in generation of wafer defects like dishing and erosion during copper CMP process (Mudhivarthi et al., 2006).
Pad	Relative pad hardness	As pad speed increases, the effective hardness of the pad increases and the penetration depth of grit into the pad drops. This reduces the conditioning effect.
	Soaking time of pad	Soaking time of pad significantly influences the dynamic shear modulus of pad. Also, the pad structure would become more flexible, and the removal degree of pad material would increase gradually.
	Ph value of slurry	The workpiece to be polished dictates the pH value of slurry. The intensity of the diamond grit drops with increasing alkalinity. This means that the removal degree of conditioning pad material will decrease because of the abrasion of incisive edge of diamond grits.
	Working Grit Density	If the downforce is increased and a very small fraction of grit is in contact with the pad, then the working grit density increases as the penetration depth increases. If the working grit density increases too much, then the pad tends to be polished rather than grooved, and the performance is reduced.
	Grit Size	Grit size is characterized by average cutting angle or groove width of diamonds. This relates to depth and width of grooves generated into polishing pad.
Conditioner	Disc Size	Disc size affects conditioner/pad ratio. Higher ratios culminate in decrease of diamond fracture rate and more effective conditioning. It is also easier to achieve better pad profile with a smaller disc diameter.
	Disk Chatter	Any change in contact area between the conditioner and the pad affects conditioning. Disk chatter can create a highly variable contact area, therefore it should be minimized by careful attention to process parameters and design of the conditioner holder and mounting hardware.
	Diamond grit wear	As the diamond grit wears, the sharp edges round off first then the entire particle slowly develops a flat top with rounded edges, Conditioning can be maintained at a constant rate only if the diamond particles are worn down to the same height as the pad penetration and there is high working grit density.

Similarly, rotational speed of the diamond disk may be varied at each section with its highest speed at an edge part of the polishing pad, a lowest rotational speed at an intermediate part, and a medium rotational speed at a center part (Lim and Lee, 2007). Such methods of variation have been adapted to uniformly condition the polishing pad and reduce costs associated with managing, maintaining, and replacing the diamond disk (Fukuzawa, 2002).

2.4.2 Measurement and Evaluation of Pad Characteristics

Metrology plays a crucial role in enabling any type of CMP process control, and may be implemented in different ways based on the measurement techniques used, its location in the process flow and the type and amount of data generated. During the CMP cycle, pad characteristics such as the thickness, Young's modulus, and viscous properties of the pad tend to be dynamic (Zhang et al., 2009). Therefore measurement of these properties is very important towards understanding polishing non-uniformity and the maintenance of acceptable WIWNU and WTWNU. Zhang et al. (2008) discuss pad thickness and hardness measurement methods.

2.5 Process Modeling

Although the last decade has seen progress in the modeling of CMP, emphasis has rather been placed on the physical interactions among the wafer, slurry, and pad (Chen et al., 2000). However, there exist proven relationships between pad conditioning and the CMP process. Various models have been proposed to describe effects of pad conditioning

on wafer surface roughness (thickness variation), MRR, pad surface profile and pad properties. The theory provides guidance on how to match or design conditioners to reach desired polishing objectives, improving process reliability and yields and process control. Such understanding is vital in semiconductor manufacture to advance cost control, process optimization and automation.

As conditioning is primarily considered as mechanical process characterized by a two-body abrasive wear mechanism (Krishnan et al., 2009), the classical Preston equation (Preston, 1927) - originally used to model polishing of glass - has been widely used to describe removal (polishing) rate in wafers (Chen et al., 2000). Considering the similarity between wafer-pad interaction and pad-conditioner interaction, the Preston's equation has been adopted by many to model pad wear due to conditioning. The Preston equation states that *MRR* is proportional to the applied pressure *P* and the relative velocity *V* between the wafer and the pad and K_p is a constant, called Preston's coefficient.

$$MRR = K_p PV$$

The use of the Preston equation has been successful due to its simplicity and computability. However the equation has been modified by various researchers to accommodate differences in application. Some researchers suspect that the value of K_p involves advanced physics (Nanz and Camilletti, 1995, Lai, 2001, Yeh and Chen, 2010) and may be dependent on the pad roughness, asperities, elasticity, surface chemistry and abrasion effects as well as conditioner characteristics among others. More analytical and

experimental studies are needed to understand the role of K_p in modeling of pad conditioning.

Other investigators use different approaches. Modeling approaches commonly used are categorized into two groups, namely *kinematic* and *statistical*. The kinematic approach uses the motion and associated forces of the conditioner and pad to describe the conditioning process. The statistical approach uses statistical models such as probability of locating a point on the pad surface for the same purpose. A classification of process models identifying key variables and major modeling objectives is presented in Table 2.4.

In Appendix I, representative figures, key formulae, assumptions, and modeling conclusions for various analytical models developed to describe diamond disc pad conditioning are presented. All the models presented take into account conditioning kinematics (conditioning pressure, conditioning time, relative velocity, and sweeping pattern). In practice, the kinematics are the most controllable aspects of the process.

Table 2.4. Classification of pad conditioning analytical models

Year	Investigator	Objective	Key Assumption	Mathematical Approach	Key Variables				
					Kinematics	Time	Diamond features	Temperature	Pad properties
1999	Zhou and Davis	Pad profile	Preston eqn.	Kinematic	x	x			
2000	Chen <i>et al.</i>	Pad profile	Preston eqn.	Kinematic	x	x			
2003	Horng	Pad deformation	Elastic deformation	Kinematic	x				x
2004	Liao <i>et al.</i>	Pad MRR	Power consumed	Kinematic	x		x		
2004	Tso and Ho	Pad MRR	Preston eqn.	Kinematic	x		x		x
2004	Borucki	Variability of pad surface	Equivalent bar conditioner	Statistical	x	x	x		x
2005	Tyan	Pad wear distribution	Conditioning density	Kinematic	x	x			
2006	Wiegand and Stoyan	Variability of pad surface	Equivalent bar conditioner	Statistical		x	x		x
2006	Borucki	Pad MRR	Conditioning, friction & removal	Combination	x		x	x	x
2007	Chang <i>et al.</i>	Pad profile	Preston eqn.	Kinematic	x	x			
2009	Chen and Young	Pad profile	Preston & scratch number	Kinematic	x	x			
2009	Lee et al	Pad profile	Preston & sliding distance	Kinematic	x	x			
2010	Baisie et al	Pad profile	Preston & sliding distance	Kinematic	x	x			
2010	Yeh	Recovered area ratio	Conditioning density	Kinematic	x	x			

Chen (2000), Feng (2007), Chang (2007), Lee (2009) and Baisie et al (2010) models use kinematic approaches to predict the amount of wear across the pad by employing the Preston equation. In the kinematic approaches, a major assumption is that pad wear is determined by the sliding distance on the pad. A related kinematic approach adopted by Chen and Young (2010) to relate the distribution of scratch numbers of diamond grit on pad to the pad profile. Yeh (Yeh and Chen, 2010) improved upon Chen's model to consider multiple cuts for a specific portion before the glazed layer is finally removed and the effective Preston's constant is restored. To measure the effectiveness of conditioning, Yeh (Yeh and Chen, 2010) defines a performance metric called recovered area ratio which is the ratio between the recovered and total pad areas.

Tso and Ho's (2004) and Liao's (2004) models focus more on the relationship between conditioner parameters and the pad wear rate (MRR). However, Tso and Ho utilize the Preston equation while Liao's model presumes metal cutting theory. On the other hand, Horng's (2003) model calculates pad deformation across the pad which is not accounted for by the other models.

The CMP process is rather complex with nonlinear and sometimes non-Gaussian process dynamics, which brings significant challenges for process monitoring and control (Zhenyu et al., 2010). Borucki (2004) and Wiegand and Stoyan's (2006) models use statistical approaches to investigate the variability and extent of pad surface roughness. A later model by Borucki et al (2006) combines pad surface topography from conditioning and coefficient of friction to predict MRR.

Other investigators have employed the FEA approach to model the interactions between the pad, wafer and abrasive particles to predict wafer MRR (Bozkaya and Muftu, 2009, Che et al., 2002, Yan et al., 2004, McGrath and Davis, 2003), WIWNU (Lee et al., 2004, Lin et al., 2008), wafer flatness (Zhang et al., 2005), pad surface asperities (Jiang and Muldowney, 2007), and pad wear (Pei-Lum and Rick, 2007, Li et al., 2010, Nishioka et al., 2001). This powerful computational approach allows for 3-D geometries and more detailed representation of physical characteristics and mechanics of the process elements in the model. However, none of the available FEA modeling reports considers the conditioning aspects and its effects on the process.

2.6 Review Summary

Out of the numerous methods, diamond disc conditioning is the most widely used in wafer fabrication facilities today to regenerate new pad asperity and maintain uniform surface profile for CMP. The conditioning tool typically consists of a metal disc with one side embedded with protruding diamond grits. Conditioner design considerations include diamond size, shape, exposure, orientation, geometric arrangement, density, disc size, disc front-side flatness, bond thickness and manufacturing methods.

The main process control avenues are conditioning time and conditioning kinematics such as pressure, relative velocity and sweeping pattern (sweeping profile). The Preston equation has been adopted by many researchers to model the conditioner-pad interaction. Key modeling variables include pressure, pad velocity, conditioner velocity,

conditioning time, disc radius, grit size, grit density, pad temperature, and pad relative hardness. Available analytical models predict pad wear rate, pad height distribution, rms pad roughness, pad deformation, wafer material removal rate and pad surface recovered area ratio. Many avenues exist for the optimization of conditioning towards more uniform pad surface characteristics and longer lasting consumables, amidst constraints such as conditioner design, pad characteristics and CMP process parameters.

CHAPTER 3

SURFACE ELEMENT MODEL

3.1 Introduction

It has been challenging to attain a flat pad surface profile in diamond disc conditioning. Moreover, there are limited reports in the literature focusing on the pad surface profile resulting from the diamond disc conditioning (Feng, 2007, Chang et al., 2007, Zhou and Davis, 1999). Freeman and Markert (1996) claimed that a mathematical model was developed to accurately predict the pad surface profile. But there was no detailed information about the model development. Zhou and Davis (1999) reported the influence of the diamond disc conditioning on the pad surface profile. Their experimental results showed that a concave pad surface profile led to a convex surface profile for the wafer. Chang et al. (2007) presented a mathematic model to reveal the concavity of the pad surface profile with experimental validation. Their research was focused on the relationship between the pad surface profile and the pad conditioning time. It was reported that longer conditioning time resulted in higher concavity of the pad surface profile. Recent research works on the pad surface profile are summarized in Chapter 2. Findings from this review showed that no such mathematic model was developed with consideration of the effect of conditioner sweeping profile.

In this chapter, a surface element method is proposed to develop a mathematic model to predict the pad surface profile resulting from diamond disc conditioning. First,

the mathematic model is developed with consideration of the conditioner sweeping profile. Then, the developed model is used to predict the pad surface profile and validated by published experimental data. Based upon the validated model, effects of conditioning parameters (including sweeping profile, pad rotating speed, conditioner rotating speed, and conditioner diameter) on the pad surface shape are further investigated and discussed.

3.2 Model Development

3.2.1 Assumptions

Figure 3.1 illustrates a cycle of pad conditioning. Initially, the pad is rotating about its center with an angular speed of ω_p at an overhead position and descends onto the pad.

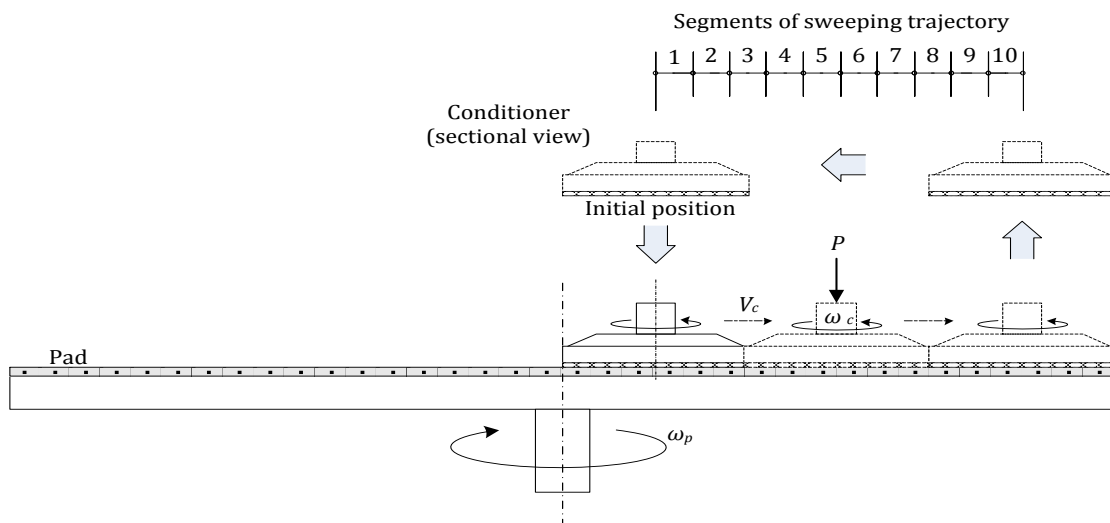


Figure 3.1. Illustration of a diamond disc conditioning cycle

The conditioner then sweeps in a straight line from the pad center to the pad periphery at a speed of V_c . The sweeping trajectory of the conditioner center is divided into 10 equal sections (or 10 annular segments). The time taken by the conditioner to traverse each section is adjustable. V_c will be a constant only if the same time value is assigned to all sections, otherwise, it will be a discrete variable. When the conditioner touches the pad periphery, it lifts off the pad surface and moves back to its initial position for the next cycle. The following assumptions are made to estimate the pad wear thickness due to conditioning:

1. Initially, the pad surface profile is assumed to be flat. However, the final profile is determined by the amount of pad material removal resulting from diamond disc conditioning (Chang et al., 2007, Zhou et al., 2008).
2. Diamond exposure is assumed to be uniform across the surface of the conditioner and hence the depths of grooves generated on the polishing pad are equal.
3. Since there is abrasive contact between the conditioner and the pad, the pad material removal due to conditioning can be represented by the Preston equation (Preston, 1927):

$$\frac{d\xi}{dt} = k_p \cdot p \cdot v_{p/c}; \quad (3.1)$$

where ξ the pad material removal, t the conditioning time, K_p a Preston coefficient determined by the pad and the conditioner properties, p the constant pressure applied on the conditioner, and $V_{p/c}$ the relative velocity between the pad and the conditioner.

4. K_p and p are assumed to be constant values. Therefore, the amount of pad material removal is only related to $V_{p/c}$ and can be rewritten as:

$$d\xi = k_p \cdot p \cdot v_p \cdot dt = k_p \cdot p \cdot dl; \quad (3.2)$$

where dl is the distance a diamond abrasive sweeps on the pad surface.

5. Now, assuming there is a surface-to-surface contact between the conditioner and the pad, Equation (3.3) can be further derived as:

$$d\xi = k_p \cdot p \cdot dA; \quad (3.3)$$

where dA is the area the diamond disc conditioner swept on the pad surface. A general equation to estimate the pad wear thickness due to the conditioning can then be described as:

$$dh = \frac{k_p \cdot p \cdot dA}{A_p} = k \cdot \frac{dA}{A_p}; \quad (3.4)$$

where dh is the pad wear thickness, A_p the pad surface area, and k is a coefficient determined by pad/conditioner properties, conditioning pressure, and pad surface area. This assumption has been successfully used by Pietsch and Kerstan (2005) to predict the wafer surface profile in simultaneous double side grinding.

3.2.2 Model Derivations

The pad conditioning kinematics is shown in Figure 3.2. The pad of a radius of R_p rotates in the clockwise direction about its center (O_p) at an angular speed of ω_p . The

conditioner of a radius of R_c rotates in the counter-clockwise direction about its center (O_c) at an angular speed of ω_c . The conditioner center (O_c) has an offset distance of R_c from the pad center (O_p). It then sweeps in a straight line from the pad center to the pad periphery till the edge of the conditioner is tangent to the pad edge. The sweeping trajectory can be obtained as $R_p - 2R_c$ and divided into 10 equal sections by 11 positions as shown in Figure 3.2.

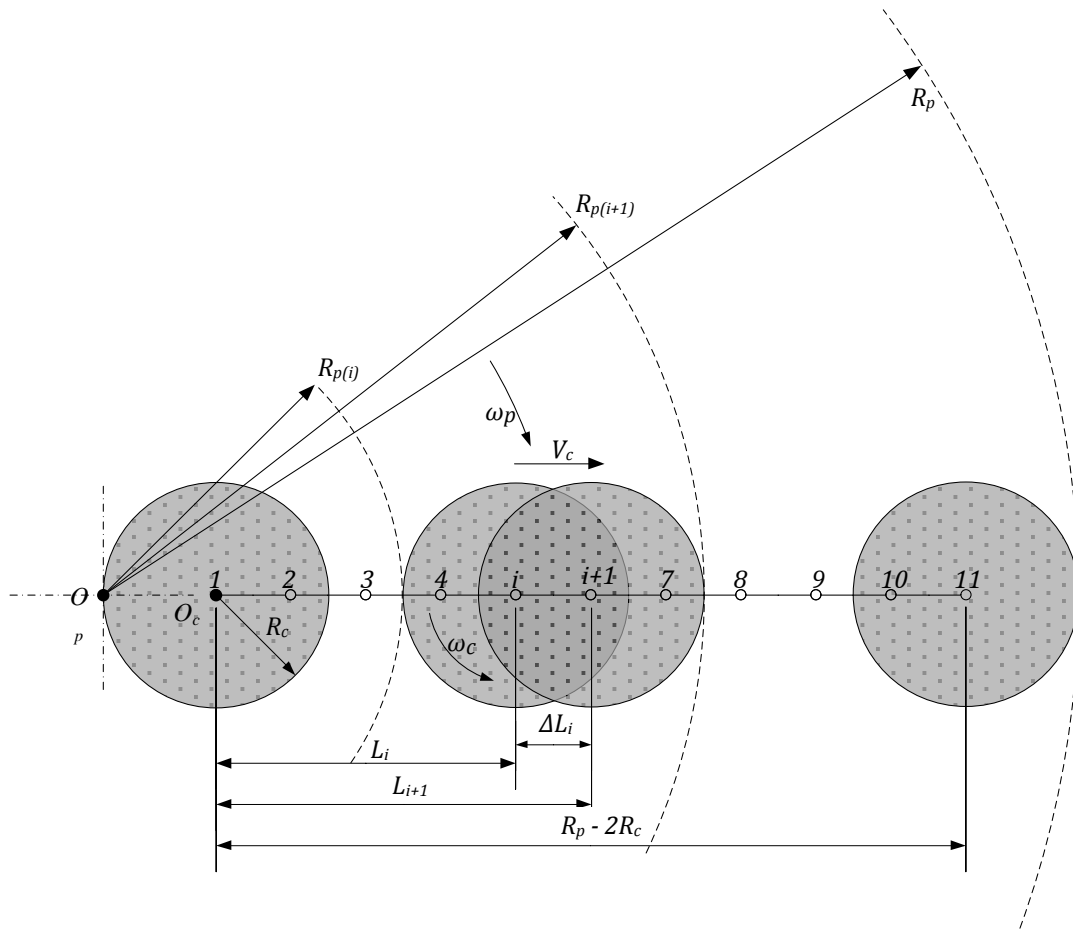


Figure 3.2. Schematic of pad conditioning kinematics

A value t_i is assigned as the time the conditioner center takes to traverse a random section ΔL_i ($1 \leq i \leq 10$). A sequence of t_i (i from 1 to 10) is defined as the conditioner's sweeping profile (Freeman and Markert, 1996). The sweeping velocity V_c can then be described as:

$$V_c = \frac{\Delta L_i}{t_i} = \frac{L}{\sum_{i=1}^{10} t_i} = \frac{R_p - 2R_c}{\sum_{i=1}^{10} t_i}, \quad i = 1, 2, 3, \dots, 10. \quad (3.5)$$

In Figure 3.2, L_i is defined as the distance between the i^{th} position and the initial conditioner center position (i.e. I^{st} position). The same definition is applicable for L_{i+1} . For a random section ΔL_i between the position i and position $i+1$, the radius of the pad area swept by the conditioner ranges from $R_{p(i)}$ to $R_{p(i+1)}$ as shown in Figure 3.2. It is easy to determine that $R_{p(i)}$ and $R_{p(i+1)}$ are equal to L_i and $L_{i+1} + 2R_c$, respectively.

Figure 3.3 shows the mathematical model to calculate the pad area swept by the conditioner when the conditioner center traverses the i^{th} section. A surface element is defined as a tiny sector on the conditioner as shown in Figure 3.3. r_c ($0 < r_c < R_c$) is the distance between the surface element and the conditioner center. After a time period of t , the surface element moves from position A to position B . The motion of the surface element can be decomposed into three parts. Firstly, the rotation of the pad in the clockwise direction is treated by rotating the center of the conditioner at an angle of $\omega_p t$. Hence, the surface element on the conditioner also rotates the same angle about the pad center and its displacement can be described as:

$$\vec{r}_p = (R_c + L_i) \cdot e^{i\omega_p t}. \quad (3.6)$$

Secondly, due to the conditioner rotation in the counter-clockwise direction, the surface element rotates an angle of $\omega_c t$ about the conditioner center during the time period t . This displacement is represented as follows:

$$\vec{r}_c = r_c \cdot e^{-i\omega_c t}. \quad (3.7)$$

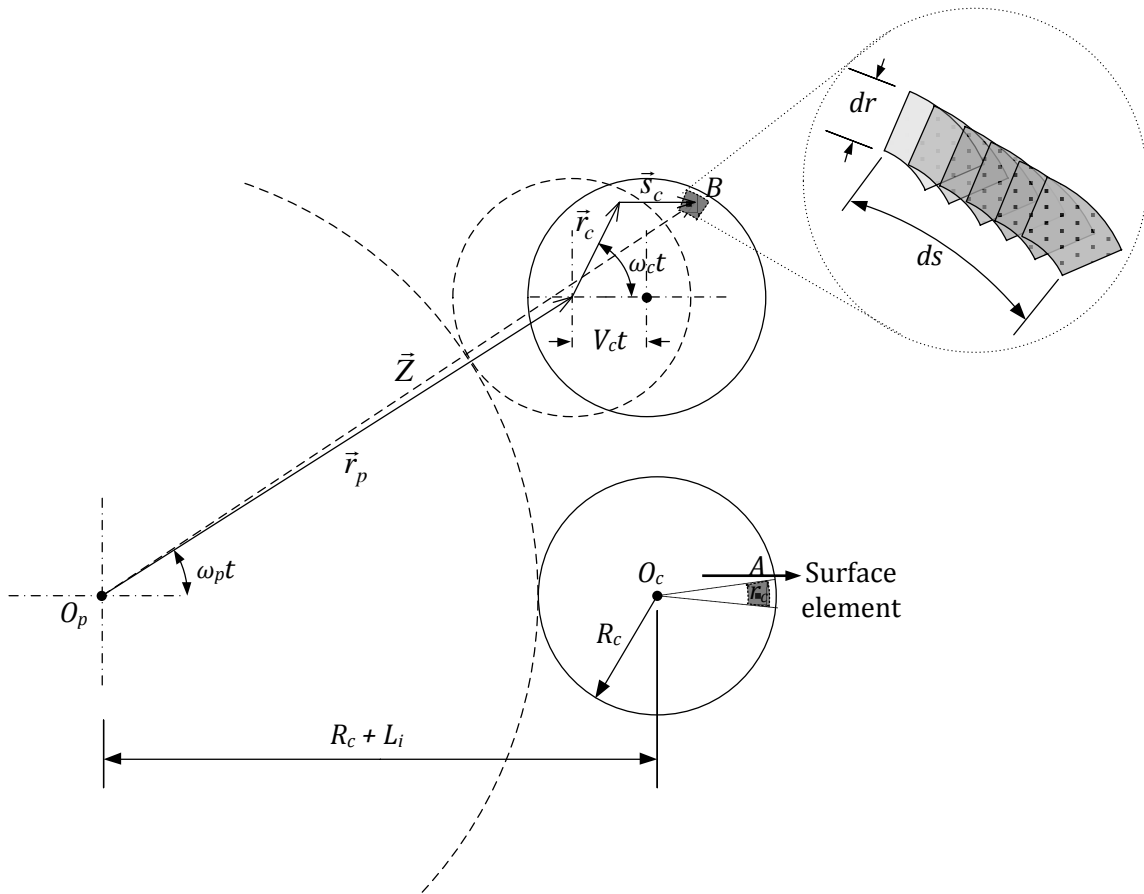


Figure 3.3. Model to calculate the pad area swept by the conditioner

Thirdly, the surface element moves along the horizontal direction due to the conditioner sweeping motion. The displacement resulted from the sweeping motion can be described as:

$$\vec{s}_c = V_c \cdot t. \quad (3.8)$$

\vec{s}_c can be further derived by substituting Equation (3.5) into Equation (3.8):

$$\vec{s}_c = \frac{\Delta L_i}{t_i} \cdot t = \frac{R_p - 2R_c}{\sum_{i=1}^{10} t_i} \cdot t. \quad (3.9)$$

From Equation (3.6), (3.7), and (3.9), the displacement to describe the motion of the surface element can be represented as follows:

$$\vec{Z} = \vec{r}_p + \vec{r}_c + \vec{s}_c = (R_c + L_i) \cdot e^{i\omega_p t} + r_c \cdot e^{-i\omega_c t} + \frac{R_p - 2R_c}{\sum_{i=1}^{10} t_i} \cdot t. \quad (3.10)$$

Equation (3.10) can be derived and rewritten in the complex number form as:

$$\vec{Z} = a + i \cdot b;$$

where

$$\begin{cases} a = (R_c + L_i) \cdot \cos \omega_p t + r_c \cdot \cos \omega_c t + \frac{R_p - 2R_c}{\sum_{i=1}^{10} t_i} \cdot t; \text{ and} \\ b = (R_c + L_i) \cdot \sin \omega_p t - r_c \cdot \sin \omega_c t. \end{cases} \quad (3.11)$$

Then the displacement \vec{Z} can be further represented by the polar form:

$$\vec{Z} = [r(t), \varphi(t)];$$

where

$$\begin{cases} r(t) = r = |\vec{Z}| = \sqrt{a^2 + b^2}; \text{ and} \\ \varphi(t) = \varphi = \tan^{-1} \frac{b}{a}. \end{cases} \quad (3.12)$$

The arc trajectory swept by the surface element within the time period t_i is calculated as:

$$s(t) = \int_0^{t_i} \sqrt{\dot{\varphi}^2 r^2 + \dot{r}^2} dt. \quad (3.13)$$

From Equation (3.13), the pad area swept by the conditioner during t_i can be integrated as follows:

$$A_{swept(i)} = \int_0^{2\pi} \int_0^{R_c} \int_0^{t_i} \sqrt{\dot{\varphi}^2 r^2 + \dot{r}^2} dt dr_c d\varphi. \quad (3.14)$$

Since the conditioner may sweep for multiple cycles, the number of cycles is calculated as $N = \frac{t_c}{t_l + \sum_1^{10} t_i}$ where t_c is the total conditioning time and t_l time the conditioner takes to lift off the pad and move back to the initial position, with the total pad area swept by the conditioner as the conditioner center traverses from the i^{th} position to the $i+1^{th}$ position during the total conditioning time period of t_c being calculated as:

$$Total A_{swept(i)} = N \cdot A_{swept(i)}. \quad (3.15)$$

Then a pad sectional wear Δh_i due to pad conditioning can be represented by combining Equation (3.15) with Equation (3.4):

$$\Delta h_i = k \cdot \frac{Total A_{swept(i)}}{A_{p(i)}};$$

where

$$A_{p(i)} = \pi \cdot R_{p(i+1)}^2 - \pi \cdot R_{p(i)}^2 = \pi \cdot (L_{i+1} + 2R_c)^2 - \pi \cdot L_i^2. \quad (3.16)$$

For $i= 1, 2, 3, \dots, 10$, Δh_i can be further described as follows:

$$\left\{ \begin{array}{l} \Delta h_1 = k \cdot \frac{Total A_{swept(1)}}{\pi \cdot (L_2 + 2R_c)^2}; \\ \Delta h_2 = k \cdot \frac{Total A_{swept(3)}}{\pi \cdot (L_3 + 2R_c)^2 - \pi \cdot L_2^2}; \\ \Delta h_3 = k \cdot \frac{Total A_{swept(3)}}{\pi \cdot (L_4 + 2R_c)^2 - \pi \cdot L_3^2}; \\ \dots \\ \dots \\ \dots \\ \Delta h_{10} = k \cdot \frac{Total A_{swept(10)}}{\pi \cdot R_p^2 - \pi \cdot L_{10}^2}. \end{array} \right. \quad (3.17)$$

It is important to note that there exists overlapped conditioning area as the conditioner traverses two or more successive sections. This means the same section of the pad surface (for example $R_{p(i)} \rightarrow R_{p(i+1)}$) could be conditioned several times when the conditioner sweeps through different sections (for example $\Delta L_{i-1}, \Delta L_i, \Delta L_{i+1}$). Because of these overlapped conditioning areas, actual pad wear $\Delta H(r_p)$ has to be treated as a result of multiple sectional pad wear. As shown in Figure 3.4, for any random position r_p along the radial direction on the pad surface, the actual pad wear $\Delta H(r_p)$ is calculated by adding all sectional pad wear Δh_i , which are overlapped to each other during conditioning.

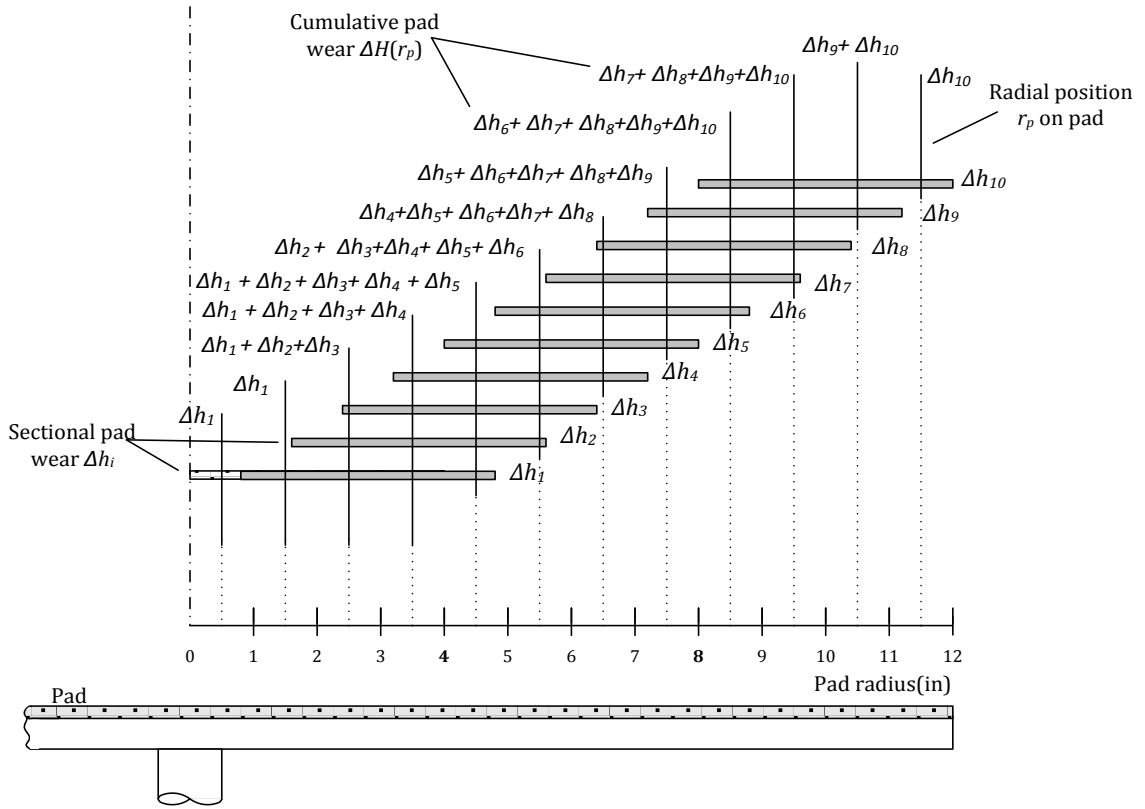


Figure 3.4. Illustration of cumulative wear thickness

The actual pad wear $\Delta H(r_p)$ is defined as cumulative pad wear and is described as follows:

$$\Delta H(r_p) = \begin{cases} \sum_1^{[|r_p - \Delta L_i| / \Delta L_i]} \Delta h_i & \text{if } r_p \leq 2R_c; \\ \sum_{[(r_p - \Delta L_i) / \Delta L_i]}^{[(r_p - \Delta L_i) / \Delta L_i]} \Delta h_i & \text{if } 2R_c < r_p < R_p - 2R_c; \\ \sum_{[(r_p - \Delta L_i) / \Delta L_i] - (m-1)}^{10} \Delta h_i & \text{if } r_p \geq R_p - 2R_c; \end{cases} \quad (3.18)$$

where r_p from 0 to R_p and m the number of sections is represented as:

$$m = \frac{2R_c}{\Delta L_i} = \frac{2R_c}{\frac{(R_p - 2R_c)}{10}}.$$

The initial pad thickness is assumed to be H_0 . Then the pad surface profile along the pad radial direction after pad conditioning can be described as:

$$H(r_p) = H_0 - \Delta H(r_p). \quad (3.19)$$

3.2.3 Simulation

The mathematical model developed above was run in a commercial software package Matlab (The MathWorks, Inc., 3 Apple Hill Drive, Natick, MA 01760, USA).

The computer program accepts these conditioning parameters:

- Pad angular speed $\omega_p = N_p/2\pi$ where N_p rotation speed in rpm;
- Conditioner angular speed $\omega_c = N_c/2\pi$ where N_c rotation speed in rpm;
- Pad radius R_p in inch;
- Conditioner radius R_c in inch;
- Conditioning time t_i assigned for section ΔL_i in second;
- Conditioning sweeping profile $\{t_i\}$; and
- Total conditioning time t_c in minute

as input variables and plots $\{t_i\}$, the sectional pad wear, the cumulative pad wear, and the pad surface profile as outputs.

3.3 Simulation Results and Experimental Validation

3.3.1 Simulation Conditions

Conditioning parameters adapted for simulation are listed in Table 3.1. More detailed information can be found in published literature (Freeman and Markert, 1996) provided in Appendix II.

Table 3.1. Experimental conditions (Adapted from Freeman and Markert, 1996)

Polish Parameters		Conditioning Parameters	
<i>Time</i>	2 min	<i>#sweeps</i>	1 post polish
<i>Downforce</i>	41.37 kPa	<i>Time</i>	1 min
<i>Pad temp</i>	37.78 °C	<i>Downforce</i>	15.38 kPa
<i>Platen RPM</i>	36 rpm	<i>End RPM</i>	70 rpm
<i>Pad type</i>	RodelEX1400	<i>Platen speed</i>	75 rpm
<i>Back pressure</i>	0 kPa	<i>Platen Ø</i>	60.96 cm
<i>Flow rate</i>	150 ml/min	<i>Profile</i>	Variable
<i>Oscillation</i>	10 mm	<i>End effector</i>	5.08 cm Ø / 200 diamond grits

Three sweeping profiles named as FLAT 1, FLAT 2, and BELL are listed in Table 3.2. FLAT 1 increases linearly in time from the pad center to the periphery. FLAT 1 is proposed to test a hypothesis that the conditioning time should increase linearly along the pad radius to compensate for the increase of the pad area. FLAT 2 has a constant sweeping profile to test the hypothesis that the pad surface profile is independent of the increase of the pad area along radial direction. BELL is proposed to generate a bell shape

sweeping profile by using high sweeping time periods at the beginning and the end and reducing the time around the middle.

Table 3.2. Sweeping profiles used for pad surface profile simulation (Adapted from Freeman and Markert, 1996).

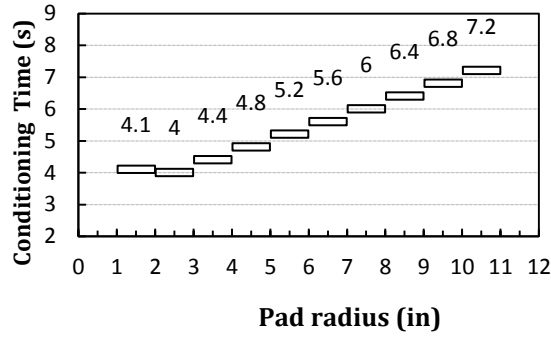
Sweeping profile (sec)	Pad center				#Section			Pad Periphery		
	1	2	3	4	5	6	7	8	9	10
FLAT 1	4.1	4.0	4.4	4.8	5.2	5.6	6.0	6.4	6.8	7.2
FLAT 2	5.5	5.5	5.5	5.5	5.5	5.5	5.5	5.5	5.5	5.5
BELL	8.1	5.4	4.0	2.2	2.4	2.6	2.8	5.8	9.8	13

3.3.2 Simulation Results and Discussion

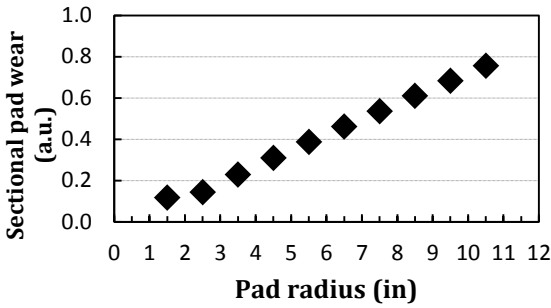
Figure 3.5 shows simulation results for the conditioner sweeping profile, the pad sectional wear Δh_i , and the pad cumulative wear $\Delta H(r_p)$ for the sweeping profile FLAT 1. There exists a significant linear increase of the pad sectional wear along the pad radial direction as shown in Figure 3.5(b). As for the pad cumulative wear, a sharp linear increase can be observed near the pad center area. It is then followed by a slower linear increase and ended with a sharp linear decrease around the pad's periphery.

Simulation results for the sweeping profile FLAT 2 are shown in Figure 3.6. The pad sectional wear shows a very slight increase with the increase of pad radius as shown in Figure 3.6(b). Concerning the pad cumulative wear thickness, a constant wear can be observed in between a sharp increase wear near the pad center and a sharp decrease wear

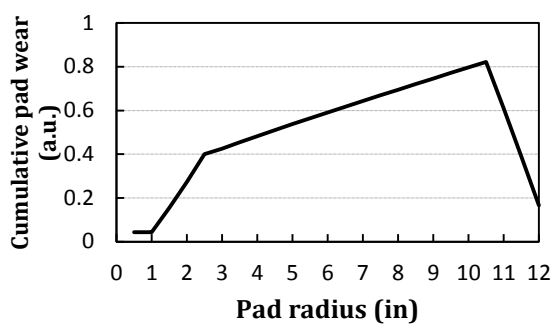
near the pad periphery as shown in Figure 3.6(c). Figure 3.7 shows simulation results for the sweeping profile BELL.



(a) Sweeping profile

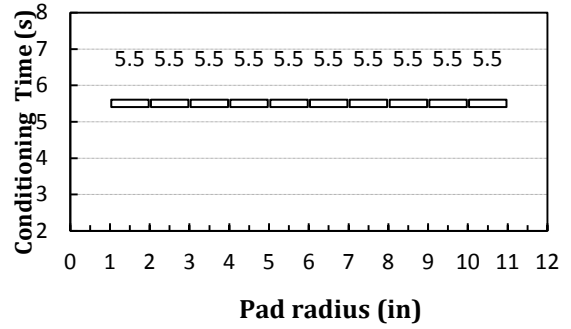


(b) Sectional pad wear

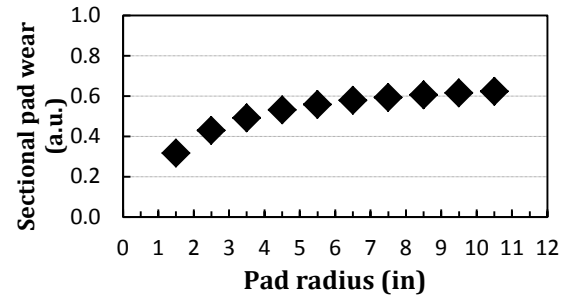


(c) Cumulative pad wear

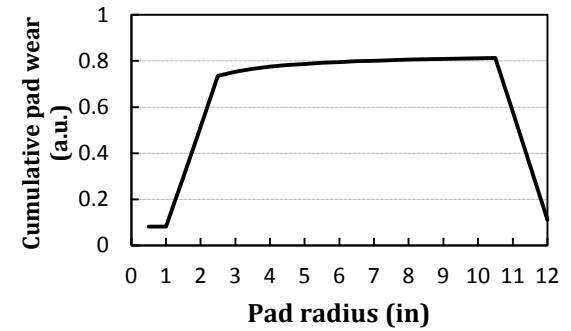
Figure 3.5. Simulation results for sweeping profile FLAT 1.



(a) Sweeping profile

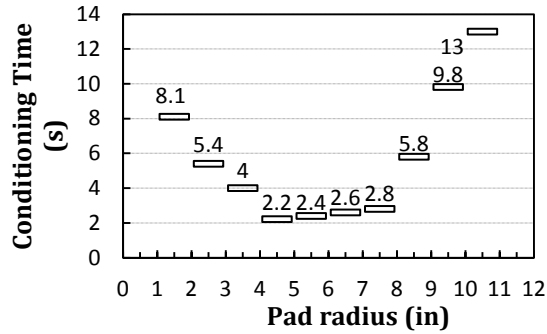


(b) Sectional pad wear

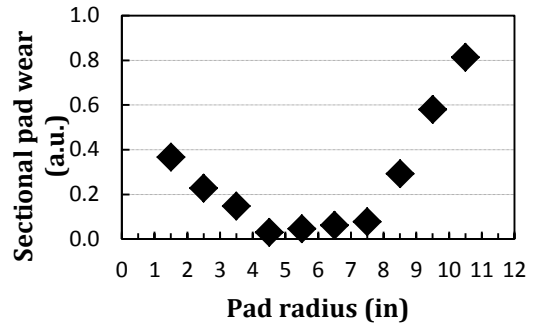


(c) Cumulative pad wear

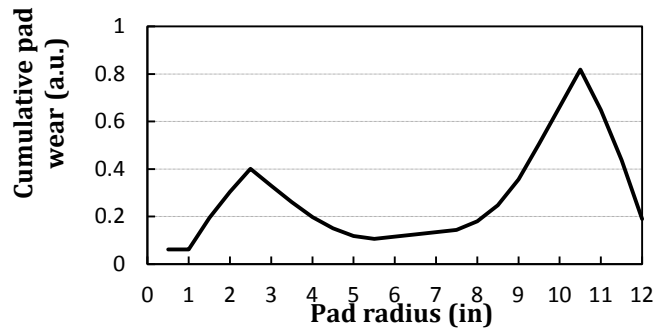
Figure 3.6. Simulation results for sweeping profile FLAT 2.



(a) Sweeping profile



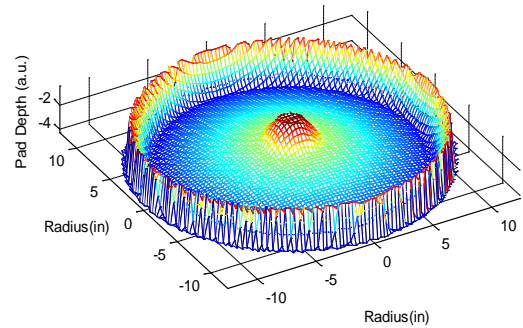
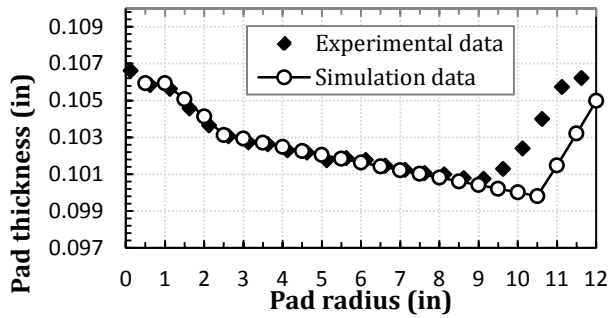
(b) Sectional pad wear



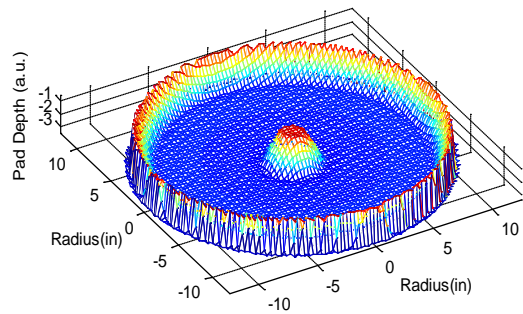
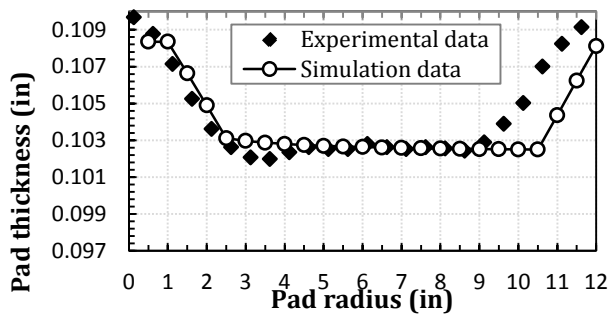
(c) Cumulative pad wear

Figure 3.7. Simulation results for sweeping profile BELL

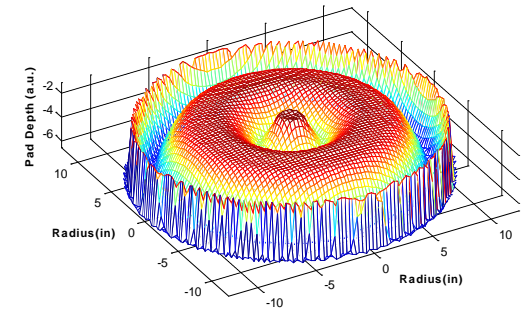
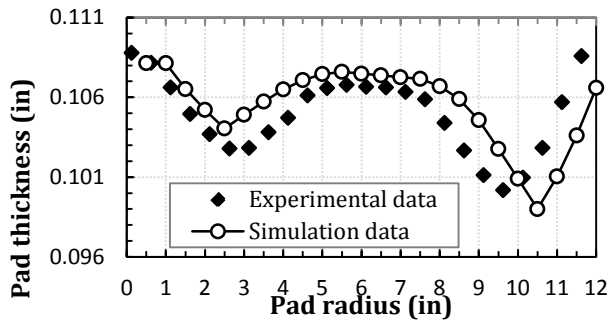
The pad sectional wear is shown in Figure 3.7(b). A nearly constant pad sectional wear can be observed in between a linear decrease wear near the pad center and a sharp increase wear near the pad periphery. The pad cumulative wear shows a saddle-curve as illustrated in Figure 3.7(c). From Figure 3.5 to 3.7, it can be observed that the cumulative pad wear always shows a sharp linear increase near the pad center and a sharp linear decrease near the pad periphery to form transition regions. These transition regions are resulting from overlapped conditioning and can be correlated with the conditioner radius R_c .



(a) FLAT 1



(b) FLAT 2



(c) BELL

Figure 3.8. Simulation results vs. experimental data showing 3-D views of pad surface profiles

The simulation results are then compared with the published experimental data. The constant k in Equations (3.4), (3.16), and (3.17) is estimated empirically by substituting the experimental data into the simulation results using the expression

$k = \Delta h_i A_{p(i)} / Total A_{swept(i)}$. A simple experimental procedure may be used where the outer section (where $i = m$) is polished for a known period, in the absence of the conditioner sweeping motion, such that $Total A_{swept(m)}$ can be easily calculated and actual Δh_m measured afterward. Figure 3.8 shows the comparison between simulation results obtained from the developed model and experimental data reported in published literature. It can be seen that the simulation results agree well with the experimental data. A slight deviation near the pad periphery area may be attributed to conditioning tests setup, pad deformation, and process variations due to polishing wafers.

From Figure 3.8, it also can be observed that the sweeping profile has a great effect on the pad surface profile. Different sweeping profiles will generate significantly different pad surface profiles. For the surface profile in between the pad center and the pad periphery, FLAT 1 generates a negative slope surface profile as shown in Figure 3.8(a), FLAT 2 generates a flat surface profile as shown in Figure 3.8(b), and BELL generates a convex surface profile as shown in Figure 3.8(c).

3.4 Effect of Conditioning Parameters on Pad Surface Profile

3.4.1 Metrics for Pad Surface Profile Evaluation

By utilizing the verified model, the effects of diamond disc conditioning parameters including sweeping profile, pad rotating speed, conditioner rotating speed, and conditioner diameter on the pad surface profile can be further investigated. Three

metrics are proposed to evaluate the flatness characteristics of the pad surface profile. They are Total Thickness Variation (TTV), Bow, and Non-uniformity (NU).

TTV is used to measure the range and extent of pad wear observed due to conditioning. A larger TTV value indicates excessive conditioning or inadequate conditioning in localized area(s) of the pad. It is defined as the difference between the maximum and minimum values of pad thickness for a series of point measurements across the diametrical section of a pad. As illustrated in Figure 3.9(a), TTV is described as:

$$TTV = H_{rpMAX} - H_{rpMIN}. \quad (3.20)$$

Bow is used to measure the concavity of the pad surface profile. A negative value of Bow indicates a convex pad surface profile while a positive value of Bow indicates a concave surface profile. As shown in Figure 3.9(b), Bow is defined as the deviation of the mid radius point of the median surface of the pad from a median surface reference plane. The median surface is the locus of points on the pad equidistant between the pad surface and the platen surface. The reference plane as shown in Figure 3.9(b) is established by three points equally spaced in one half of the pad diametrical section and with equal spaces away from the pad center and edge. In this paper, Bow is described mathematically as:

$$Bow = \frac{1}{2} \left[\frac{(H_{rpL} - H_{rpR})}{2} - H_{rpC} \right]. \quad (3.21)$$

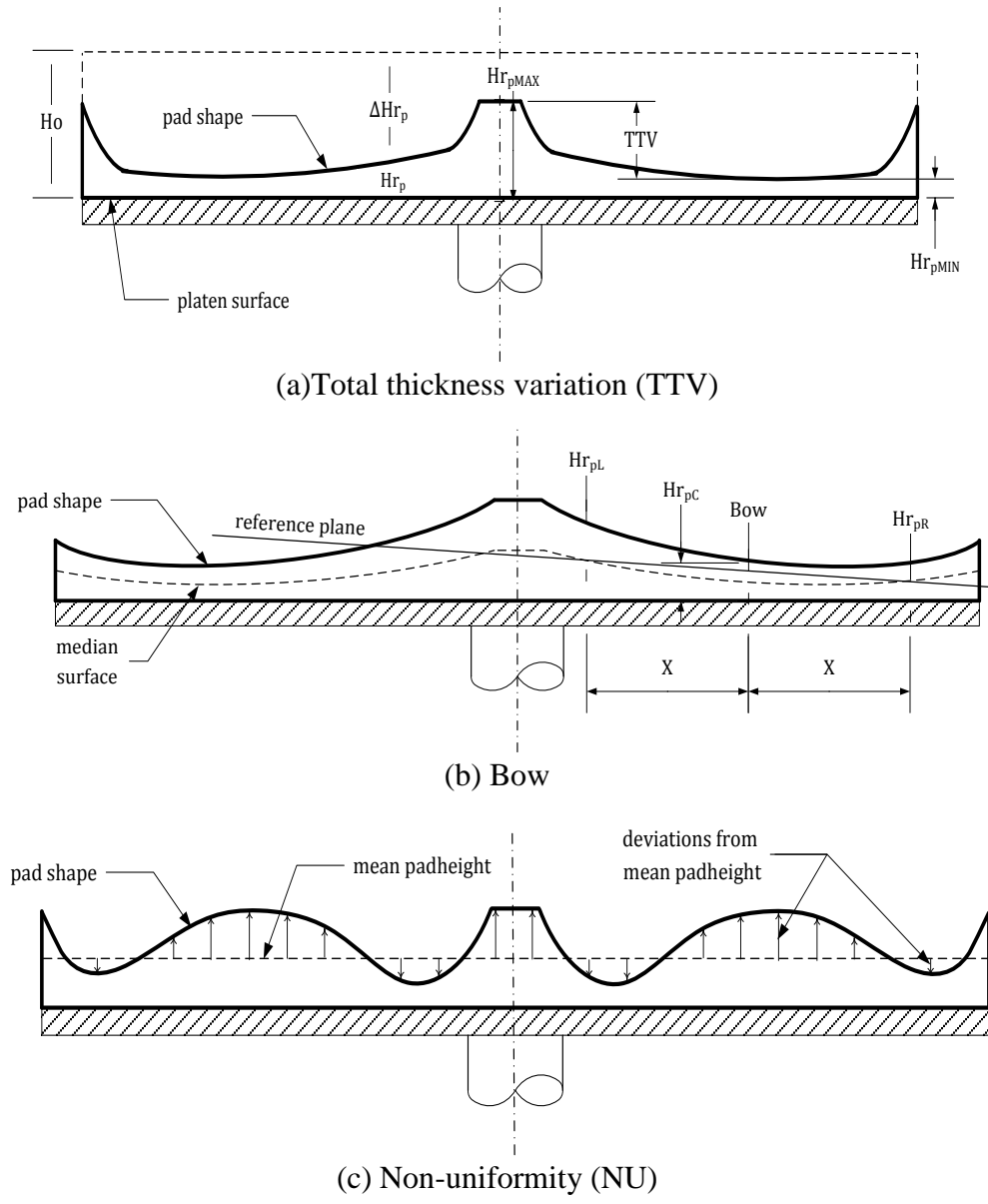
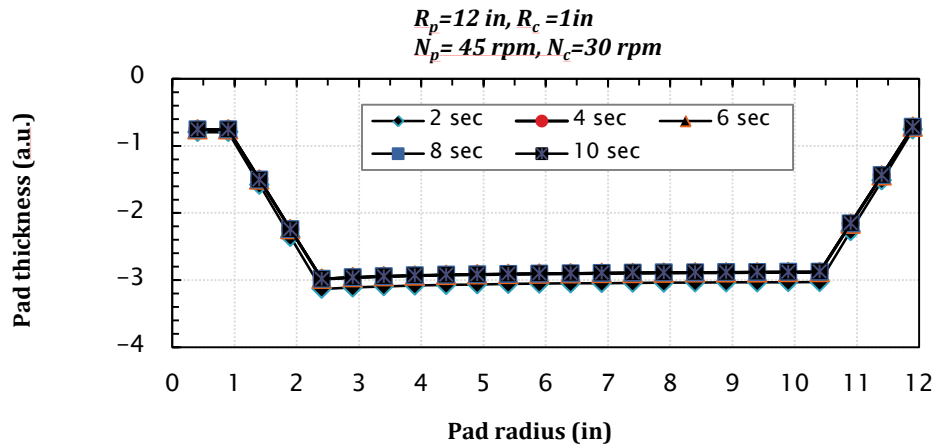


Figure 3.9. Metrics to evaluate the pad surface profile

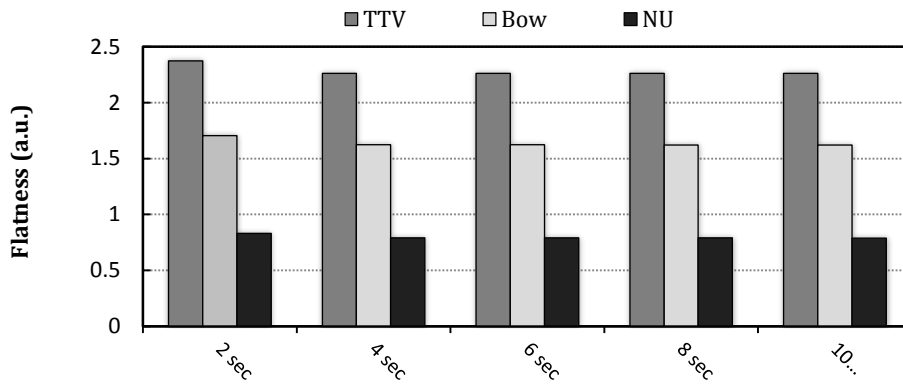
NU is used here to evaluate the waviness of the pad profile. Pad profile non-uniformity is defined as the mean deviation of the series of pad thickness values across the pad diametric section from the mean pad thickness value. The standard deviation of

the thickness values is employed as the measurement of variation. As illustrated in Figure 3.9(c), NU is described mathematically as:

$$NU = \sqrt{\frac{1}{n} \sum_{rp} (H_{rp} - \overline{H_{rp}})^2} \quad (3.22)$$



(a)



(b)

Figure 3.10. Effect of section sweeping time t_i showing (a) pad profile comparison and (b) flatness evaluation

3.4.2 Effect of Section Sweeping Time t_i

Figure 3.10 shows the effect of section sweeping time t_i on TTV, Bow, and NU when the sweeping profile is uniform (i.e. $t_i = \text{constant}, \forall i = 1, 2, \dots, 10$). The section sweeping time t_i is increased from two sec to ten sec whilst the total conditioning time remains constant. In Figure 3.10(a), it can be seen that all the pad surface profiles are overlapped to each other. In Figure 3.10(b), TTV, Bow and NU appear to be constant for all five levels of section sweeping time. Thus, it can be concluded that the section sweeping time t_i does not affect the pad surface profile significantly.

Table 3.3. Sweeping profiles used for pad surface profile simulation

Sweeping profile	Sweeping time for segment i (sec)																			
	1	2	3	4	5	6	7	8	9	10	11	12	13	14	15	16	17	18	19	20
UNIFORM	2	2	2	2	2	2	2	2	2	2	2	2	2	2	2	2	2	2	2	2
CONCAVE	3.76	3.30	2.85	2.43	2.05	1.72	1.44	1.23	1.08	1.01	1.01	1.08	1.23	1.44	1.72	2.05	2.43	2.85	3.30	3.76
CONVEX	0.24	0.70	1.15	1.57	1.95	2.28	2.56	2.77	2.92	2.99	2.99	2.92	2.77	2.56	2.28	1.95	1.57	1.15	0.70	0.24
DESCENT	4	3.8	3.6	3.4	3.2	3	2.8	2.6	2.4	2.2	2	1.8	1.6	1.4	1.2	1	0.8	0.6	0.4	0.2
ASCENT	0.2	0.4	0.6	0.8	1	1.2	1.4	1.6	1.8	2	2.2	2.4	2.6	2.8	3	3.2	3.4	3.6	3.8	4

3.4.3 Effect of Sweeping Profile $\{t_i\}$

Table 3.3 lists five sweeping profiles used to simulate the pad surface profiles. They are UNIFORM, ASCENT, DESCENT, CONVEX, and CONCAVE. In UNIFORM, all pad sections are conditioned equally for 2 sec. In ASCENT, t_i is varied from 0.65 sec to 3.5 sec in increments of 0.15 sec to form a linear diagonal pattern. DESCENT is

obtained by reversing ASCENT. In CONVEX, t_i is varied to achieve a convex pattern. CONCAVE is obtained by inverting CONVEX. From Figure 3.11(a), it can be seen that the sweeping profile shows a significant effect on the pad surface profile. Different sweeping profiles result into significantly different pad surface profiles and the sweeping profile takes a “mirroring” effect on the pad surface profile. In Figure 3.11(b), it can be seen that DESCENT shows the highest TTV whilst CONVEX shows the highest Bow. ASCENT and CONVEX show the highest values of NU. UNIFORM exhibits the best flatness in terms of TTV and NU.

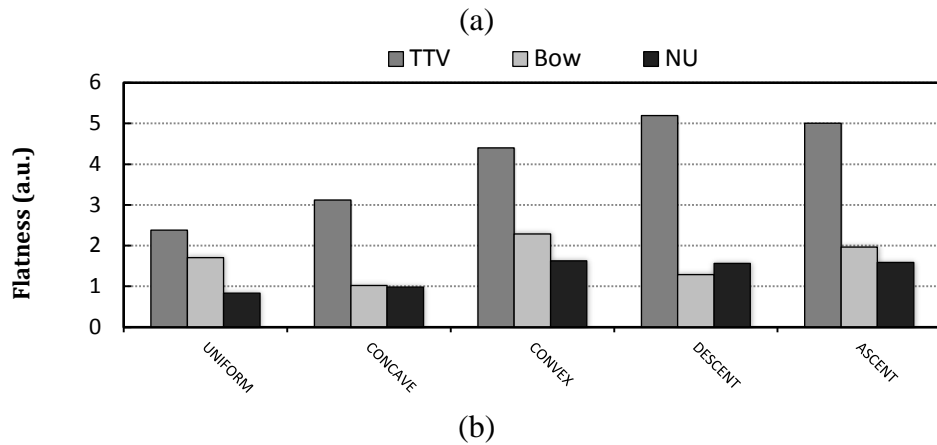
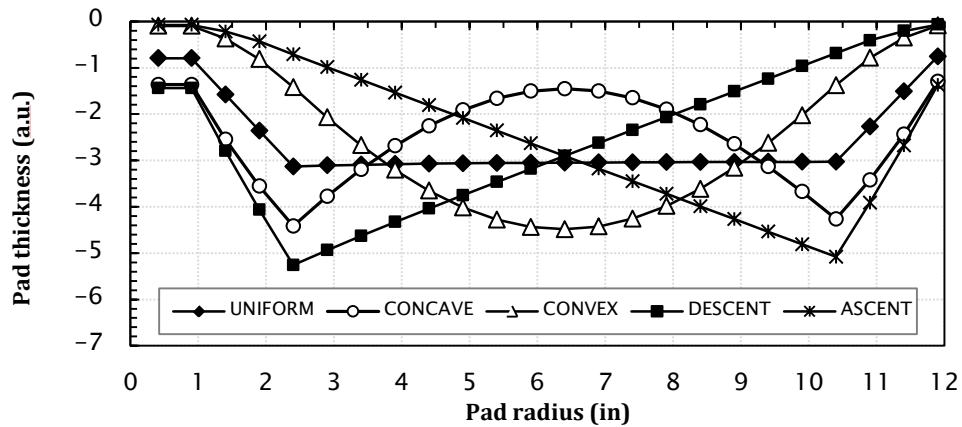


Figure 3.11. Effect of sweeping profile $\{t_i\}$ showing (a) pad profile comparison and (b) flatness evaluation at $R_p=12''$, $R_c=1''$, $N_p=45\text{ rpm}$, $N_c=30\text{ rpm}$

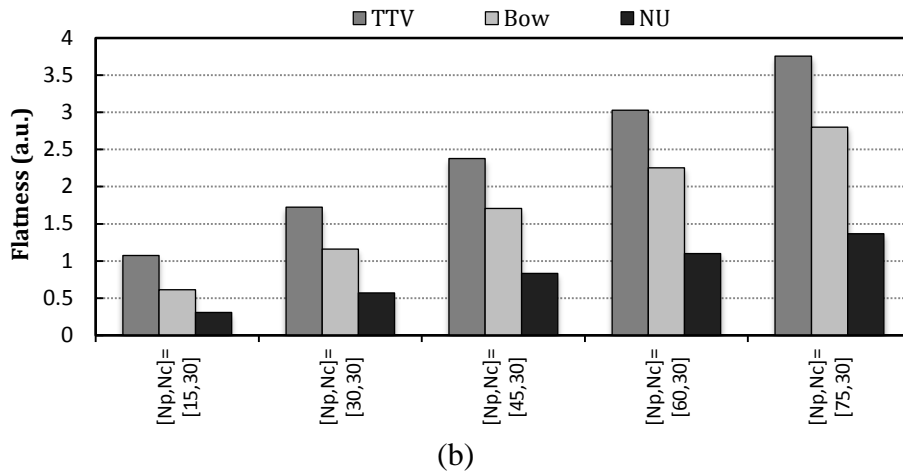
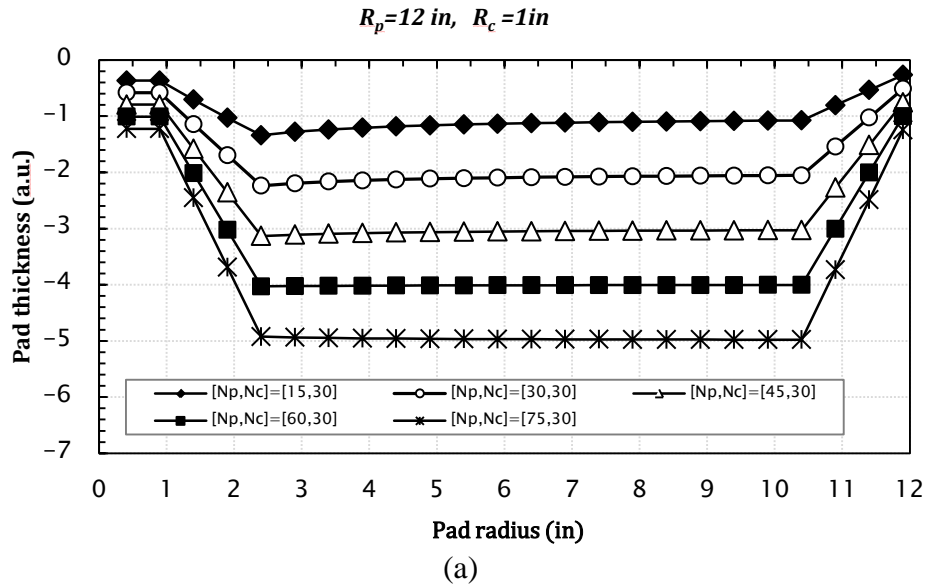


Figure 3.12. Effect of pad rotating speed showing (a) pad profile comparison and (b) flatness evaluation

3.4.4 Effect of Pad Rotating Speed

Figure 3.12(a) shows the simulation results when pad rotating speed is varied while all other parameters are held constant. From the simulation results, it can be seen that there is a significant decrease in pad thickness as the pad rotating speed increases.

This effect can be explained in the following way. Assuming the conditioner is held stationary, increasing the pad rotating speed leads to the increase of contact between the pad surface sections with the diamond disc conditioner. The pad surface profiles resulted from conditioning at various pad rotating speed are evaluated in Figure 3.12(b).

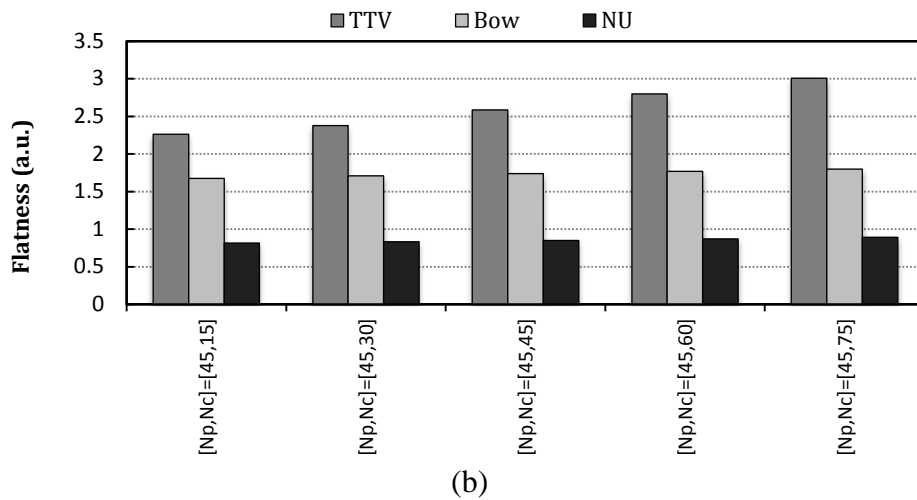
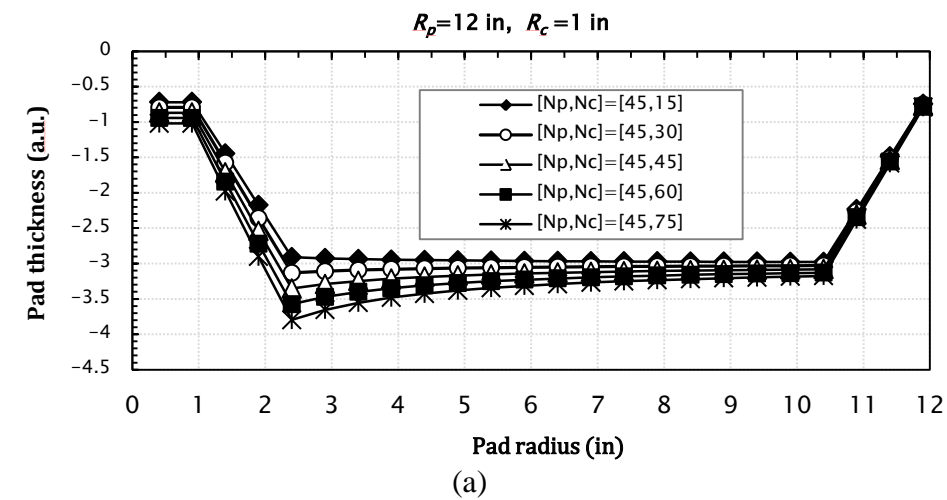


Figure 3.13. Effect of conditioner rotating speed showing (a) pad profile comparison and (b) flatness evaluation

It can be seen that TTV, Bow and NU deteriorate as the pad rotating speed increases. This is a clear indication that conditioning at a lower pad rotating speed is preferred. It can be concluded that higher pad rotating speed generates more pad wear and makes the pad profile more concave and less uniform. However, whilst considering the choice of pad rotating speed, it should be noted that the same operational parameter is directly related to the MRR of the wafer being polished. Therefore a tradeoff has to be made between pad surface characteristics and wafer MRR.

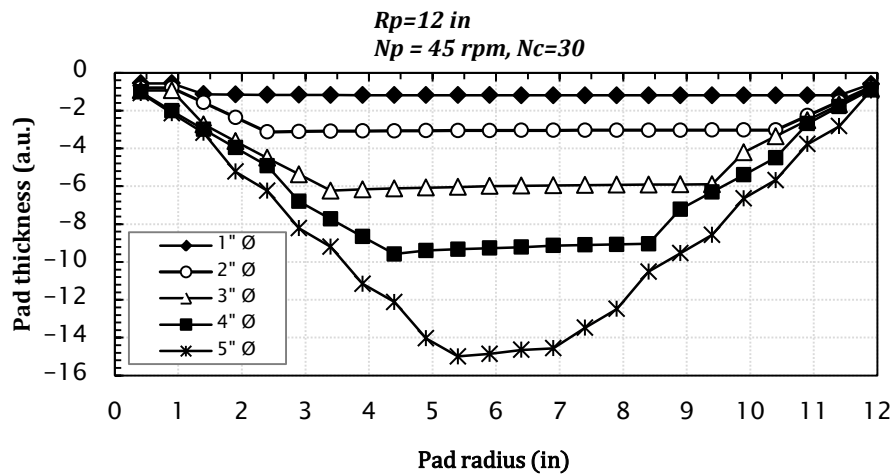
3.4.5 Effect of Conditioner Rotating Speed

Figure 3.13 shows the effect of conditioner rotating speed on the pad surface profile. From Figure 3.13(a), it can be observed that similar pad profiles are generated for five levels of conditioner rotating speed from 15 rpm to 75 rpm. There is a slight increase of pad wear around the pad center area as the conditioner rotating speed increases. In Equation (3.10), the contribution of conditioner rotating speed (ω_c) to the swept distance (Z) is less than the pad rotating speed (ω_p) because the pad always shows a much larger diameter than the conditioner. From Figure 3.13(b), it is easy to observe that TTV increases slightly with the increase of conditioner rotating speed. The conditioner rotating speed does not show a significant effect on Bow and NU.

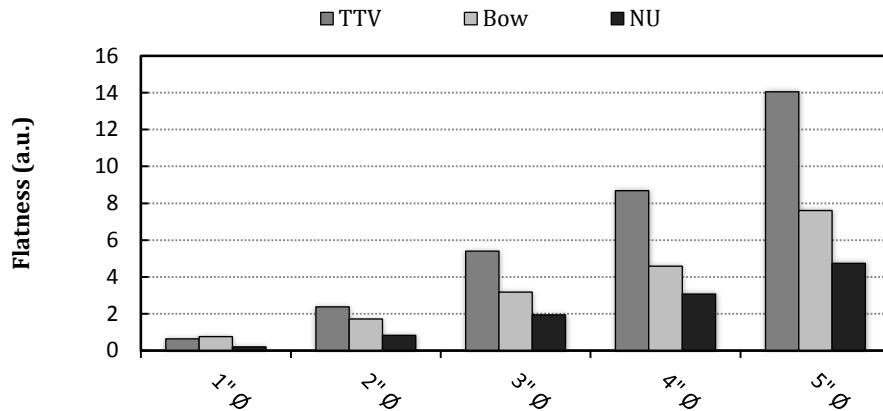
3.4.6 Effect of Conditioner Diameter

Figure 3.14 shows the effect of conditioner diameter on the pad surface profile. It indicates that the amount of pad wear resulted from conditioning increases with the increase of conditioner diameter. The larger the conditioner diameter, the more sections that are in interaction with the abrasive surface and thus the higher cumulative

conditioning times that those sections are conditioned. Figure 3.14(b) indicates that TTV, Bow and NU deteriorate significantly as the conditioner diameter increases. Hence, it can be concluded that a larger conditioner disc size makes the pad more worn, more concave and thus less uniform. Theoretically speaking, a point diamond conditioner would produce the best results but it might be practically unacceptable.



(a)



(b)

Figure 3.14. Effect of conditioner diameter showing (a) pad profile comparison and (b) flatness evaluation

3.5 Conclusions

A surface element model was utilized to develop a mathematical model to predict the pad surface profile resulted from diamond disc conditioning in CMP. The model was utilized to investigate the effect of conditioning parameters on pad surface profile. Three metrics, namely TTV, Bow, and NU, were defined and used to evaluate the pad surface profile characteristics. Major conclusions can be summarized as follows:

- The surface element model is effective to simulate the kinematics of conditioner-pad interaction in diamond disc pad conditioning and accurately predict the pad surface profile. A slight deviation between the simulation results and the experimental data can be attributed to conditioning tests setup, pad deformation and process variations due to polishing wafers.
- There always exist some transition regions in the pad profile near the pad center and the pad periphery. These transition regions show a sharp linear increase towards the pad periphery or a sharp linear decrease away from the pad center. They are resulted from cumulative wear due to overlapped conditioning and can be related to the conditioner radius. When the total conditioning time remains constant, the section sweeping time does not affect the pad surface profile.
- The sweeping profile has a “mirroring” effect on the pad surface profile. Thus the flat sweeping profile gives the flattest pad profile.
- Higher pad rotating speed generates more pad wear and makes the pad surface profile more concave. Thus, conditioning at a lower pad rotating speed is preferred. However, whilst lowering pad velocity for expected improvements, a tradeoff has to

be made between pad surface profile characteristics (TTV, Bow, and NU) and wafer MRR.

- The conditioner rotating speed exhibits a much weaker effect on the pad surface profile than the pad rotating speed.
- The smaller the conditioner diameter, the flatter the pad surface profile. Theoretically speaking, a single point diamond conditioner would produce the most flat surface profile but it might be practically unacceptable.

CHAPTER 4

CONDITIONING DENSITY MODEL

4.1 Introduction

Studies have suggested that the amount of pad wear experienced at a section has a strong correlation with the conditioning density (CD) at that area. (Byrne et al., 1999, Hooper et al., 2002, Hua et al., 2009, Qin et al., 2009, Tsai, 2010a). Initially, Hooper et al.(2002), developed a simple model where CD is determined by the sweeping velocity of the arm V_{arm} , and the radial position on the pad, R_{pad} ($CD = 1/V_{arm} \cdot R_{pad}$). Later, Feng (2007) developed a more elegant kinematic CD function based on the polishing trajectories generated by a conditioner. Feng's CD model was used as a measure of dressing performance and also, by inference, to predict pad wear rate. In the study, it was observed that to have a flat distribution of pad wear rate, the ratio of disk-radius to pad-radius must be as small as possible. Feng concluded that several concerns needed to be investigated further. Among them are; different sweeping motions, non-uniform grit distribution, the assumption of a slow sweeping motion, and ultimately the search for an optimal set of parameters to satisfy a certain criterion. Yeh and Chen (2010) also commented that Feng's model, despite its utility, does not consider the fact that a specific area of the pad may require several "cuttings" to restore it. Thus, Yeh and Chen suggested a modification of the conditioning density definition to include the influence of other related information. In addition, a mathematical relationship between CD and the

pad profile is not mentioned and only numerical examples are provided to verify the model.

With regard to these issues, a conditioning density distribution model was developed to predict the pad surface profile resulting from the diamond disc conditioning in CMP. A kinematic study was carried out to calculate and simulate the diamond grit trajectories. An analytical model was then proposed to correlate the conditioning density distribution with the wear of the polishing pad. In this model, different sweeping motions as well as user defined grit distribution are considered. Furthermore, the pad surface profile is predicted by the model and compared with experimental data.

4.2 Model Development

4.2.1 Assumptions

A typical pad conditioning cycle is illustrated in Figure 3.1. The pad and conditioner rotate about their central axis at angular speeds of ω_p and ω_c respectively. At the start of a conditioning cycle, the rotating conditioner is fed down to the pad from its initial position and pressed against the pad surface under a constant pressure P . The conditioner then moves along the radial direction of the pad at a velocity $v(t)$. As the conditioner touches the pad periphery, it lifts up from the pad surface and moves back to its initial position to repeat next conditioning cycle.

In practice, the travel distance of the conditioner center is divided into m equal sections as shown in Figure 3.1. In the configuration shown in Figure 3.1, $m=10$. The

length of each section is $w = \frac{R_p - 2R_c}{q}$, where R_p is the pad radius and R_c is the conditioner radius. The time it takes for the conditioner to traverse the section k ($k = 1, 2, 3, \dots, m$) is defined as t_k . t_k is equal to $\frac{w}{v}$ and is adjustable. A sequence of t_k which sums up to t_{cycle} is defined as a sweeping profile. The radial distance traveled by the conditioner from the pad center by time t can be obtained as:

$$d = D(t') = L + \int v dt' \quad , \quad \text{where} \quad t' = t(\text{mod}(t_{cycle})). \quad (4.1)$$

Usually, L is set to be equal to the conditioner radius R_c or larger. In the case where L is larger than R_c , the central area of the pad with radius $L - r_c$ will remain unconditioned. In addition, the following assumptions are made.

1. It is assumed that all of the diamond grits embedded on the metal disc protrude with a pyramid shape and have the same protrusion height as shown in Figure 2.2.
2. In the conditioning process, each diamond grit is in continuous contact with the pad and will generate an individual trajectory on the pad surface.
3. The concentration of these trajectories on the pad depicts the conditioning density and then pad material removal due to conditioning is assumed to be directly proportional to the conditioning density.

4.2.2 Model Derivation

The relative velocity between conditioner and pad is represented generally as:

$$\vec{v}_{p/c} = \vec{v}_p - \vec{v}_c = \vec{\omega}_p \times \vec{d} + (\vec{\omega}_p - \vec{\omega}_c) \times \vec{r}. \quad (4.2)$$

Where v_p is pad velocity, v_c is conditioner velocity and r is the radius of a point on the conditioner relative to the conditioner center. Figure 4.1 illustrates the kinematic model to generate the diamond grit trajectories. At an instant of time t in the conditioning session, the position of a diamond grit relative to the pad axes (X_{pad}, Y_{pad}) can be obtained as:

$$\begin{aligned} x = X(t) &= d \cdot \cos(w_p t) + r \cdot \cos((w_p - w_c)t - \theta); \text{ and} \\ y = Y(t) &= d \cdot \sin(w_p t) + r \cdot \sin((w_p - w_c)t - \theta). \end{aligned} \quad (4.3)$$

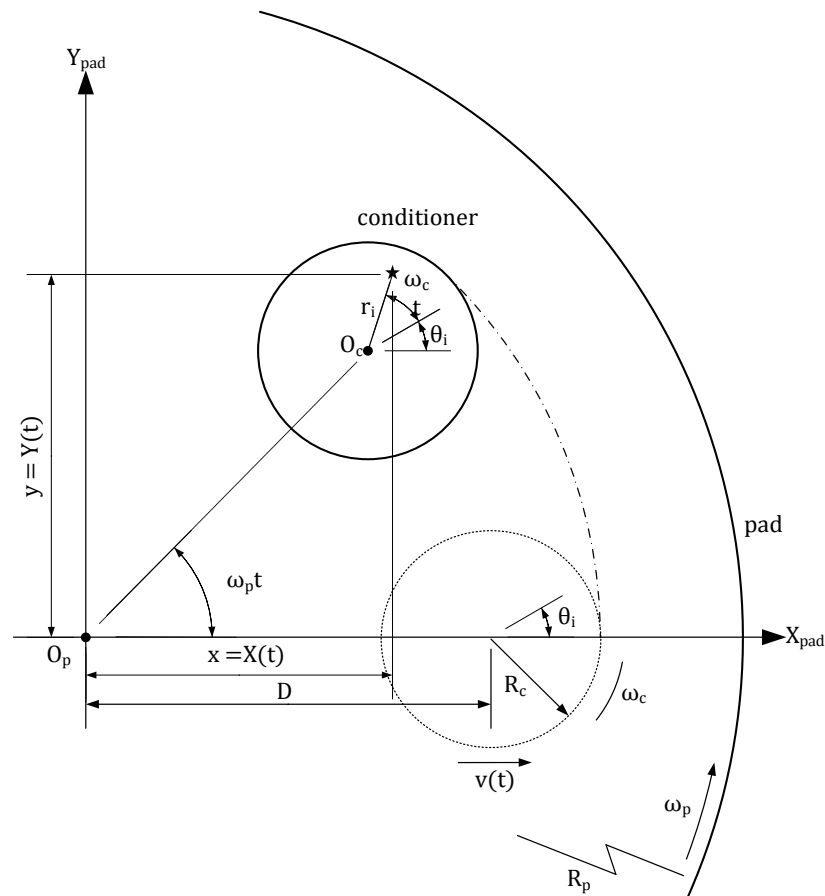


Figure 4.1. Position of diamond grit relative to the pad x-y coordinates

As illustrated in Figure 4.1, (r_i, θ_i) defines the position of the i^{th} diamond grit (out of N_d total diamonds) relative to the conditioner center. For multiple diamonds on the conditioner, the collection of trajectories on the polishing pad is described by:

$$\bigoplus_{i=1}^{N_d} \begin{bmatrix} X(t) \\ Y(t) \end{bmatrix}_i = d \cdot \begin{bmatrix} \cos(w_p t) \\ \sin(w_p t) \end{bmatrix} + \bigoplus_{i=1}^{N_d} r_i \begin{bmatrix} \cos((w_p - w_c)t - \theta_i) \\ \sin((w_p - w_c)t - \theta_i) \end{bmatrix}. \quad (4.4)$$

Equation (4.4) was utilized with Matlab to plot the conditioner trajectories. The parameters are the input variables N_p , N_c , R_p , T , t_{cycle} and the set $[r_i, \theta_i]$ which describes the conditioner diamond grit arrangement. N_p and, N_c , the rotation speeds in rpm for the pad and conditioner were converted to ω_p and ω_c respectively in rad/sec. All length units are in inches and time is in seconds. Figure 4.2 illustrates a typical single diamond grit trajectory over one cycle when the sweeping velocity is constant ($v(t) = 0.1818$ in/s). Figures 4.3 to 4.5 illustrate the trajectories produced for various conditioner diamond arrangements. The trajectory plots reveal that for different diamond arrangements, pad conditioning differs in extent of coverage of conditioner-pad interaction.

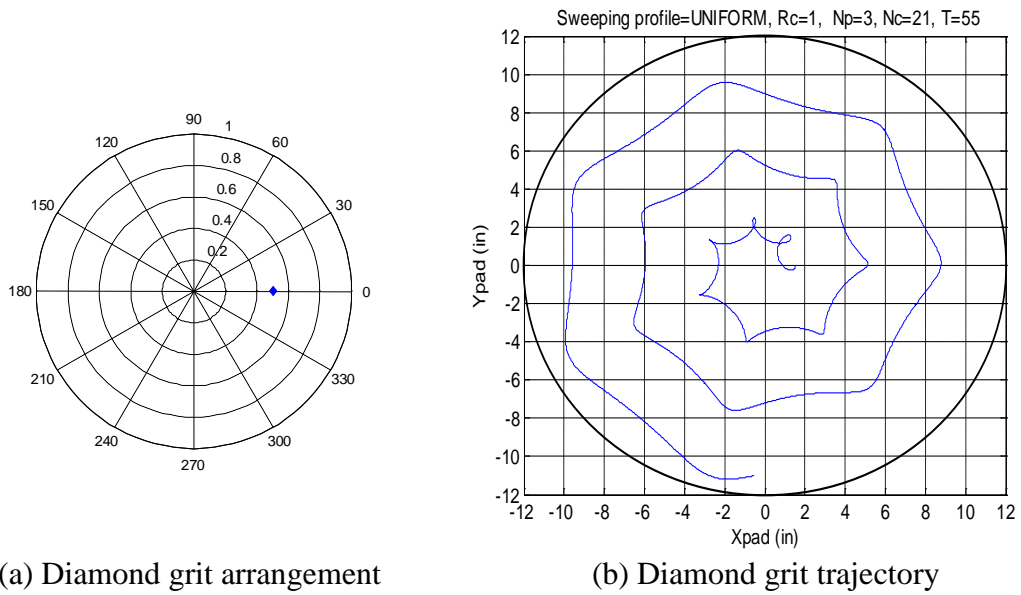


Figure 4.2. Trajectory on pad created by 2'' conditioner with single diamond

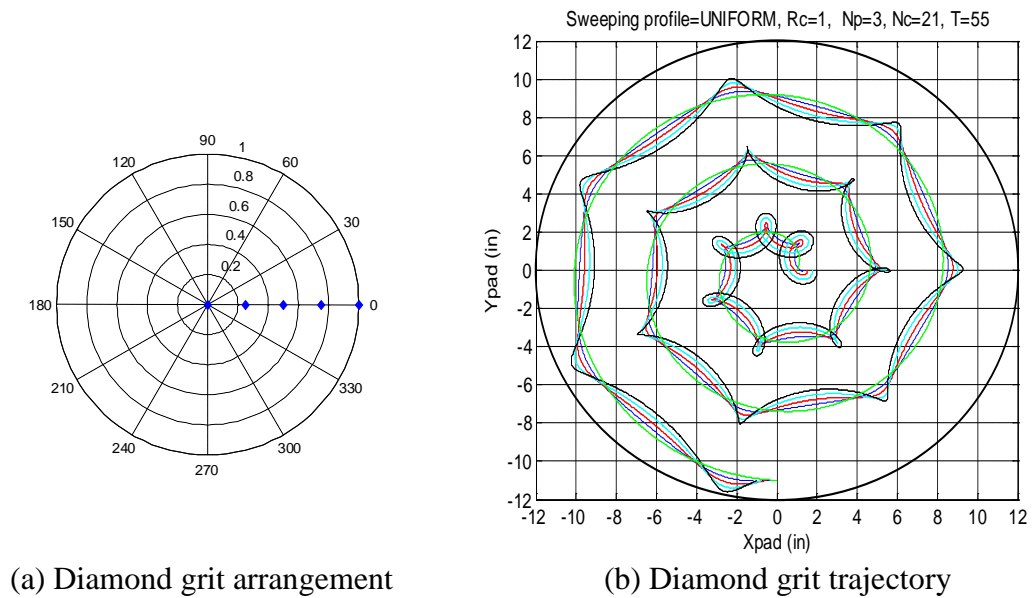


Figure 4.3. Trajectories on pad created by 5 grit/2'' conditioner with radial diamond arrangement

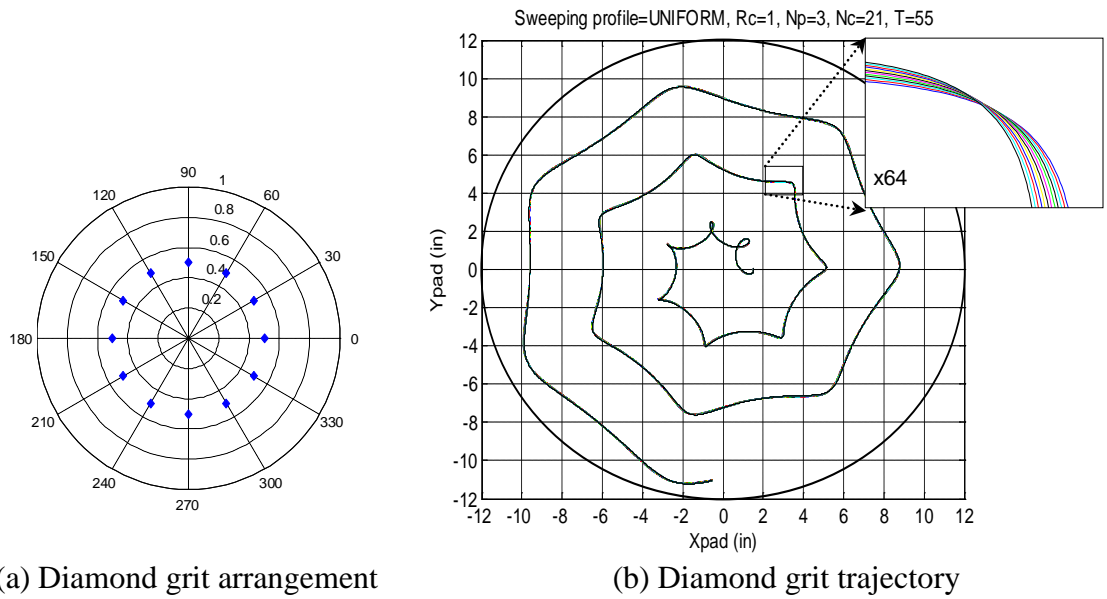


Figure 4.4. Trajectories on pad created by 12 grit/2" conditioner with annular diamond arrangement

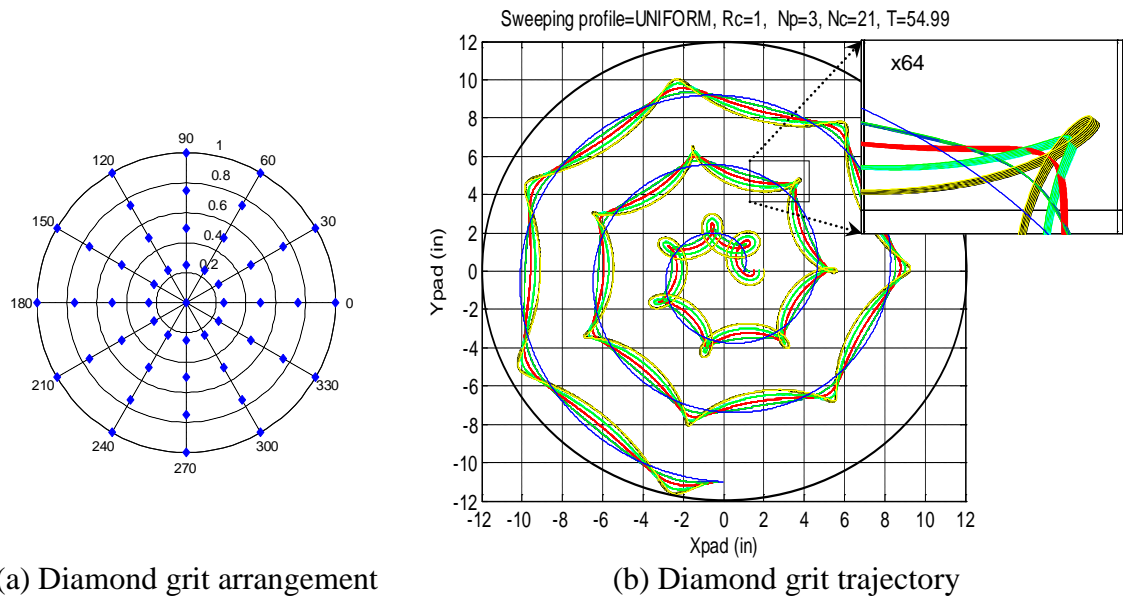


Figure 4.5. Trajectories on pad created by 49 grit/2" conditioner with combined (radial x annular) diamond arrangement

Conditioning density is defined as the average of total trajectory length per unit area in the radial direction (Feng, 2007). Considering an infinitesimal part of the trajectory, the length s of the curve generated within the time interval $[t_i, t_{i+1}]$ can be given as:

$$s = \lim \sum_{t_i}^{t_{i+1}} \sqrt{\Delta x^2 + \Delta y^2}; \quad (4.5)$$

which yields

$$S = \int_{t_i}^{t_{i+1}} \sqrt{[X'(t)]^2 + [Y'(t)]^2} dt. \quad (4.6)$$

Figure 4.6 shows how the trajectory length is measured computationally and how a surface map can be used to account for the conditioner-pad contact distribution. The scratch points indicate positions of diamond grit at specified intervals of time. In this study, the conditioning density is evaluated for a set of annular sections along the radius of the pad. Since the motion of the conditioner is restricted in one radial direction, part of the conditioner trajectory can be considered to fall within a specific section j when t (say t_{rj} and t_{Rj}) is known for the section boundary radii (say r_j and R_j). The length of a diamond grit trajectory traveled between the times that the grit i traverses section j can be determined as:

$$S_{ij} = \int_{t_{r_j}}^{t_{R_j}} \sqrt{[X'(t)]_i^2 + [Y'(t)]_i^2} dt \quad \forall j = (1,2,3 \dots n); \quad (4.7)$$

where

$$R_j = j \frac{R_p}{n} \quad , \quad r_j = (j - 1) \frac{R_p}{n}; \tag{4.8}$$

and

$$t_{R_j} = D^{-1}(d) \Big|_{d=R_j} \quad , \quad t_{r_j} = D^{-1}(d) \Big|_{d=r_j}.$$

Figure 4.7 shows the development of the pad profile from trajectory length. For the entire collection of diamonds on the conditioner, the trajectory distribution is described by:

$$S_j = \sum_{i=1}^{N_d} S_{ij} \quad \forall j = (1,2,3 \dots n). \tag{4.9}$$

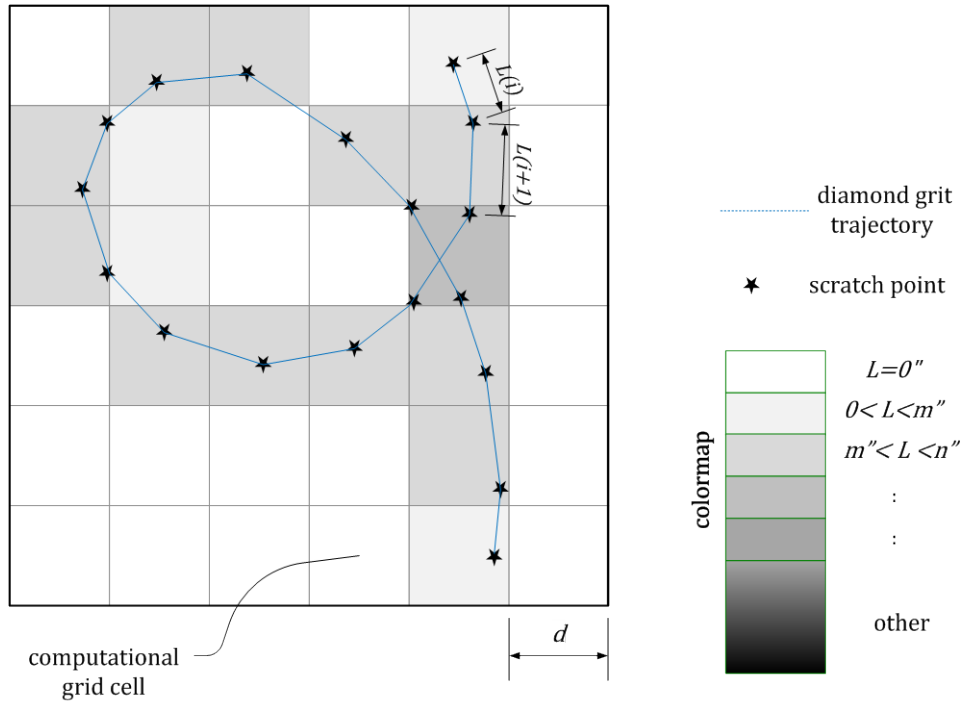


Figure 4.6. Development of surface map from trajectory length per unit area

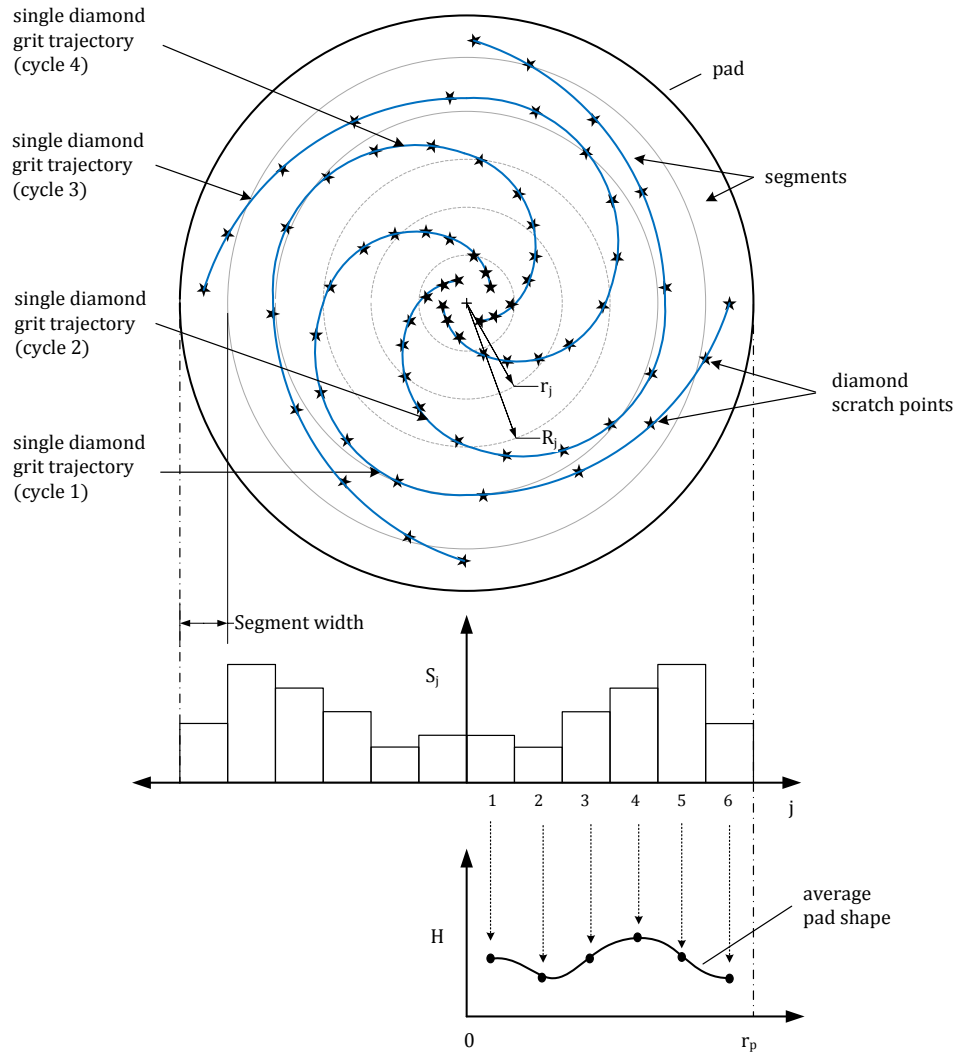


Figure 4.7. Development of pad profile from trajectory length

This distribution does not directly reflect the amount of pad removal since pad wear is affected by the size of the conditioned area. To account for the conditioned area, the average conditioning density CD_j for a specified section j is given as:

$$CD_j = \frac{NS_j}{\pi(R_j^2 - r_j^2)} \quad \forall j = (1,2,3 \dots n); \quad (4.10)$$

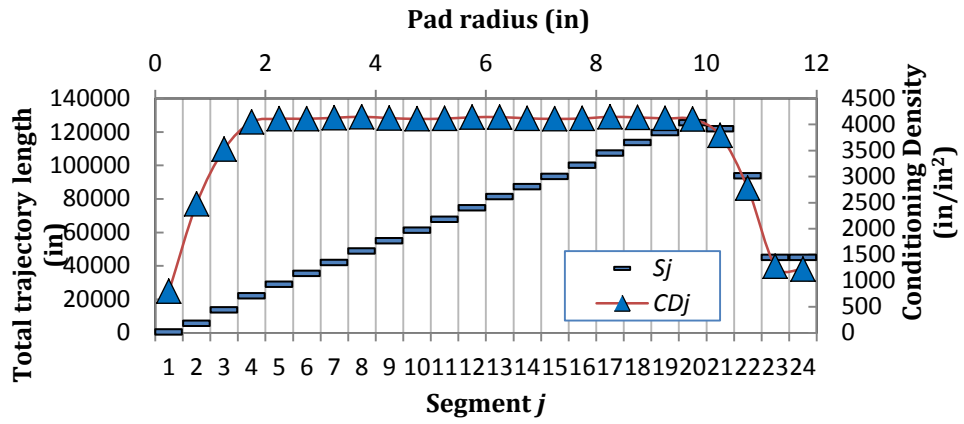
where $N = \frac{T}{t_{cycle}}$ and T = total conditioning time.

Since it is of interest to finally determine the pad profile, conditioning density is computed for the set of n annular sections of equal width. In equation (4.11), these values are then correlated with an average pad wear thickness $\Delta H(r_{pj})$ for corresponding radii r_{pj} of the pad. The description of pad profile development is illustrated in Figure 4.8.

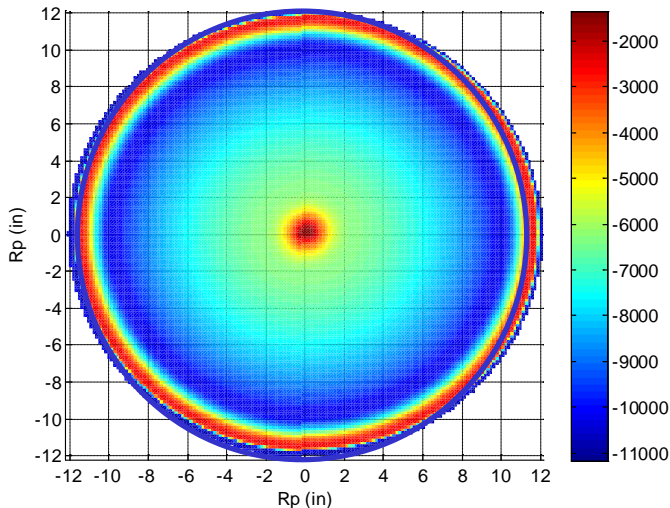
$$\Delta H(r_{pj}) = K \cdot CD_j \quad |r_j < r_{pj} < R_j \quad (4.11)$$

Coefficient K is utilized to account for other process conditions. K involves advanced physics and is reported to be dependent on the pad roughness, asperities, elasticity, surface chemistry and abrasion effects as well as conditioner characteristics (Nanz and Camilletti, 1995). In this study, the value of K is modified by substituting the experimental data into the simulation results. Considering the initial pad thickness H_o , the pad surface profile (pad thickness $H(r_p)$) along the radial direction of the pad can be obtained from the wear prediction in Equation (4.12): The plot of $H(r_p)$ against the pad radius describes one half of the pad profile.

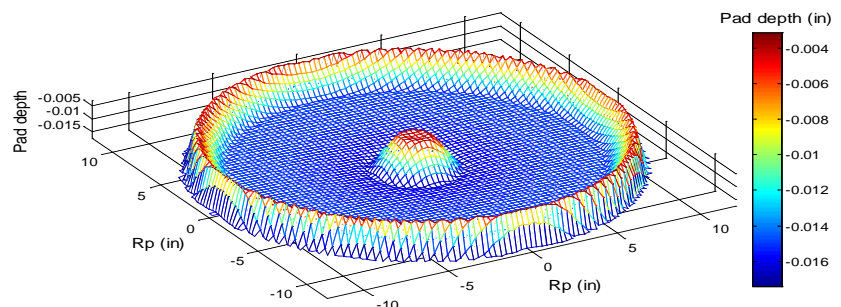
$$H(r_p) = H_o - \Delta H(r_p) \quad (4.12)$$



(a) Section trajectory length and conditioning density



(b) Surface map



(c) 3-D pad profile

Figure 4.8. Simulation results for typical conditioning case (UNIFORM)

4.3 Simulation and Experimental Validation

4.3.1 Simulation Conditions

The Matlab software package was utilized to explore simulation results for major stages in the model development. For a typical conditioning case termed UNIFORM, the parameters are chosen as $N_p=75 \text{ rpm}$, $N_c=70 \text{ rpm}$, $R_p=12''$, $T=660 \text{ s}$, $t_{cycle}=55 \text{ s}$ and $v(t)=0.1818 \text{ in/s}$. A 2'' conditioner with combined (radial x annular) arrangement of 200 diamond grits is used. The pad surface is divided into 24 annular sections.

Figure 4.8(a) shows the distribution of total contact distance S_j of the conditioner and corresponding CD_j on the pad surface. The surface map shown in Figure 4.8(b) reveals the areas where conditioning is more intense. For a UNIFORM conditioner sweeping speed, it is seen that the total contact distance experienced by the conditioner increases for the outer sections. A 3-D view of the pad surface profile for a UNIFORM sweeping profile is shown in Figure 4.8(c). Since the pad conditioner operates on one side of the revolving pad, the pad profile is symmetrical about the pad's axis of rotation. Interestingly, the 3-D view reveals a central bump and an inner surface which is correlated with the sweeping profile bounded by a peripheral wall. It is observed that the size of base of the central bump is related to L .

4.3.2 Simulation Results and Discussion

The model is verified with published experimental data by Freeman and Markert (1996). Three experimental sweeping profiles (FLAT 1, FLAT 2, and BELL) which correspond to three sweeping velocity functions are listed in Table 4.1. FLAT 1 increases

linearly in time from the pad center to the periphery. FLAT 1 is proposed to test a hypothesis that the conditioning time should increase linearly along the pad radius to compensate for the increase of the pad area. FLAT 2 has a constant sweeping profile to test the hypothesis that the pad surface profile is independent of the increase of the pad area along radial direction. BELL is proposed to generate a bell shape sweeping profile by increasing the time at the beginning and the end and reducing the time around the middle.

Table 4.1. Sweeping profiles used for model verification (Adapted from Freeman and Markert, 1996)

<i>Sweeping Profile</i>	$\int vdt$	0"	1"	2"	3"	4"	5"	6"	7"	8"	9"	10"
<i>FLAT 1</i>	$t_k(sec)$	-	4.1	4.0	4.4	4.8	5.2	5.6	6.0	6.4	6.8	7.2
	$\Sigma t_k(sec)$	0	4.1	8.1	12.5	17.3	22.5	28.1	34.1	40.5	47.3	54.5
<i>FLAT 2</i>	$t_k(sec)$	-	5.5	5.5	5.5	5.5	5.5	5.5	5.5	5.5	5.5	5.5
	$\Sigma t_k(sec)$	0	5.5	11.0	16.5	22.0	27.5	33.0	38.5	44.0	49.5	55.0
<i>BELL</i>	$t_k(sec)$	-	8.1	5.4	4.0	2.2	2.4	2.6	2.8	5.8	9.8	13.0
	$\Sigma t_k(sec)$	0	8.1	13.5	17.5	19.7	22.1	24.7	27.5	33.3	43.1	56.1

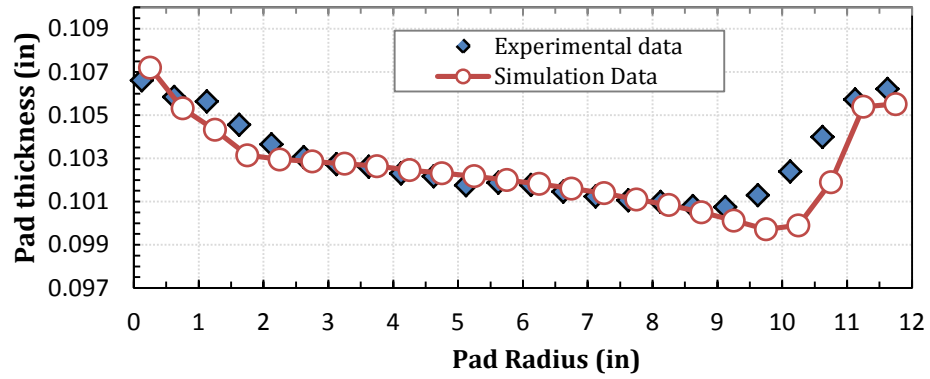
To simulate each sweeping pattern, the relationship between the swept distance $\int vdt$ and cumulative conditioning time Σt_k is fitted with a polynomial curve to derive the respective sweeping distance equations:

$$\int vdt = \begin{cases} 0.1818(t') & \text{for FLAT 2;} \\ -0.0011(t')^2 + 0.2415(t') + 0.1036 & \text{for FLAT 1; and} \\ 6 \times 10^{-6}(t')^4 - 0.0008(t')^3 + 0.0315(t')^2 - 0.1487(t') + 0.1092 & \text{for BELL.} \end{cases} \quad (4.13)$$

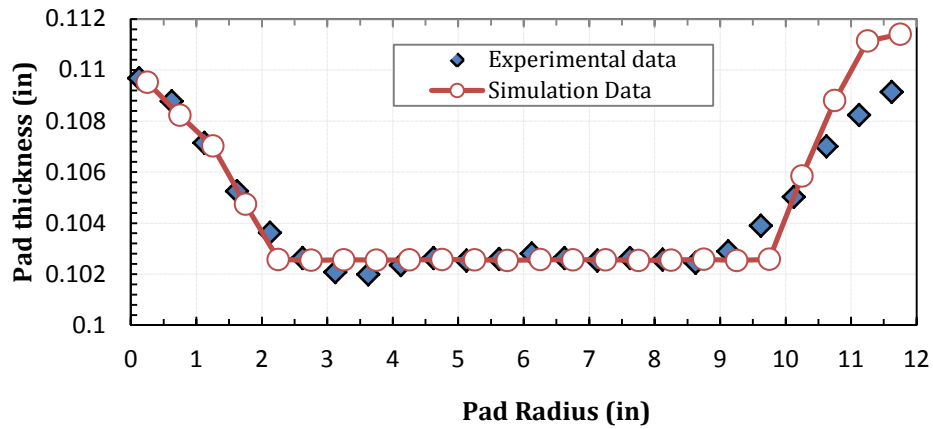
The experimental process parameters are presented in Table 3.1. Figure 4.9 shows the model simulation results overlain with experimental data when the same conditioning parameters are used. For the simulation results of FLAT 1 shown in Figure 4.9(a), a sharp linear increase in pad wear can be observed near the pad center area followed by a slower linear increase and terminated with a sharp linear decrease around the pad periphery area. For FLAT 2 a constant wear can be observed in between a sharp increase wear near the pad center and a sharp decrease wear near the pad periphery as shown in Figure 4.9(b). This confirms the initial hypothesis that the pad surface profile is largely independent of the increase of the pad area along radial direction. In a similar nature the results for BELL, as shown in Figure 4.9(c), reveal a bell-shaped wear profile.

From all three results, it is observed that the pad wear always shows a sharp linear increase near the pad center and a sharp linear decrease near the pad periphery to form transition regions. These transition regions are resulted from the inability of all the diamond grits to have full interaction with the pad during their revolution since the entire diameter of the conditioner does not sweep over the central and peripheral areas.

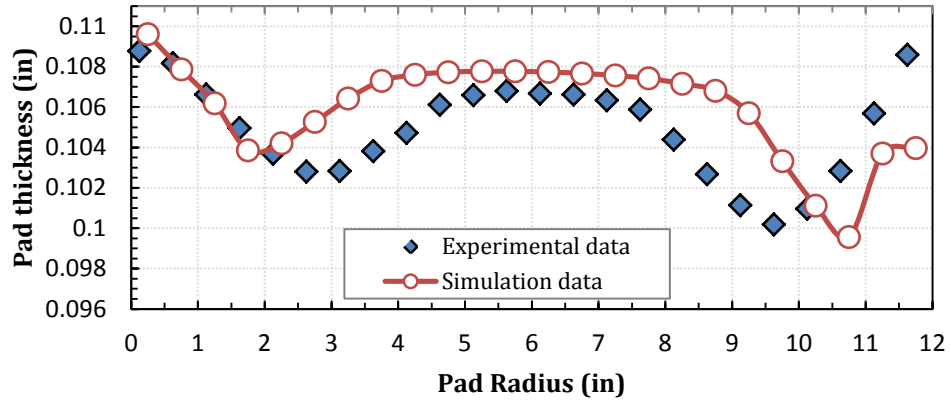
The effect of transition regions could be mitigated by reducing the conditioner disc size, allowing conditioner overhanging and possibly allowing step function modifications to the sweeping profile although further investigation is required. It can be concluded that the sweeping profile has a great effect on the pad surface profile. Different sweeping profiles will generate significantly different pad surface profiles.



(a)FLAT 1



(b)FLAT 2



(c)BELL

Figure 4.9. Simulation results vs. experimental results of three sweeping profiles

The good agreement between the simulation results and published experimental data indicates that the model developed from the conditioning density can be used to accurately predict pad surface profile resulted from diamond disc conditioning. The slight deviations observed in the comparison can be attributed to the sweeping pattern approximation and experimental conditions such as conditioning tests setup, pad deformation, and process variations due to polishing wafers.

4.4 Conclusions

An analytic model was utilized to predict the pad surface profile from the area density of conditioner-pad interaction given the sweeping profile (defined by a function), conditioner disc design and process kinematic parameters. A surface map was utilized to account for the trajectory length per unit area as a visual measure of conditioner-pad contact distribution. Major conclusions can be summarized as follows.

- The developed model was able to simulate the kinematics of diamond disc pad conditioning and accurately predict the pad surface profile.
- The model was able to account for specific conditioner diamond grit arrangement (regular/random/annular/full/etc). It was observed that under different diamond grit arrangements, the actual conditioner-pad interaction is different in terms of surface coverage.

- By investigating three sweeping profiles, it was confirmed that the sweeping profile has a strong effect on the pad surface profile and the pad profile is largely independent of the increase of the pad area along radial direction.
- There always exist some transition regions near the pad center and the pad periphery. These transition regions show either a sharp linear decrease or a sharp linear increase pad thickness. These transition regions are resulted from the inability of all the diamond grits to have full interaction with the pad during touchdown and lift off stages of the conditioning cycle. This could be mitigated by reducing the conditioner disc size, allowing conditioner overhanging and possibly allowing step function modifications to the sweeping profile.

CHAPTER 5

2-D MORPHOLOGY AND FINITE ELEMENT ANALYSIS OF PAD

5.1 Introduction

The polishing pad plays a primary role in the CMP process. The pad transports slurry to the wafer surface and also transmits normal and shear forces from the polisher to the wafer (Li, 2008). During the conditioning process, the rotating conditioner is fed down to the pad from an overhead position and pressed against the pad surface under a predetermined down force. At this point, local compression is introduced on the pad surface resulting in deformation. The pad's mechanical response (such as pad deformation, wear, stress and strain) to polishing and conditioning forces is crucial to the fundamental understanding of the material removal mechanism of CMP. Mechanical properties (composite modulus and hardness), liquid permeability and surface roughness of CMP pads are highly related to the foam morphology (Cook, 1999).

Despite the advancement of experimental and theoretical studies on diamond disc pad conditioning, there are only few published reports about the effect of conditioning on the pad deformation. Horng (2003) developed pad deformation equations for conditioning using Hertzian contact theorem and principle of elasticity. A set of CMP investigators have used the FEA approach to model the interactions between the pad, wafer and abrasive particles to predict wafer MRR (Bozkaya and Muftu, 2009), WIWNU (Lee et al., 2004, Lin et al., 2008), wafer flatness (Zhang et al., 2005), pad surface asperities (Jiang and Muldowney, 2007) and pad wear (Li et al., 2010). This powerful

computational approach allows for complex geometries and more detailed representation of physical characteristics and mechanics of the process components in the model. However, none of the available FEA modeling reports considers pad conditioning and its effects on the CMP process.

To model the CMP pad more accurately, its internal microstructure needs to be understood. This has called for studies into the morphological and mechanical properties of CMP pads. Several methods (Sexton, 2009, Ridha, 2007, Choi et al., 2011, Centeno et al., 2005, Machinski et al., 2001) have been used to examine the surface and internal structure of foam/porous media. CMP pad images have been analyzed using statistical design analysis (Centeno et al., 2005), attenuated total reflectance fourier transform infrared (ATR/FTIR) (Lu et al., 2002) and spectrometry (Machinski et al., 2001) to characterize the surface of CMP pads. However, most of these approaches are expensive and intricate. Moreover, a detailed study on the characterization of the internal morphology of CMP pads is still lacking.

In this chapter a two-dimensional (2-D) image processing procedure is proposed for the characterization of morphological and mechanical properties of CMP pads. First, assumptions are drawn, characterization parameters are defined and the procedure is described. The procedure is utilized to characterize a chosen CMP pad. Characterization data is incorporated into an FEA model to investigate the mechanical behavior of CMP pads with enhanced fidelity. A 2-D axisymmetric quasi-static FEA model is proposed to investigate the interaction between the diamond disc conditioner and the polishing pad for the first time. The FEA model is developed and utilized in the ANSYS (ANSYS Inc.,

275 Technology Drive, Canonsburg, PA 15317, USA) simulation software to study the effects of some process parameters on the pad deformation.

5.2 Image Processing

A typical CMP pad consists of two stacked components; (1) a rigid top-pad with its upper surface in contact with the wafer and bottom surface adhered to (2) a resilient soft base termed the sub-pad (Wang et al., 2008). The IC1000 and IC1400 pad are the most common CMP pads in industry today (Wang et al., 2008) and have been studied more than any other CMP pad type. With the IC1400, the top pad is a microporous filled cast polyurethane material IC1000 polymer (Doering and Nishi, 2008). The IC1000 layer has a closed cell structure with hollow spherical micropores. The sub pad is of buffed high density urethane foam (Rodel, 2001) with a closed-cell foam structure (DeNardis et al., 2006). An assumption of spherical micropores is considered valid under two conditions: (1) if the pad is unused and, (2) if the pad slice to obtain the cross section image is undeformed and obtained using a vertical plane. It is also necessary to assume that the solid (cast urethane polymer) matrix of the foam is homogenous. Figure 5.1 shows a flowchart for the logical description of the image processing procedure beginning from reading the acquired pad cross-section image to characterization results.

With good segmentation of 2-D slice images, accurate image data can be retrieved and reliable characterization can be attained. This begins by converting a gray-scale image into a binary image using the conventional thresholding method.

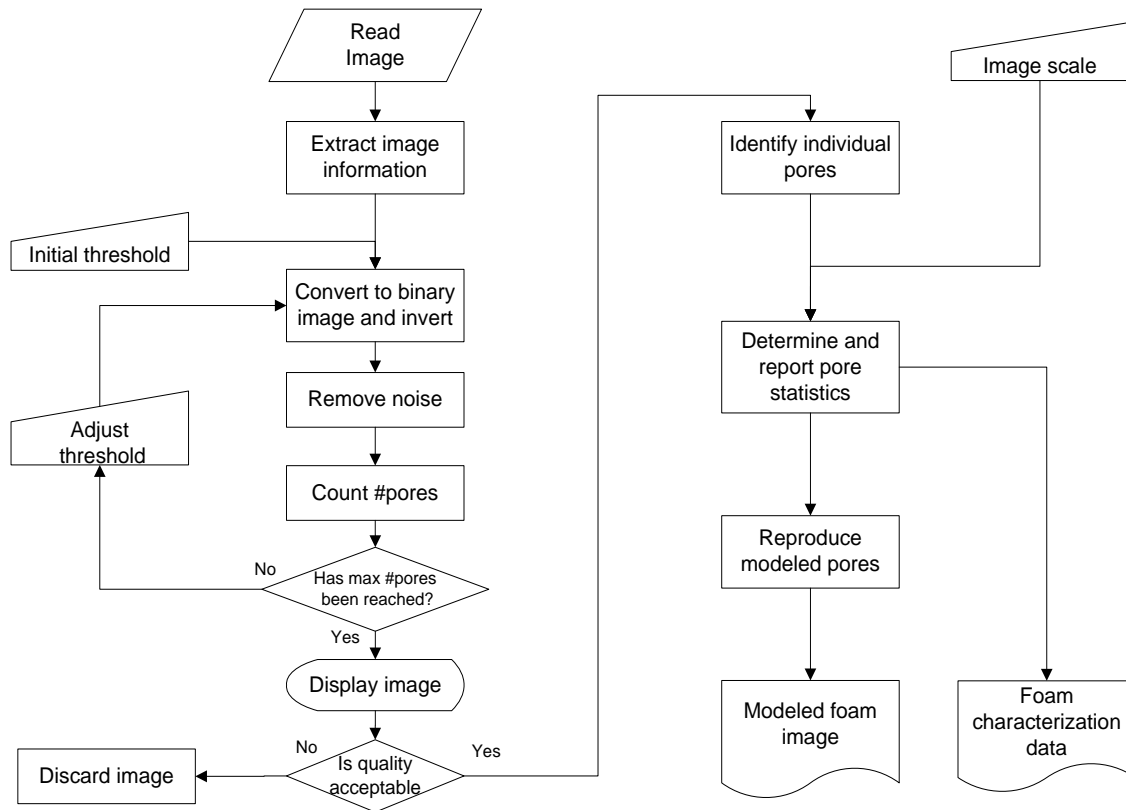
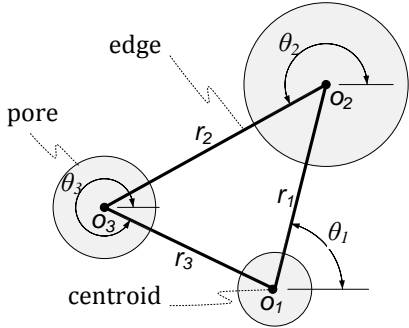


Figure 5.1. Image processing procedure

The 8-connected neighborhood criteria (Chugh, 2010) is used to determine connected pixels and subsequently to identify and label all individual components in the image. Shape measurements such as area (a_i), centroid (o_i), equivalent diameter (d_i) and perimeter (p_i) of all n components are computed. With this data, values of morphological characterization parameters can be extracted. Table. 5.1 lists and defines the parameters chosen to characterize the morphology of the pad. The eccentricity for each pore is measured. The average value assists in accessing the validity of the assumption of spherical pores. The mean, median and standard deviation of the pore size

also provide a general description of the pore geometry. From observation of several fitted pore data, the statistical distribution of the pore size is appropriately described by a lognormal distribution.

Table 5.1. Pad morphological parameters

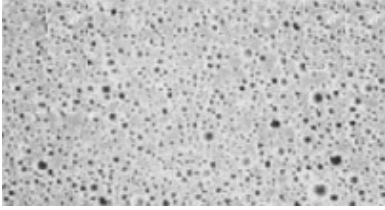
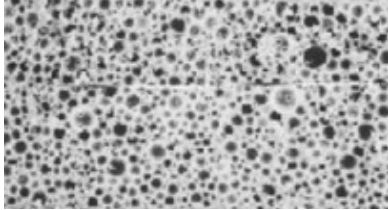
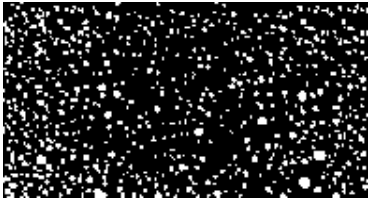
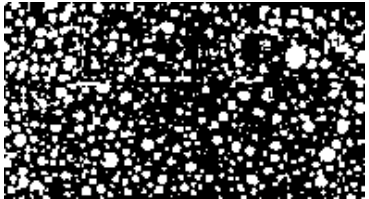
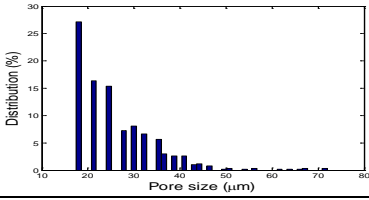
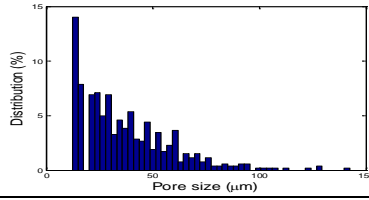
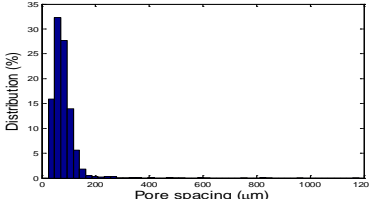
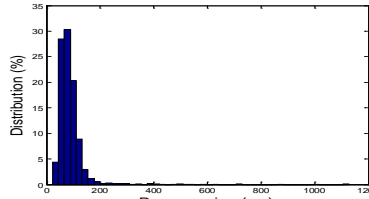
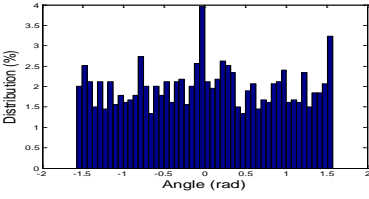
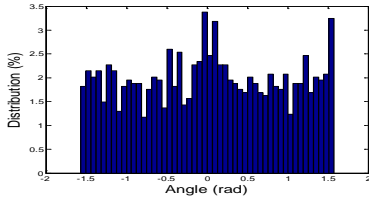
Parameter	Definition
<i>Eccentricity</i>	The ratio \mathcal{E} of the distance between the foci of the ellipse (that has the same second-moments as the pore component) and its major axis length. The value is between 0 (for a circle) and 1 (for a line segment).
Pore size	<i>Mean</i> Mean pore diameter given by: $\mu_d = \frac{S \cdot \sum_{i=1}^n d_i}{n}$; where S is the scale (μm /pixel).
	<i>Median(μm)</i> Median pore diameter given by: $\tilde{d} = S \cdot \text{median} \{d_i\}$.
	<i>Distribution</i> Probability distribution of pad pore diameter fitted with a log-normal distribution specified by mean μ_2 and standard deviation σ .
<i>Pore linear spacing (μm)</i>	Distance r_i between pore centroid and centroid of closest neighbors (lengths of edges of Delaunay triangulation). A log-normal distribution is adapted for r_i . <div style="text-align: right;">  </div>
<i>Pore angular spacing (rad)</i>	The angle θ_i that an edge connecting two pore centroids makes with the horizontal.
<i>Pore density (void fraction)</i>	Ratio of the area of void-space (pores) and the total or bulk area of the pad (including the matrix and pore components) given by: $\phi = \frac{\sum_{i=1}^n a_i}{lh}$; where l and h are the length and height of the image respectively.

The x and y values of the component centroid define the position of the pores distributed within the pad polymer matrix. The pore centroid distribution provides a general description of the pore formation. To adequately model the structure of the foam, it is important to understand the morphological relationship between pores.

Delaunay's approach is adapted to characterize this relationship. Given the set of pore centers, the Delaunay triangulation generates a set of lines connecting each pore to its natural neighbors. These lines form a set of triangles such that no data points (pore centers) are contained in any triangle's circumscribed circle. The set of triangle edge lengths is used to infer the pore spacing distribution and homogeneity.

SEM images of IC1400 (top-pad and sub-pad) were obtained from published sources (Shown in Table 5.2) and prepared for processing. The preparation involved removal of image boundaries and non-foam features (such as scale bar, etc) followed by enhancement of the contrast and brightness. The scale of each image was determined manually by using the image processing toolkit ImageJ (National Institutes of Health, USA). The computations described in the image processing procedure were carried out using the Matlab Image Processing toolbox.

Table 5.2. Image processing results

<i>Pad Type</i>	IC 1400 Top-pad	IC 1400 Sub-pad
<i>Original Image</i>		
<i>Source</i>	DeNardis et al. (2006)	DeNardis et al. (2006)
<i>Binarized and filtered image</i>		
<i>Distr. of pore sizes</i>		
<i>Pore morphological relationship</i>		
	<i>Distribution of pore linear spacing</i>	
		
<i>Distribution of pore angular spacing</i>		
\mathcal{E}	0.68	0.55
μ_1 (μm)	26.5	37.5
\tilde{d} (μm)	24.7	32.7
<i>Distr. of d [$\mu\text{m}, \mu\text{m}$]</i>	Lognormal [3.2256,0.311]	Lognormal [3.463,0.577]
<i>Distr. of r [$\mu\text{m}, \mu\text{m}$]</i>	Lognormal [4.2893,0.4421]	Lognormal [4.388,0.428]
<i>Distr. of θ [rad,rad]</i>	Uniform $[-\pi/2, -\pi/2]$	Uniform $[-\pi/2, -\pi/2]$
ϕ	0.1427	0.2889

5.3 Characterization Results

Table. 5.2 shows the results for the characterization of IC1400. In the binarized and filtered image, white pores are shown against a black background of the polymer matrix. A histogram of the pore size d corroborates that the distribution of the pore size follows a lognormal distribution. Similarly, pore linear spacing r follows a lognormal distribution. However, the pore angular spacing θ is better described by a uniform distribution (except a slight spike in 0° and 90° neighbours). The eccentricity values being less than 0.68 indicate that the characterized pores are fairly circular. It is expected that higher resolution images will provide better eccentricity values.

A visual comparison of the top-pad and sub-pad (from both Table. 5.2 and Figure 5.2) shows that the sub-pad is more porous than the top-pad (DeNardis et al., 2006). This is confirmed by the higher ϕ value for the IC1400 sub-pad. In Figure 5.2, the geometrical model of the cross section of the characterized pads is shown overlain with a Delaunay triangulation connecting all the centers of the circular pores. The geometrical model provides a close representation of the actual pad morphology (including the shape, size and position of pad pores within the polymer matrix) required for the finite element model.

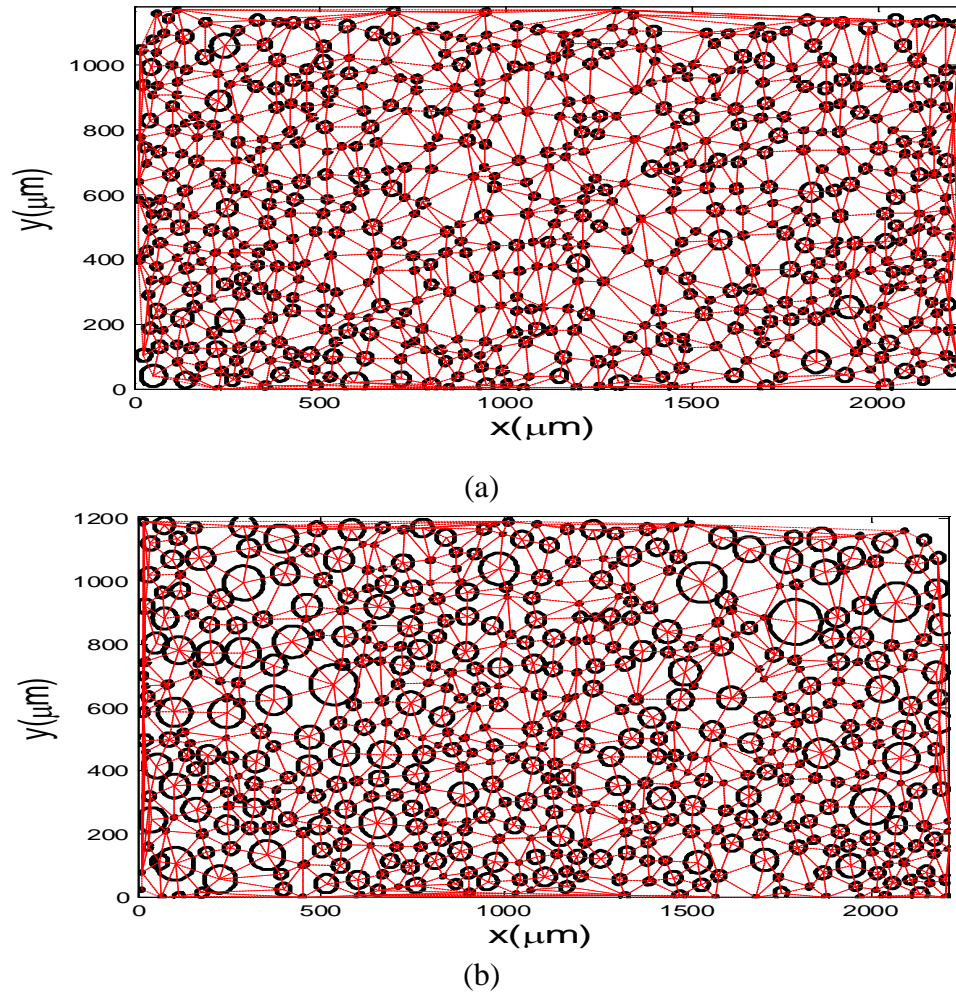


Figure 5.2. Geometric model of IC1400 (a) top-pad and (b) sub-pad cross sections overlain with corresponding Delaunay triangulations

5.4 FE Model Development

5.4.1 Assumptions

The pad is modeled as a solid block impregnated with circular holes to represent the foam microstructure. Here, the effect of the gas trapped in the pores is ignored. The

pad block is in contact with a conditioner block. Stresses on the pad surface arise mainly from two sources; (1) down pressure from the conditioner head and (2) shear forces due to the relative motion of the conditioner and pad. For simplicity, the contact surface between the conditioner and pad can be considered as a smooth plane. Then a uniformly distributed normal pressure acts on the head of the conditioner block. Sliding contact between the conditioner and pad causes a traction force which can be correlated to the relative velocity between the conditioner and pad. This can be ignored if the pad and conditioner rotating speeds are similar. With the given configuration, static equilibrium is necessitated to solve the deformation equations. A quasi-static simulation is thus employed. Considering symmetry of pad profile and quasi-static conditions, loading can be assumed to be axisymmetrically distributed. In this model, the pad and the conditioner are assumed to be free from internal forces prior to the application of loads.

5.4.2 Model Parameters

Geometric and material properties of interest include the elastic modulus of the foam matrix, poisson ratio, pad thickness and porosity. Due to the considerable anisotropic properties of the pad and difficulty in obtaining consistent data, the model parameters are chosen based on empirical relations and the image processing results. First, the matrix of the pad is assumed to possess isotropic mechanical properties. To avoid convergence errors, a Poisson's ratio of $\nu = 0.35$ is chosen as a compromise to a value near 0.5 for polyurethane elastomers. For the conditioner, $\nu = 0.3$.

There are several differing reports on the Young's modulus E of the IC1400 pad (ranging from 4Mpa to 350Mpa). This is probably due to anisotropy of the pad, diverse

testing methods/conditions or reference to other elastic moduli. However, reports on the hardness of the pad are consistent. Thus, in this study, E is derived from knowledge of the pad's shore hardness. Qi et al. (2003) stated that a linear relation between the Shore hardness and the logarithm of E is applicable over a large range of Shore A and Shore D hardnesses for elastomeric materials. The relation is given as:

$$\log_{10} E = 0.0235 \cdot S - 0.6403; S = \begin{cases} S_A & \text{for } 20 < S_A < 80 \\ S_D & \text{for } 30 < S_D < 85 \end{cases}; \quad (5.1)$$

where S_A is the Shore A hardness and S_D is the Shore D hardness. Provided with the average IC1000 S_D of 57 (Rohm&Haas, 2004), E of the bulk top-pad is determined to be approximately 75 Mpa. The subpad can have a Shore A hardness between 35 to 50 (Prasad, 2007). Thus, E of the bulk subpad is determined to be approximately 2.3 Mpa.

Since the pad is modeled with consideration of the internal microstructure, E_0 is assigned to the pad polymer matrix only and not the bulk pad. Hence, a correlation between ϕ , E_0 and E is necessary. Based on a large number of experimental observations of pore deformation, Lu et al. (Lu et al., 1999) developed a simple model to correlate the macro-properties of porous materials from the micromechanics viewpoint. The bulk elastic modulus, E , for high values of porosity such as for foams is given as:

$$E = E_0(1 - \phi)^2; \quad (5.2)$$

where E_0 is the elastic modulus when the porosity ϕ is zero. Figure 5.3 shows the determination of the E_0 of the pad matrix polymer. Considering an IC1400 top-pad with $E = 75$ Mpa at $\phi = 0.35$, E_0 of the modeled top-pad is obtained to be 130 Mpa at $\phi =$

0.1427 and 177 Mpa at $\phi = 0$. Considering a subpad with $E = 2.3$ Mpa at $\phi = 0.5$, E_0 of the modeled sub-pad is obtained to be 4.7 Mpa at $\phi = 0.2889$ and 9.3 Mpa at $\phi = 0$.

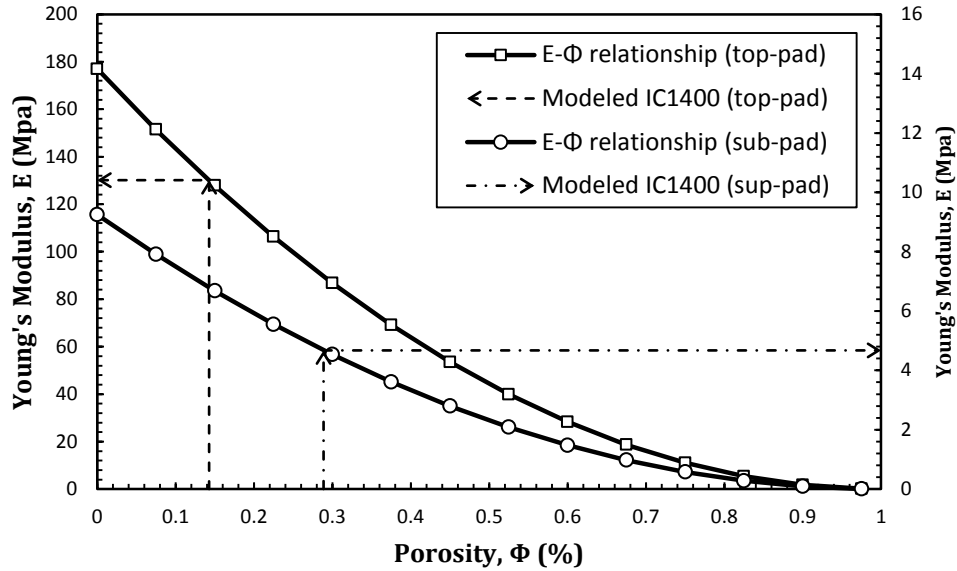


Figure 5.3 Relationship between the porosity and elastic modulus

5.4.3 Finite Element Model

The deformation problem is modeled using a structural mechanics approach in ANSYS. Contact is simulated by defining a set of elements (with a considerably small height) inbetween the contacting surfaces. The defined elements share the same nodes with the contact surfaces. In this way, the target surface elements can directly impact the contact surface upon loading. 2-D 4-node structural solid elements were used. Figure 5.4 shows the boundary conditions for the 2-D FEA model.

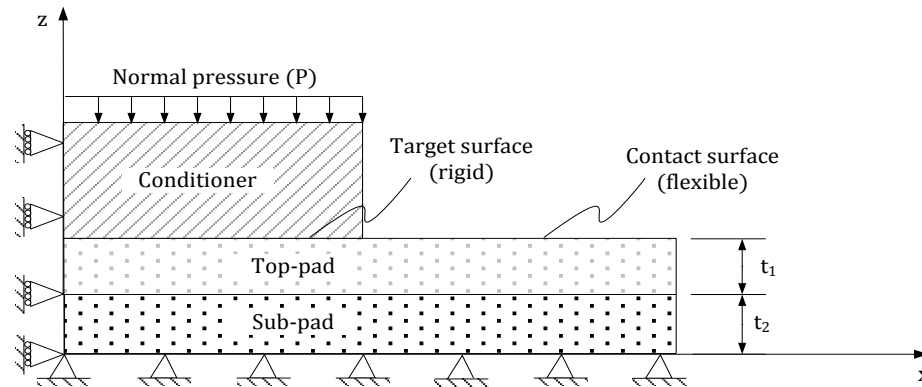


Figure 5.4 Boundary conditions of 2-D FEA model

The pad is modeled by stacking the geometric models of the top-pad and sub-pad (from Figure 5.2) together into a block. The model is discretized into 87767 elements and 56509 nodes. Since it is of interest to visualize the surface and sub-surface deformation, a much finer mesh was used for the pad in comparison to the conditioner. Meshing was performed such that the displacements at the surfaces of contact between the conditioner and top-pad and also the top-pad and sub-pad were identical in all directions. Since the bottom surface of the pad is fixed, all nodes lying on the bottom plane are fixed in all degrees of freedom. Displacement of all nodes lying along the axis of symmetry are restricted to the z-axis.

5.5 Results and Discussion

To investigate the effect of process parameters including, pad stiffness and conditioning pressure on the pad deformation, three levels of each parameter are

simulated. Table 5.3 provides a list of the parameter values used at each level. Figure 5.5 shows the variation of deformation of the pad surface and subsurface. It can be seen that upon deformation, the pad surface directly under the conditioner remains flat and experiences the most deformation. The surface out of contact with the conditioner inclines upward away from the edge of the conditioner. Also, the intensity of deformation reduces away from the bottom of the conditioner with the deformation of the top-pad only as much as the deformation at the top of the sub-pad. A slight bulge is also observed at the free end of the sub-pad.

Table 5.3 Parameters used for simulation

Parameter	Levels		
	1	2	3
E_0 of top-pad matrix (MPa)	83	130	177
Conditioning Pressure P (N)	40	70	100
E of conditioner (MPa)	180×10^3		
E_0 of sub-pad matrix (MPa)	9.30		
Thickness of top-pad t_1 (μm)	1181.00		
Thickness of sub-pad t_2 (μm)	1203.00		
Porosity of top-pad (%)	14.27		
Porosity of sub-pad (%)	28.89		
Poisson ratio of matrix	0.35		

Considering the microstructure of the pad, it can be seen that the pores of the sub-pad deform into an ellipsoid shape whilst those of the top-pad remain fairly circular. This suggests that, as intended, the sub-pad enables the stacked pad to be more flexible, while still maintaining high enough stiffness of the top surface layer.

In CMP, conditioning pressure is usually increased to intensify the regeneration of pad surface. In Figure 5.6, the conditioner is subjected to three conditioning loads. Results show that deformation increases with increasing conditioning pressure P . The evenly spaced deformation profiles suggest that conditioning pressure may have a linear relationship with the depth of deformation. The graph also confirms the initial observation that the surface of the top-pad deforms only as much as the surface of the sub-pad except at the edge of the conditioner.

The effect of pad hardness is investigated by varying E_0 of the top-pad material. Results from Figure 5.7 show that deformation increases as expected when pad material becomes softer. However, unlike the resulting deformation profiles for P , the range of deformation (both top-pad and sub-pad) over the length of the pad increases as the pad gets softer.

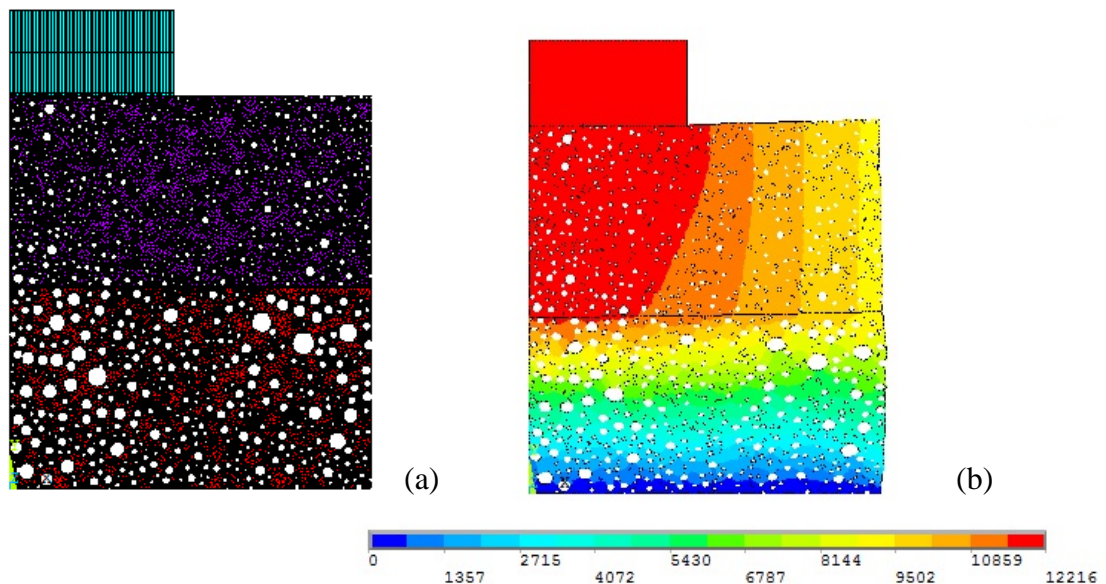


Figure 5.5. (a) FEA model and (b) variation of average pad deformation at $E_0=130$ Mpa and $P=70$ N

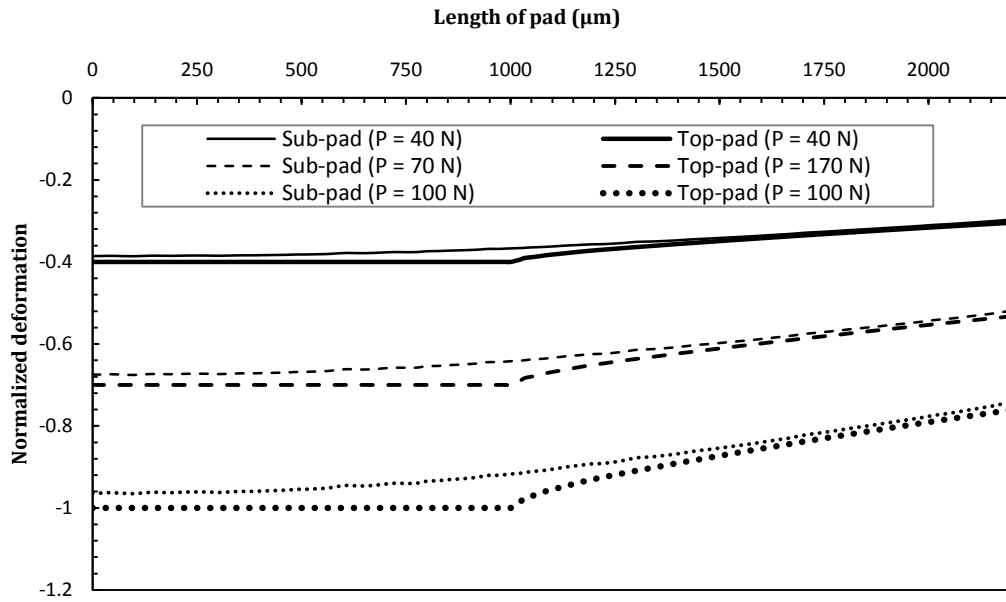


Figure 5.6. Effect of conditioner pressure (P) on deformation ($E_0 = 177 \text{ Mpa}$)

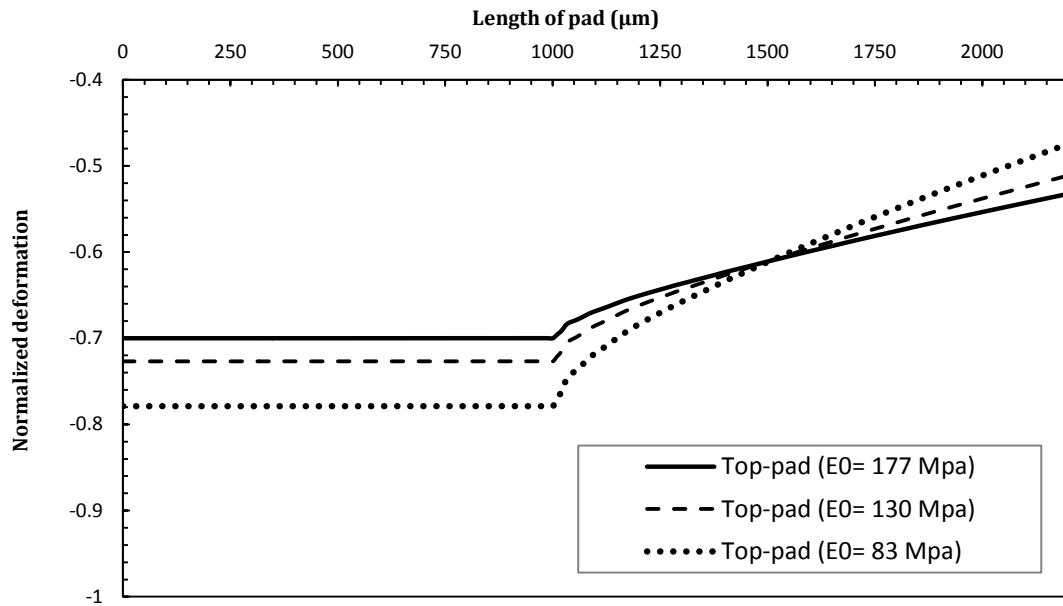


Figure 5.7. Effect of pad stiffness (E_0) on deformation at $P = 70 \text{ N}$ for top-pad

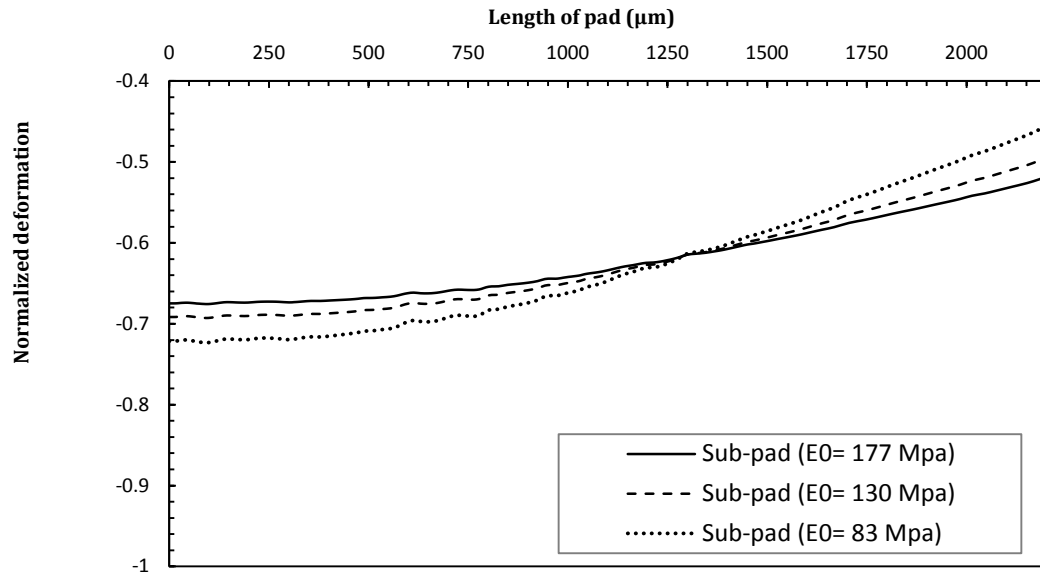


Figure 5.8. Effect of pad stiffness (E_0) on deformation at $P = 70$ N for sub-pad

5.6 Conclusions

Pad deformation due to pad conditioning during CMP affects several aspects of the process output. Analysis of these effects is crucial to the fundamental understanding of the material removal mechanism of CMP. A 2-D image processing procedure has been developed for the characterization of the morphological and mechanical properties of CMP pads. Characterization data was incorporated into a 2-D axisymmetric quasi-static FEA model to investigate effects of process parameters (pad stiffness, and conditioning pressure) on the pad deformation with enhanced fidelity. Three levels of each parameter were simulated. Results show that: (1) the conditioner slightly indents the pad with its top surface inclined away from the edge of the conditioner, (2) the softer sub-pad deforms to permit a more planar profile of the top-pad (3) deformation increases as the pad's elastic

modulus decreases, and (4) deformation increases with increasing conditioning pressure. Since the mechanical properties, liquid permeability and surface roughness of CMP pads are highly related to the foam morphology, the model provides an avenue for more accurate quantitative comparison of pads of different composition and design for high performance industrial applications.

CHAPTER 6

CONDITIONER DESIGN OPTIMIZATION

6.1 Introduction

Despite the progress made to control the pad surface profile, attaining a uniform pad surface texture (from the homogenous distribution of regenerated asperities) still remains a challenge. As mentioned in Section 1.5, CMP suppliers (system and consumables) and end users are more interested in collaborative evaluation of new consumables geared towards reducing CMP Cost of Ownership. This is achieved primarily through extended pad and conditioner lifetime and minimizing development/optimization time and repetition of efforts (Singh et al., 2011). Pad conditioner performance must be optimized not only for maintaining desired pad surface morphology but also for preserving device yield, reducing defectivity and enhanced process stability throughout pad's lifetime. This calls for more stringent control of diamond disc design features. Generation of optimal pad surface texture requires the optimization of various conditioner design parameters.

Pysher et al. (2010) proposed the concept of a pad conditioner design space (plot of conditioner surface finish against aggressiveness number) to understand different classifications of diamond pad conditioners to facilitate the selection of a disk design for a particular CMP application. Their efforts were experimental and directed towards pad MRR and surface finish of the disk by improving the diamond tip height distribution.

Hwang et al. (2007) used experimental methods to compare conditioner design parameters (diamond size, shape, distribution, concentration and bond type) and improve wafer defect rates through generation of desirable pad textures. In a similar study, Hwang's research group (2009) performed numerical simulations to enable a visual comparison of the pad texture generated by two conditioner designs. These studies present only some degree of effort towards the optimization of conditioner design in a quantitative manner.

In terms of evaluating conditioner design quantitatively, Feng (2007) developed a kinematic conditioning density (CD) function (based on the polishing trajectories generated by a conditioner) as a measure of conditioning performance. Yeh and Chen (2010) suggested a modification of the CD definition (by introducing "recover-area ratio") in order to consider the fact that a specific area of the pad may require several "cuttings" to restore it. It is generally desired that a conditioner design is evaluated independent of process parameters. However, Yeh and Chen's module does not consider conditioner design features except disc size. In lieu of these challenges, the CD model developed in Chapter 4 accounts for conditioner design features such as grit density, disc size and shape as well as diamond distribution provided the positions of the individual diamond grits are known. Baisie et al. (2011) and Feng (2007) compared the collection of trajectories generated by different kinds of diamond grain distributions. Despite the usefulness of the traditional CD approach, it is computationally intensive for the evaluation of the pad surface texture. Hence its use is currently limited to determine pad

cross-sectional profile in relation to pad wear. A simple method to quantitatively evaluate pad surface texture generated by a specific conditioner design is needed.

Following this introduction, conditioner design considerations are briefly discussed and the concept of genetic algorithms (GA) is introduced as a platform for the optimization of conditioner design in Section 6.2. In Section 6.3, the constructs of the GA optimization model are developed. Here, a new metric to evaluate conditioning performance based on the conditioning density generated by a specific conditioner design is proposed as well as a special reproduction operator based on linear crossover. In Section 6.4, the metric is applied in the model to optimize conditioner design for the first time. The model searches for the design parameters that produce a desired CMP pad surface texture. Search results are analyzed in Section 6.5 and conclusions are drawn.

6.2 Disc Design

As mentioned earlier in Section 2.3.2, product performance of CMP conditioners is characterized by diamond grit pop out, wafer removal rate, conditioner life, and consistency of conditioners among batches (Ohi, 2004). Process performance is characterized by regeneration of pad surface characteristics such as texture (described by the nature of asperities) and profile. It is well known that diamond characteristics such as size, shape, and exposure strongly influence these pad surface characteristics. The disc assembly as well as the distribution of diamond grits on the disc (Hua et al., 2009) also play an important role in conditioning outcome such as uniformity and thoroughness of

conditioning. Figure 6.1 shows various types of diamond geometric arrangements and disc shape. In the manufacture of diamond disc conditioners, the diamond grits are distributed in a random or structured pattern using conventional techniques or more modern surface engineering techniques mentioned in Section 2.3.1 which promise high regularity of diamond shape and uniform regeneration of pad asperities. Due to the increasing intensity, complexity and changing requirements of next-generation CMP processes, requirements for the performance of CMP conditioners have diversified (Singh et al., 2011). Thus CMP pad conditioner designs are currently selected for particular applications based on the pad type, wafer size, and slurry (Ohi, 2004, Pysher et al., 2010). Optimization methods are sought to determine the best diamond disc design features for each application.

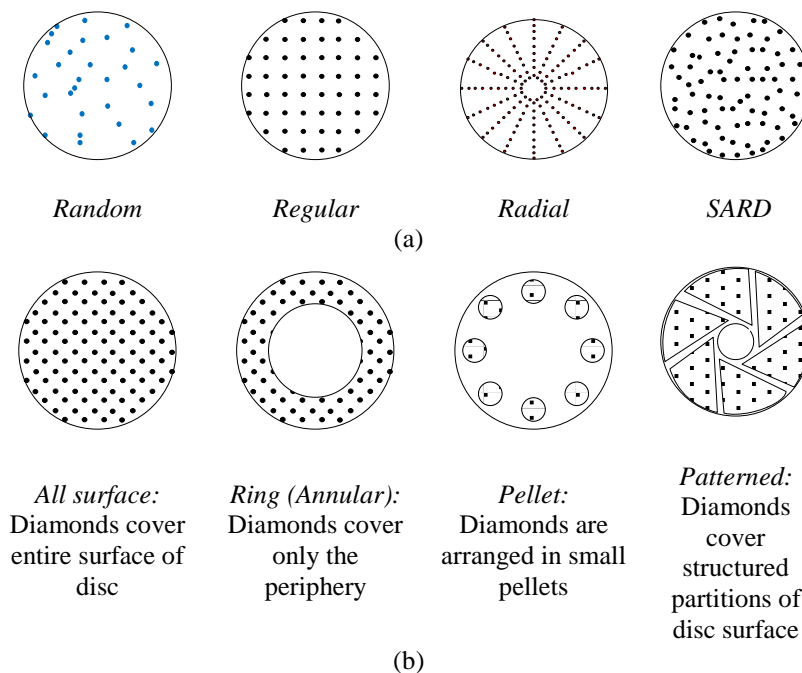


Figure 6.1. Types of (a) diamond geometric arrangements and (b) disc shape

6.3 Genetic Algorithms in Design Optimization

Most practical design optimizations are highly nonlinear, multimodal, and under various complex constraints where different objectives are often conflicting (Yang, 2012). Such is the conditioner design optimization problem being addressed. Genetic algorithms constitute a popular class of (adaptive and stochastic) metaheuristic search algorithms especially suited to solving complex optimization problems in engineering. GAs transpose the notions of evolution in nature to computers and imitate natural evolution. Basically, they find solution(s) to a problem by maintaining a population of possible solutions according to the ‘survival of the fittest’ principle (Renner, 2004). GAs only use the objective function while searching for optimized result and not the derivatives, therefore it is a direct search method. Design can be conceived as a search for a suitable or optimal construction, where the term search is used in a technical sense.

A search problem consists of a desired state (goal state), a search space and a search process. In design the goal state represents the characteristics of the final design. The search space is the set of all designs characterized by all allowable values of the design parameters (Renner, 2004). GAs work with a coding of the parameter set (set of strings/individual chromosomes) and use probabilistic transition rules (Goldberg, 1989). Renner (2004) discusses in more detail the features of GAs, how they work and provides an overview of applications of GAs to different domains of engineering design. Solving a problem with GA starts with designing a proper representation, fitness measure and termination criterion. The termination criterion usually allows at most some predefined

number of generations and checks whether an acceptable solution has been found. The GA procedure modified for this study is presented in Figure 6.2.

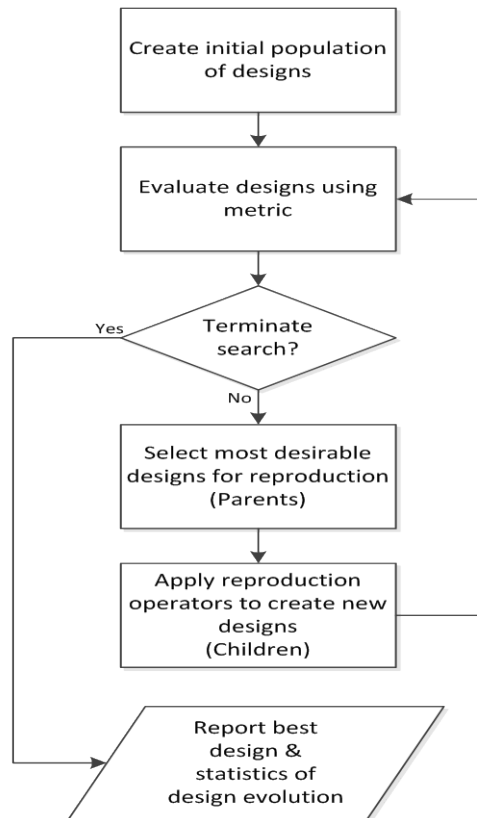


Figure 6.2. Genetic Algorithm (GA) process

6.4 Problem Representation

6.4.1 Solution Representation

In this study, three design parameters are considered: Geometric arrangement of diamonds (G_{ij}), Grit Density (D_{ij}) and Size (S_{ij}) of conditioner disc j in generation i . The

shape of the conditioner is restricted to the “all surface” type shown in Figure 6.1(b). A fourth parameter R_{ij} is introduced to specify the number of rays in the case of a radial geometric arrangement. Table 6.1 describes the constraints associated with each of these parameters.

Table 6.1. Constraints on conditioner design parameters

Parameter	Constraints
Geometric arrangement of diamonds (G_{ij})	The value of G_{ij} is a discrete variable which could assume one of four values where 1 represents Regular, 2-Random, 3-SARD and 4-Radial design. (SARD -Self Avoiding Random Distribution).
Grit Density (D_{ij})	$0 < D_{ij} \leq \frac{1}{\delta * \mu_{grit}^2};$ where $D_{ij} = \frac{ND_{ij}}{\pi * S_{ij}^2}$. ND_{ij} is the number of diamonds over the corresponding conditioner surface area, δ is a diamond pitch factor to control the proximity of diamond grits to each other, and μ_{grit} is the average diamond grit size.
Size (S_{ij})	$0 < S_{ij} \leq 0.5 \times R_{pad};$ where R_{pad} is the pad radius.
Number of rays (R_{ij})	$1 \leq R_{ij} \leq \frac{2\pi S_{ij}}{\delta * \mu_{grit}}$ R_{ij} must be a positive integer.

The usual method of applying GA to real-parameter problems is to encode each parameter as a bit string using either a standard binary coding or a Gray coding. The bit strings for the parameters are concatenated together to give a single bit string (or "chromosome") which represents the entire vector of parameters. In biological terminology, each bit position corresponds to a gene of the chromosome, and each bit

value corresponds to an allele. Wright (1991) showed that in terms of reproduction, binary crossover is exactly the same as real crossover and a mutation can also be considered as a perturbation of some of the real valued parameters. Thus, in this study, it is deemed sufficient that, a chromosome corresponds to a vector of real parameters (G_{ij} , D_{ij} , S_{ij} , R_{ij}), a gene corresponds to a real number, and an allele corresponds to a real value.

6.4.2 Design Evaluation

A typical pad conditioning cycle is illustrated in Figure 3.1. The kinematic model developed in Chapter 4 is used to simulate the diamond grit trajectories. It is assumed that all of the diamond grits embedded on the metal disc protrude with a pyramid shape and have the same size and protrusion height as shown in the Figure 2.2(b). It is also assumed that during the conditioning process, each diamond grit is in continuous contact with a flat and homogenous pad surface and will generate an individual trajectory. The collection of these trajectories depicts the pad's surface texture resulted from the conditioning process.

From Section 4.2, the radial distance d traveled by the conditioner from the pad center by time t is given by:

$$d = D(t) = L + \int v dt. \quad (6.1)$$

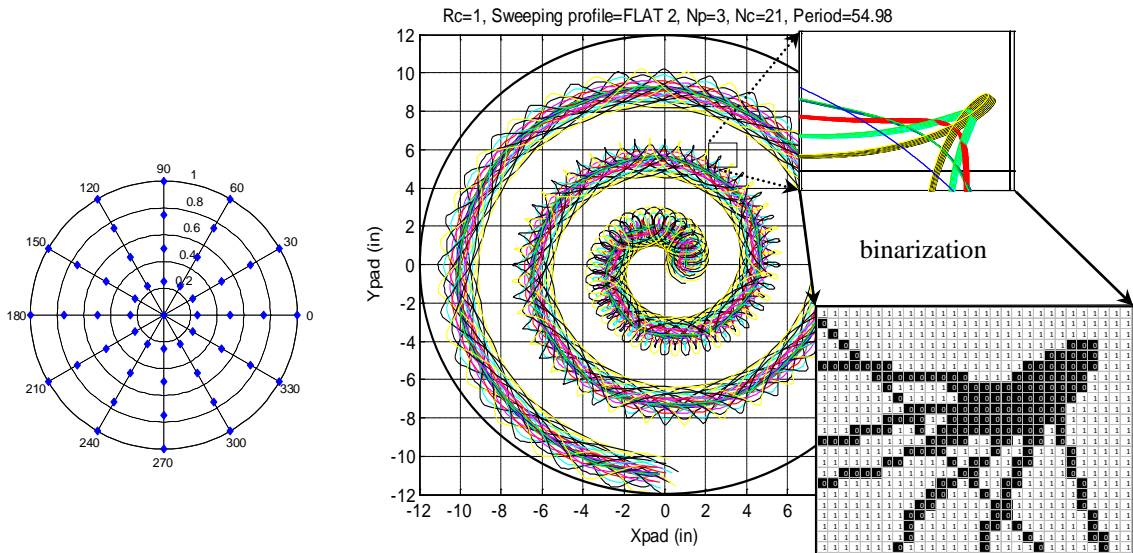
L is set to be equal to the conditioner radius S_{ij} and overhanging is not allowed. For multiple diamonds on the conditioner, the collection of trajectories on the polishing pad is described as:

$$\bigoplus_{k=1}^{ND} \begin{bmatrix} X(t) \\ Y(t) \end{bmatrix}_k = d \cdot \begin{bmatrix} \cos(w_p t) \\ \sin(w_p t) \end{bmatrix} + \bigoplus_{k=1}^{ND} r_k \begin{bmatrix} \cos((w_p - w_c)t - \theta_k) \\ \sin((w_p - w_c)t - \theta_k) \end{bmatrix}. \quad (6.2)$$

Equation (6.2) is utilized to plot the conditioner trajectories. The parameters are the input variables N_p , N_c , R_p , T , t_{cycle} and the set $[r_k, \theta_k]$. N_p and N_c , the rotation speeds in rpm for the pad and conditioner are converted to ω_p and ω_c respectively in rad/sec. R_p is the pad radius, T is total conditioning time and, t_{cycle} is the time for a single cycle. All length units are in inches and time in seconds. A function is developed to generate the set $[r_k, \theta_k]$ that satisfies the conditioner design specified by the chromosome $[G_{ij}, D_{ij}, S_{ij}, R_{ij}]$. To evaluate the pad surface texture generated, a simple conditioning density (CD') metric is proposed that compares the area covered by trajectories (Ac_{ij}) to the total area of the pad (Ap) hence:

$$CD'_{ij} = \frac{Ac_{ij}}{Ap} = \frac{\text{Number of black pixels}}{\text{Pixel value of pad circular area}}. \quad (6.3)$$

To implement CD' , the plot of trajectories on the pad surface area is converted to a binary image (as shown in Figure 6.3(b) inset), where each pixel assumes one of two discrete values: 1 for white or 0 for black. All positions that contain a pixel of value 0 indicate conditioned area and 1 otherwise. The value of CD' ranges between 0 and 1. A CD' value closer to 1 indicates that the conditioner design achieves more coverage of the pad surface area and hence a more homogeneously regenerated pad texture. Therefore in an application where uniform conditioning of the entire pad surface area is desired, the goal of the search is to seek a design that maximizes CD' .



(a) Conditioner design
 $(G_{ij}, D_{ij}, S_{ij}, R_{ij}) =$
 $(4, 15.59, 1, 12).$

(b) Binarized diamond grit trajectory. Colors are used here to differentiate trajectory generated by different diamond grit

Figure 6.3. Binarized trajectories generated by a specified conditioner design

6.4.3 Selection

The fitness of each individual design solution in the current population is evaluated using the CD' function. An elitist strategy is adapted to select the proportion of the existing population to breed a new generation. After ranking current population according to CD' , the best 50% of the solutions are selected to serve as parents in the subsequent reproduction stage for the next generation of solutions. The same population size is maintained throughout subsequent generations.

6.4.4 Reproduction

An efficient optimization algorithm must use two techniques to find a global maximum: *exploration* to investigate new and unknown areas of the search space, and *exploitation* to make use of knowledge found at points previously visited to help find better points (Beasley et al., 1993). Accordingly, new designs (offspring) are generated by applying three genetic operators (traditional crossover, linear crossover and mutation) to parent designs. Crossover essentially performs an exploitive role while mutation performs an explorative role.

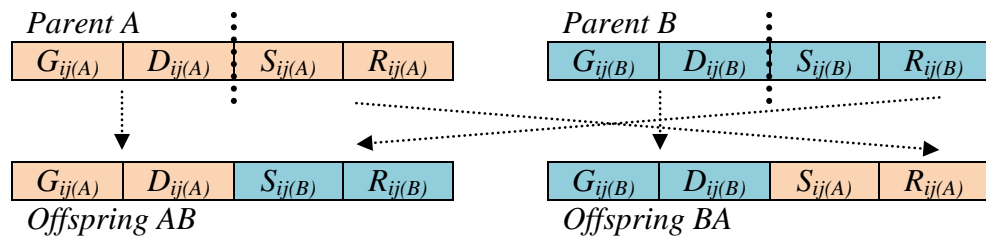
A one-point traditional crossover operator combines the representation of two parent individuals to produce two children by swapping between the two parent design parameters as shown in Figure 6.4(a). The problem with traditional crossover is that it tends to be less and less effective as the similarities between organisms increases (due to recurrence of alleles) as the population converges. At this stage, mutation becomes more and more necessary as variation in the population is reduced (Beasley et al., 1993). To overcome this problem, a different form of operator to be termed '*random linear crossover*' is proposed. Instead of swapping alleles, corresponding alleles of two parent genes P_{ij}^A and P_{ij}^B are recombined using a linear operator to produce two offspring O_{ij}^{AB} and O_{ij}^{BA} (as shown in Figure 6.4(b)) using the equations:

$$O_{ij}^{AB} = P_{ij}^A * Rand(0,1) + P_{ij}^B * (1 - Rand(0,1)); \quad (6.4)$$

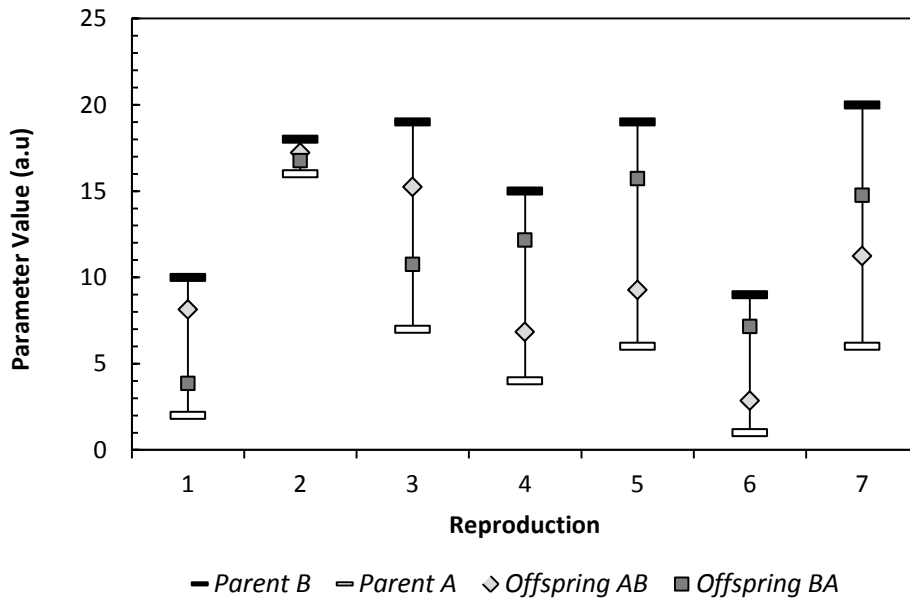
and

$$O_{ij}^{BA} = P_{ij}^A * (1 - Rand(0,1)) + P_{ij}^B * Rand(0,1). \quad (6.5)$$

The mutation operator introduces local changes to the genetic code of an individual parent design by randomly reassigning new allele(s) to the design parameters within their specified constraints. Each selected parent was randomly assigned to one of the three reproduction operators. By proportion, 45% of the selected parent designs reproduce by traditional crossover, 45% by linear crossover and the remaining 10% by mutation.



(a)



(b)

Figure 6.4. (a) Traditional crossover and (b) random linear crossover operations

6.5 Results and Discussion

6.5.1 Simulation Parameters

Conditioning parameters were chosen such that conditioning performance was minimally influenced by process parameters not related to conditioner design. $N_p = 3$ rpm, $N_c = 2$ rpm, $R_p = 12$ in, and $v = 0.1818$ in/s. The average diamond grit size (μ_{grit}) was set to 150 microns and a pitch factor (δ) of 10 was chosen. To minimize computational cost, only one conditioning cycle was simulated. The pad and conditioner speed were chosen to minimize periodicity in the generation of trajectories.

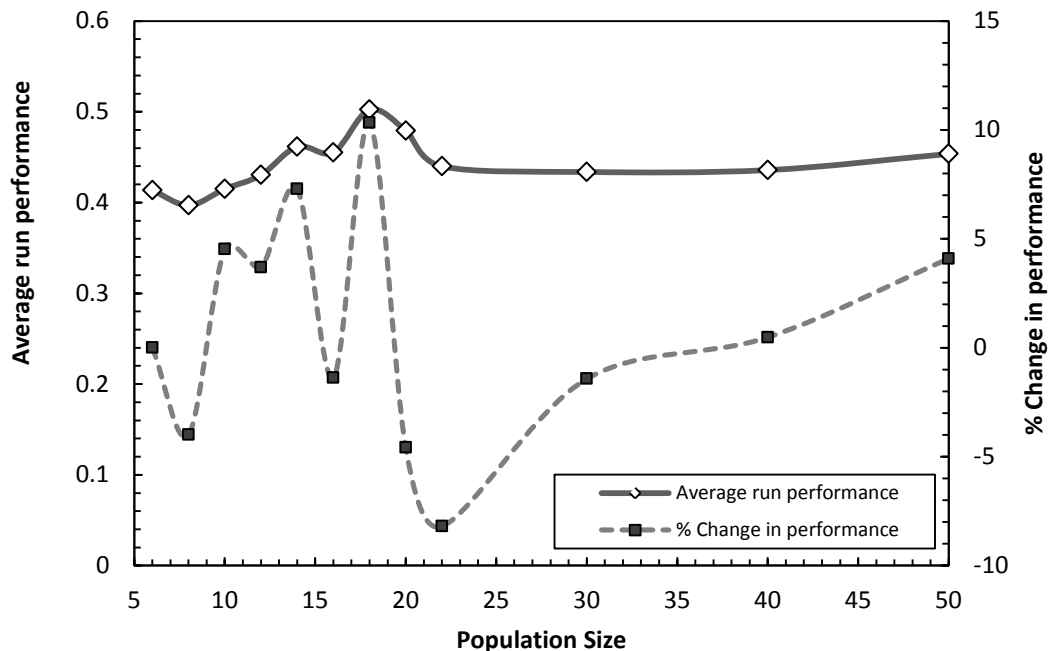


Figure 6.5. Effect of population size on run performance

Reed et al. (Reed et al., 2000) proposed a well-known 3-step methodology for the tuning of population size, selection pressure, and the influence of crossover and mutation in the design of simple genetic algorithms for practical computationally intensive problems. However, Reed's guidelines are intended for binary coded GA and are not generally extendable to real value GAs. In this study, the population size is decided by performing some trial GA runs for a small number of generations with each run having different population size. In Figure 6.5, the average run performance and the percentage change in performance is plotted against the population size. The graph shows that a population size of 18 was sufficient to provide promising results. Thus, an initial population size of 18 was chosen to evolve over a period of 30 generations with 9 individuals surviving 9 offspring being born in each generation. The individuals in the initial population were chosen such that there were an equal proportion of solutions with the same G_{ij} value and the remaining design parameter values (D_{ij} , S_{ij} and R_{ij}) were chosen at random.

6.5.2 Search Results

6.5.2.1 Performance of Design Optimization

Figure 6.6(a) is a plot of the best and average fitness values in each generation. The reproduction operators were able to maintain a diverse and yet an increasingly 'fit' population within feasible region throughout the evolution period. The selection criteria also proved to maintain an even, controllable selection pressure to push for the selection of better individuals appropriate for the conditioner design optimization problem. It can be seen that the average population fitness improves quickly and reaches a plateau close

to the value 0.75. This means that the designs of the latter generations may well suggest parameter values that are more desirable. The best solution in each population does not seem to improve significantly over the generations. This may be due to limitations imposed by the chosen process parameters values and the limited number of conditioner design features considered in the model. Figure 6.7 shows areas in the search space where the solutions emerged. Judging from the location of the best solution in the last generation, the search converged to the region with the highest concentration of solutions and thus more desirable design parameter values.

6.5.2.2 Evolution of Size

Figure 6.6(b) shows a plot of the average relative disc radius (S_{ij}/R_{pad}) over the simulation run. It can be seen that designs with smaller conditioner size tend to quickly hover around a relative radius of 30% of the pad radius. This is attributed to two reasons. First, larger conditioners are not able to adequately condition the central portion of the pad. Secondly, there tends to be larger gaps between the trajectories generated by the wider spaced diamonds on larger conditioners. The tendency of the specific relative radius is dependent on the conditioning process parameters such as the relative speed of the conditioner. Other studies (Baisie et al., 2010) have shown that in this configuration of pad conditioning, total thickness variation, concavity and waviness of the pad profile tend to deteriorate significantly as the conditioner size increases.

6.5.2.3 Evolution of Grit Density

Figure 6.6(c) shows the plot of the average density over the simulation run. It is expected that conditioners with higher grit density will achieve better coverage of the pad

surface area and hence better conditioning performance. However, it can be seen that the conditioning density increases steadily and converges around 40 grits/in². This limit is imposed by the practical constraints associated with the diamond pitch factor and grit size.

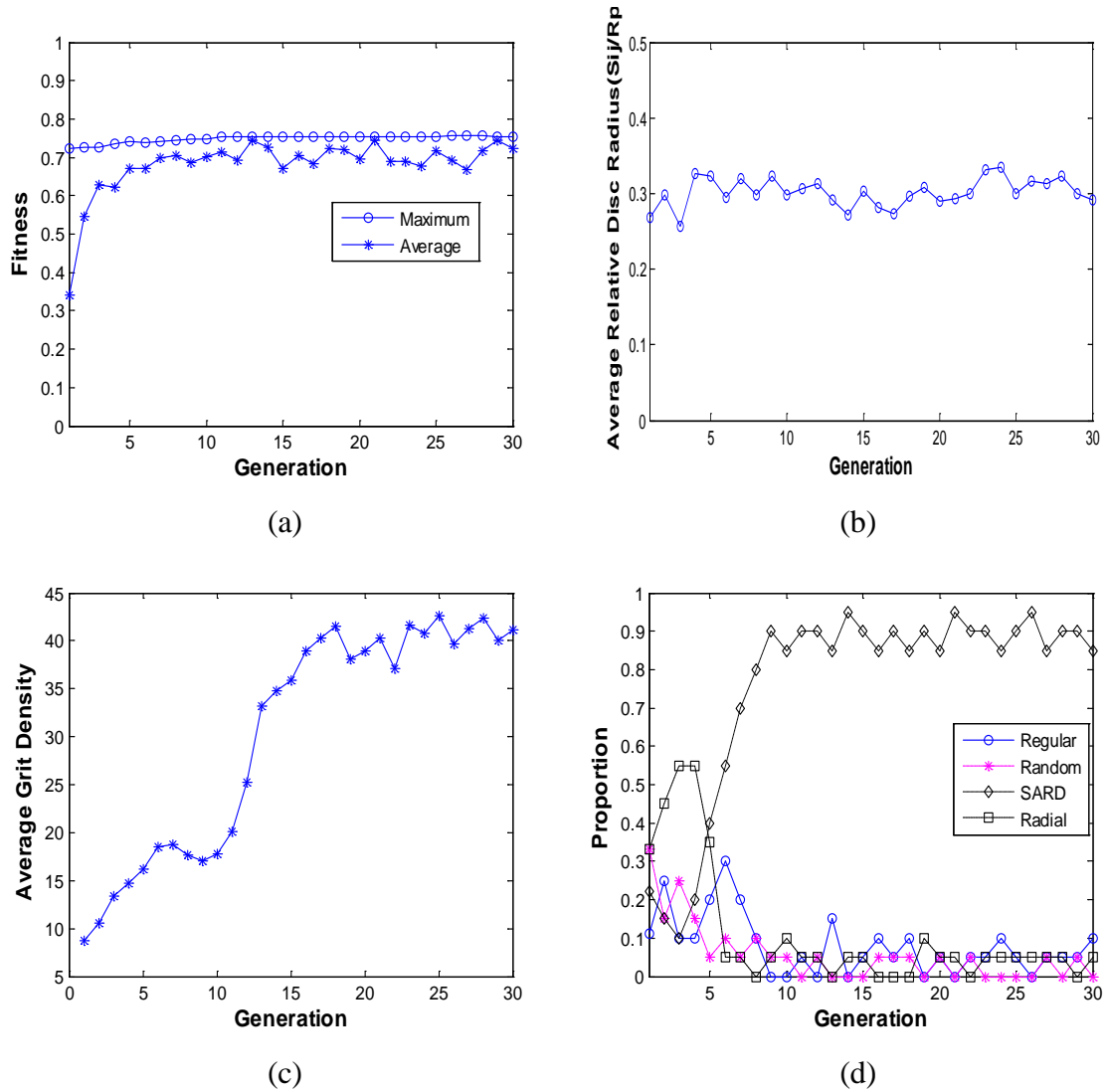


Figure 6.6. Evolution of (a) fitness, (b) disc size, (c) grit density, and (d) geometric arrangement

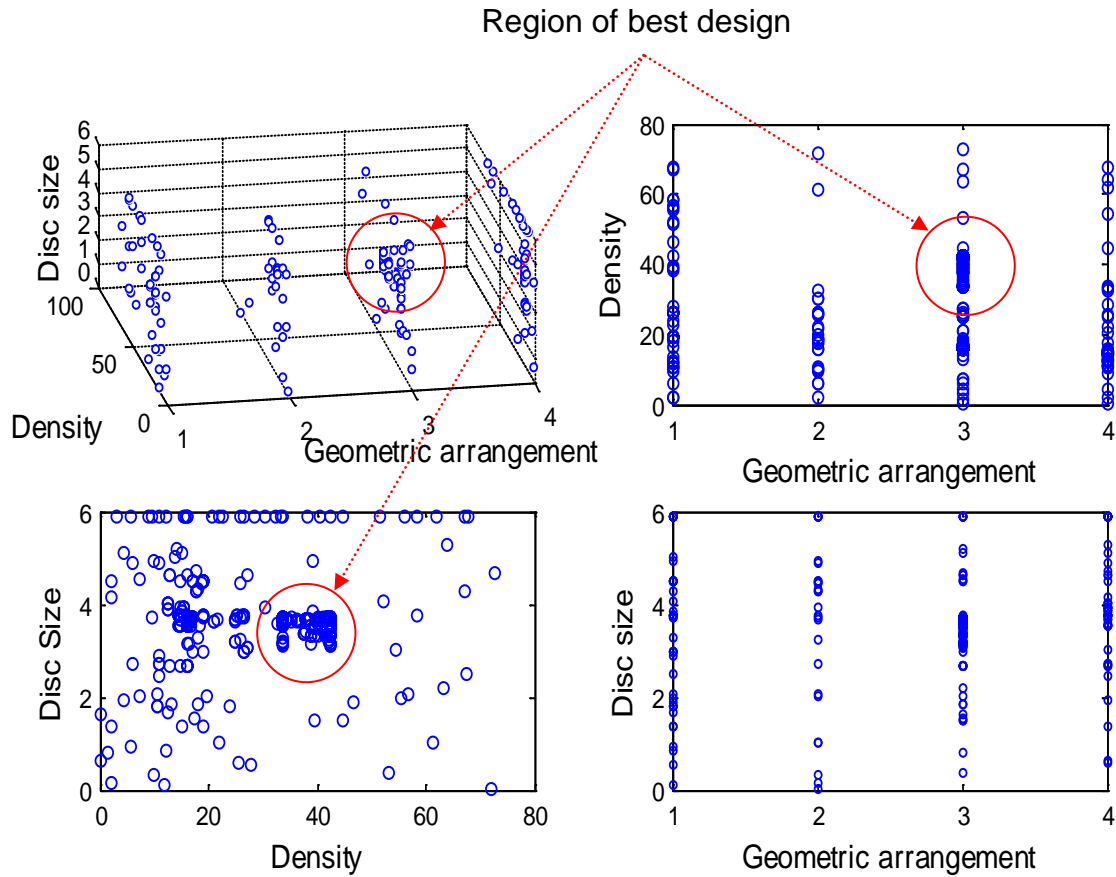
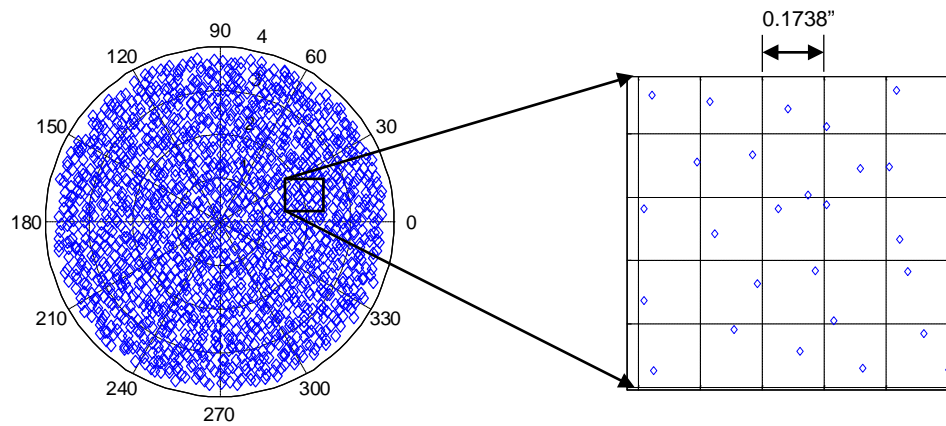


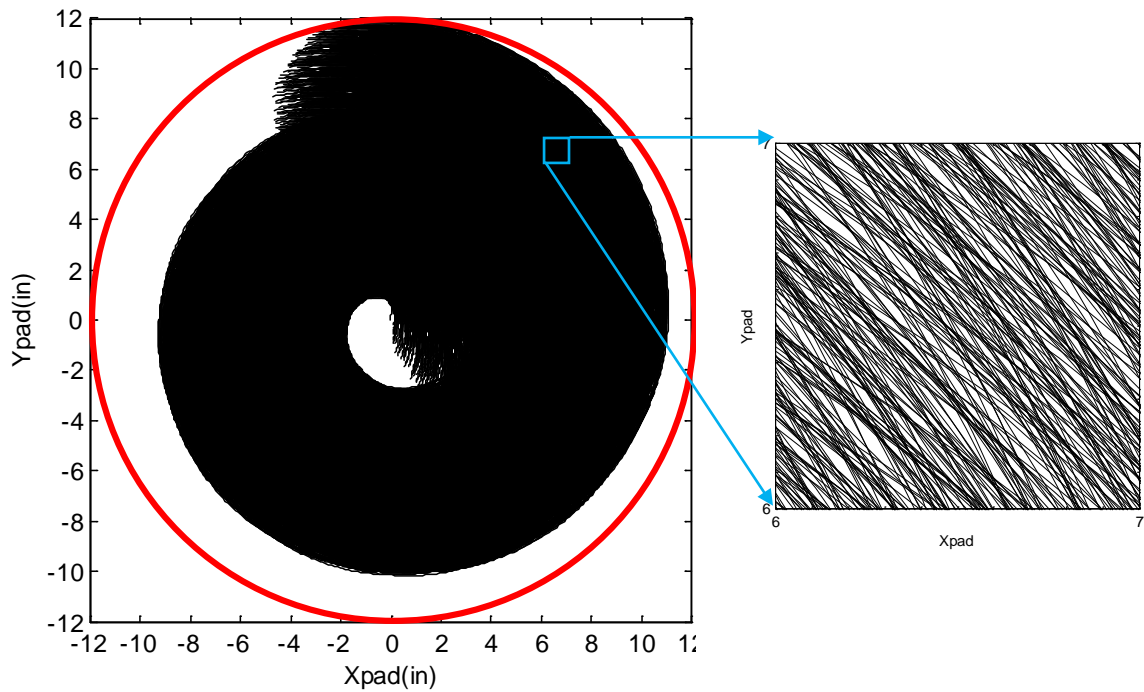
Figure 6.7. Solution space

6.5.2.4 Evolution of Geometric Arrangement

Figure 6.6(d) shows the proportion of Regular, Random, SARD and Radial diamond geometrical arrangements within each generation. It can be seen that designs with SARD diamond arrangement quickly begin to dominate the population of solutions. This means the geometric arrangement of the diamonds showed a more dominant impact on the search outcome.



(a)



(b)

Figure 6.8. Best design in last generation showing (a) (3, 42.14, 3.69, 0) design displayed on polar grid and (b) its corresponding $CD' = 0.75$

Figure 6.8 shows the SARD design of the most ‘fit’ individual in the last generation of individuals. Regular and Radial distributed diamonds tend to generate periodic patterns where often times a single diamond’s trajectory may partially overlap another. This reduces the chances of achieving more coverage of the pad surface area and hence a more homogeneous spread pad texture. Although a Random diamond arrangement may seem to overcome this challenge, it is difficult to achieve manufacturing consistency and hence poor process repeatability and reproducibility. The SARD was developed by Hwang et al.(2007) in an attempt to eliminate periodicity in trajectories and also to avoid diamond free zones in the coverage of the conditioner surface as seen in truly random diamond arrangements. In the SARD, each diamond grit is randomly positioned in a grid as shown in the Figure 6.8(a) inset. In Figure 6.8(b), it can be seen that the conditioner’s diamond trajectories cover 75% of the region within the pad’s circumferential boundary in red. The inset also shows a close up view of the surface texture of a 1”x1” cake of the pad.

6.6 Conclusions

Currently, CMP conditioner suppliers and end users are more interested in collaborative evaluation of new consumables geared towards reducing CMP Cost of Ownership by minimizing development/optimization efforts. There has been only little degree of effort towards the optimization of conditioner design in a quantitative manner. In this study, a new metric to evaluate conditioning performance based on the

conditioning density generated by a specific conditioner design was developed. The metric was further applied in a genetic algorithm to optimize the conditioner design parameters (including geometric arrangement of diamonds, grit density and disc size) for the first time. It can be concluded that the GA framework is well suited for the design optimization of diamond disc pad conditioners. It was observed that better designs tend to exhibit features with higher grit concentration, smaller disc size and a structured randomization of the diamond grit arrangement. Geometric arrangement of the diamonds showed a more dominant impact on the search outcome. The model is useful for the prediction of conditioning performance and tuning of conditioner design to specific applications.

CHAPTER 7

CONCLUSIONS AND FUTURE WORK

7.1 Research Overview

This research sought to address the concern about the lack of models that are reliable enough to be used for verification and optimization of the diamond disc pad conditioning process in three main steps. First, three models to simulate, predict, and evaluate the pad's mechanical response and surface characteristics resulting from conditioning were developed. Secondly, the effects of pad conditioning parameters on conditioning uniformity were evaluated. Finally, a new framework for the optimization of the conditioner design was developed. The modeling results mainly suggested that it is possible to advance pad conditioning towards high uniformity and predictability if as many of the process parameters can be controlled and incorporated in the analytical models. A recap of the major research contributions and findings is provided below.

7.1.1 Findings from Literature Review

Pad conditioning had developed to an advanced stage where all dimensions are highly controlled. As conditioning is primarily considered as a two-body abrasive wear mechanism, the Preston equation has been widely adopted to model the conditioner-pad interaction. It was revealed that the main process control avenues were conditioning time and conditioning kinematics such as pressure, relative velocity and sweeping profile.

Modeling approaches commonly used were categorized into two groups, namely *kinematic* and *statistical* approach.

7.1.2 Modeling and Prediction of Pad Surface Profile

In this research, two new kinematic models were developed to predict the pad surface profile due to wear from diamond disc conditioning. The first model was developed using a surface element approach where the motion of a tiny sector on the conditioner is decomposed into its rotational and linear components to simulate the wear area that a diamond abrasive sweeps on the pad surface. The actual pad profile was determined by considering overlapped pad areas and the size of the pad section being conditioned. In the second model, a plot of the collection of trajectories generated by individual diamonds on the conditioner was generated. The conditioning density, determined by the ratio of total trajectory length per unit area in the radial direction, is used to infer the pad profile.

Three metrics, namely TTV, Bow, and NU, were developed to evaluate the pad surface profile characteristics. Experimental data was used to confirm that both models were able to simulate the kinematics of diamond disc pad conditioning and accurately predict the pad surface profile. Simulation results revealed that: (1) there are always some transition regions present in the pad profile near the pad center, and the pad periphery; (2) the sweeping profile has a “mirroring” effect on the resulting pad surface profile; and (3) a lower pad rotating speed and a smaller conditioner size allow a flatter pad profile.

7.1.3 2-D Morphology and Finite Element Analysis of Pad

The pad's mechanical response affects the conditioning process and is highly dependent on its foam morphology. A 2-D image processing procedure combined with a 2-D axisymmetric quasi-static FEA model were developed for the first time to investigate effects of process parameters (pad stack, pad stiffness, and conditioning pressure) on the pad deformation with enhanced fidelity. Results showed that: (1) softer sub-pads deform to permit a more planar profile of the top-pad; (2) the conditioner slightly indents the pad with its top surface inclined away from the edge of the conditioner; and (3) deformation increases as the pad's elastic modulus decreases, and conditioning pressure increases.

7.1.4 Conditioner Design Optimization

To suggest ways to further improve the conditioning process, a new metric to evaluate pad surface texture was developed and applied in a GA model to optimize the conditioner design parameters (including geometric arrangement of diamonds, grit density and disc size) for the first time. In the GA model, a new way to quantitatively characterize conditioner design was developed as well as a special GA reproduction operator. It was concluded that: (1) the GA framework is well suited for the design optimization of diamond disc pad conditioners; and (2) better conditioner designs tend to exhibit features with higher grit concentration, smaller disc size and a structured randomization of the diamond grit arrangement.

7.2 Future Work

7.2.1 *Control of Pad Profile*

Considering the current understanding of pad profile development and the availability of metrics to measure conditioning performance, future work can consider applying an optimization model to the developed kinematic models to determine the optimal set of parameters to further eliminate pad wear transition regions and achieve desired pad profiles. The kinematic models could be further developed to consider non-linear sweeping paths and conditioner overhanging. The two kinematic process models can be compared to evaluate model capabilities, differences and similarities and permit a more informed decision on the choice of application.

7.2.2 *Finite Element Analysis*

Following the findings of the Finite Element Analysis, a 3-D as well as a dynamic analysis of the conditioner-pad interaction is needed. Here, the shear forces involved in the process can be considered in detail. The model can further be utilized to evaluate the effect of conditioner design features such as convex or contoured cross sections on the pads mechanical response. A study is also needed to investigate the effect of different pad stacks and microstructures on the pad's mechanical response. The results should be related to the evolution of the pad profile due to conditioning.

7.2.3 Understanding and Characterizing the Preston Coefficient K in Pad

Conditioning

In-house experiments need to be carried out to verify the kinematic models, to determine the Preston coefficient K and also to verify the Finite Element model. Some researchers suspect that the value of K in the pad conditioning process involves advanced physics and may be dependent on the pad roughness, asperities, elasticity, surface chemistry and abrasion effects as well as conditioner characteristics among others. Based on the results of Chapters 5 and 6, and consideration of the analytical models summarized in Appendix I, an initial deduction of the relationships which a set of chosen parameters have with K is provided in Table 7.1. Experimental studies are needed to develop an empirical model to further understand and characterize the underlying parameters that affect K and their influence on modeling of pad conditioning.

Table 7.1. Relationship of chosen parameters with K

Relationship with K	Parameter
Positive correlation	1. Density of abrasive grit distribution
	2. Disc diameter
	3. Total number of working diamonds
	4. Average groove width or cross-sectional area of diamond
	5. Power consumed to remove unit volume of pad
	6. Poisson ratio of pad
	7. Temperature of pad
	8. Soaking time of pad
	9. Porosity of pad
Negative correlation	10. Hardness of pad
	11. Knife-edge or sharpness of diamond grit
	12. Slurry viscosity
	13. Young's modulus of pad
	14. Pad surface variation due to morphology

7.2.4 Conditioner Design Optimization

Although the Genetic Algorithm platform was successful in the conditioner design optimization effort, other metaheuristics could be tested. The optimization model could further be developed to consider more design features such as disc shape. More so, future work could concern the development of a model capable not only of optimizing available designs, but also creating new conceptual designs from scratch. With regard to the geometric arrangement of diamonds, functional biological patterns such as phyllotactic and Fibonacci patterns could be explored.

7.2.5 Process Model Integration

Finally, a more comprehensive process model that integrates multiple analytical models and captures all the key operational factors needs to be developed. The models should be linked to both up-stream as well as down-stream CMP processes to allow series process improvement.

REFERENCES

- Andersson, J., Hollman, P., Forsberg, M. & Jacobson, S. Year. A geometrically defined all-diamond pad conditioner. *In*, 2005 New York, NY 10016-5990, United States. American Society of Mechanical Engineers, 361-362.
- Baisie, E. A., Li, Z. C. & Zhang, X. H. 2009. Diamond disc pad conditioning in chemical mechanical polishing: A literature review of process modeling. *4th Annual 2009 ASME International Manufacturing Science and Engineering Conference* West Lafayette, IN, United states: ASME.
- Baisie, E. A., Li, Z. C. & Zhang, X. H. 2010. Simulation of Diamond Disc Conditioning in Chemical Mechanical Polishing: Effects of Conditioning Parameters on Pad Surface Shape. *ASME Conference Proceedings*, 2010, 169-177.
- Baisie, E. A., Li, Z. C. & Zhang, X. H. 2011. Diamond Disc Pad Conditioning in Chemical Mechanical Polishing: A Conditioning Density Distribution Model to Predict Pad Surface Shape. *Accepted in International Journal of Manufacturing Research (IJMR)*.
- Ballhaus, W., Pallega, A. & Constantin, V. 2009. A change of pace for the semiconductor industry. Dusseldorf, Germany: Pricewaterhouse Coopers.
- Beasley, D., Bull, D. R. & Martin, R. R. 1993. An Overview of Genetic Algorithms : Part 1 , Fundamentals. *University Computing*, 15, 1-16.
- Benner, R. L., Benner, S. J. & Benner, R. L. 2003. *Polishing pad conditioning system*, US Patent 6508697 B1.
- Borucki, L., Lee, H., Zhuang, Y., Nikita, N., Kikuma, R. & Philipossian, A. 2009. Theoretical and experimental investigation of conditioner design factors on tribology and removal rate in copper chemical mechanical planarization. *Japanese Journal of Applied Physics*, 48.
- Borucki, L. J., Rikita, N., Zhuang, Y., Lee, H., Zhuang, R., Yamishita, T., Kikuma, R. & Philipossian, A. 2006. Causal Analysis of Conditioner Design Factors on Removal Rates in Copper CMP. *11th International CMP-MIC Conference*. Fremont, California.
- Borucki, L. J., Witelski, T., Please, C., Kramer, P. R. & Schwendeman, D. 2004. A theory of pad conditioning for chemical-mechanical polishing. *Journal of Engineering Mathematics*, 50, 1-24.

- Bozkaya, D. 2009. *Mechanics of the pad-abrasive-wafer contact in chemical mechanical polishing*. Doctor of Philosophy Dissertation, Northeastern University.
- Bozkaya, D. & Muftu, S. 2009. A material removal model for CMP based on the contact mechanics of pad, abrasives, and wafer. *Journal of the Electrochemical Society*, 156, H890-H902.
- Breivogel, J. R., Blanchard, L. R. & Prince, M. J. 1993. *Polishing pad conditioning apparatus for wafer planarization process* US Patent 5216843.
- Bubnick, M., Qamar, S., Mcgregor, S., Namola, T. & White, T. 2010. Effects of Diamond Shape and Size on Polyurethane Pad Conditioning. *Abrasive Technology TECHVIEW* [Online], Article retrieved from: <http://www.abrasive-tech.com/literature#CMP>. [Accessed 8/10/2010].
- Byrne, G., Mullany, B. & Young, P. 1999. The Effect of Pad Wear on the Chemical Mechanical Polishing of Silicon Wafers. *CIRP Annals - Manufacturing Technology*, 48, 143-146.
- Centeno, G., Sampath, V., Moreno, W., Tadi, B. & Maignel, J. 2005. Nondestructive characterization of CMP pads using statistical design analysis. *Semiconductor Manufacturing, IEEE Transactions on*, 18, 664-671.
- Chang, O., Kim, H., Park, K., Park, B., Seo, H. & Jeong, H. 2007. Mathematical modeling of CMP conditioning process. *Microelectronic engineering*, 84, 577-583.
- Charm, L. & Tam, H. 2006. Methods for Determination of CMP Pad Life: Simulation by Conditioning vs. Wafer Passes. *11th International CMP-MIC Conference*. Fremont, California.
- Che, W., Guo, Y., Bastawros, A. & Chandra, A. Year. Mechanistic understanding of material detachment during CMP processing. *In: 2002 MRS Spring Meeting, April 1, 2002 - April 5, 2002, 2002 San Francisco, CA, United states. Materials Research Society*, 90-95.
- Chen, C.-Y., Yu, C.-C., Shen, S.-H. & Ho, M. 2000. Operational aspects of chemical mechanical polishing polish pad profile optimization. *Journal of The Electrochemical Society*, 147, 3922-3930.
- Chen, K.-R. & Young, H.-T. 2010. Modelling on dressing effects in chemical mechanical polishing with diamond dressers. *International Journal of Abrasive Technology*, 3, 1-10.

- Choi, W. J., Jung, S. P., Shin, J. G., Yang, D. & Lee, H. B. 2011. Characterization of wet pad surface in chemical mechanical polishing (CMP) process with full-field optical coherence tomography (FF-OCT). *Optics Express*, 19, 13343-13350.
- Chugh, S. 2010. Algorithm for counting overlapping red blood cells using Matlab. *Knol* [Online]. Available: <http://knol.google.com/k/samiksha-chugh/algorithm-for-counting-overlapping-red/jrj7q3z0tyuk/13>.
- Clennon, E. 2007. Texas Semiconductor Industry Report. *In: TOURISM, O. O. T. G. E. D. A. (ed.)*. Austin, TX: Business Research Staff.
- Cook, L. M. 1999. Chapter 6 CMP Consumables II: Pad. *In: WILLARDSON, R. K. & EICKE, R. W. (eds.) Semiconductors and Semimetals*. Elsevier.
- Daane, J. 2010. The Challenges Ahead for the Semiconductor Industry. Special Talk by CEO of Altera at the University of Toronto.
- Denardis, D., Doi, T., Hiskey, B., Ichikawa, K., Ichikawa, D. & Philipossian, A. 2006. Modeling Copper CMP Removal Rate Dependency on Wafer Pressure, Velocity, and Dissolved Oxygen Concentration. *Journal of the Electrochemical Society*, 153, G428-G436.
- Doering, R. & Nishi, Y. 2008. *Handbook of semiconductor manufacturing technology*, Boca Raton, CRC Press.
- Dornfeld, D. 2010. CMP Process Modeling for Improved Process Integration, Development and Control. *JSPS Japan Society for Precision Engineering* [Online]. Available: http://planarization-cmp.org/contents/houkoku/2002_message.html [Accessed July 28, 2010].
- Dyer, T. & Schlueter, J. 2002. Characterizing CMP pad conditioning using diamond abrasives. *Wet Surface Technology*, MICRO January 2002, 47-53.
- Feng, T. 2007. Pad conditioning density distribution in CMP process with diamond dresser. *IEEE Transactions on Semiconductor Manufacturing*, 20, 464-75.
- Forsberg, M., Andersson, J. & Jacobson, S. 2006. Geometrically Defined All-Diamond Abrasive Surfaces for Pad Conditioning in Chemical Mechanical Polishing. *Journal of The Electrochemical Society*, 153, G1-G6.
- Freeman, P. W. & Markert, L. 1996. Characterization of pad conditioning profiles in oxide CMP. *Chemical Mechanical Polish for ULSI Multilevel Interconnection Conference (CMP-MIC)*. Fremont, CA, USA.

- Fukushima, D., Tateyama, Y. & Yano, H. 2001. Impact of pad conditioning on CMP removal rate and planarity. *Advanced Metallization Conference (AMC)*. Montreal, Que., Canada: Materials Research Society.
- Fukuzawa, H. 2002. *Chemical-mechanical polishing apparatus*, US Patent 6364742.
- Garretson, C. C., Mear, S. T., Rudd, J. P., Prabhu, G., Osterheld, T., Flynn, D., Goers, B., Laraia, V., Lorentz, R. D., Swenson, S. A. & Thornton, T. W. 2000. New pad conditioning disc design delivers excellent process performance while increasing CMP productivity. *CMP Technology for ULSI Interconnection, SEMICON West 2000*.
- Goldberg, D. E. 1989. *Genetic algorithms in search, optimization, and machine learning*, Addison-Wesley Pub. Co.
- Hooper, B. J., Byrne, G. & Galligan, S. 2002. Pad conditioning in chemical mechanical polishing. *Journal of Materials Processing Technology*, 123, 107-13.
- Hornig, T.-L. 2003. An analysis of the pad deformation for improved planarization. *Key Engineering Materials*, 238-239, 241-246.
- Hua, Q.-F., Fang, H.-S. & Yuan, J.-L. 2009. Influencing Factors of Conditioning Effect about Polishing Pad Conditioning for Chemical Mechanical Polishing. *Light Industry Machinery*, 27, 48-51.
- Huang, W., Chou, C.-H. & Chou, C.-C. 2008. *Diamond disc manufacturing process* US Patent 7717972.
- Hwang, T., Baldoni, G., Vedantham, R. & Puthanangady, T. 2007. Optimized and Customized CMP Conditioner Design for Next Generation Oxide/Metal CMP. *International conference on Planarization/CMP Technology* berlin-Offenbach.
- I.T.R.S.Roadmap.Committee 2010. International Technology Roadmap for Semiconductors 2010 Update Overview. ITRS.
- Jackson, P. D., Schultz, S. C., Sanford, J. E., Ong, G., Rice, R. B., Modi, P. S. & Baca, J. G. 1995. *Conditioner for a polishing pad and method thereof*, US Patent 5456627.
- Jeong, I. 1999. *Chemical mechanical polishing systems including brushes and related methods*, US Patent 5961377.
- Jiang, B. & Muldowney, G. P. Year. Computational solid mechanics modeling of asperity deformation and pad-wafer contact in CMP. *In: 2007 MRS Spring Meeting, April 10, 2007 - April 12, 2007, 2007 San Francisco, CA, United States. Materials Research Society*, 39-44.

- Karuppiyah, L., Swedek, B., Thothadri, M., Hsu, W.-Y., Brezoczky, T. & Ravid, A. 2006. Overview of CMP Process Control Strategies. *11th International CMP-MIC Conference*. Fremont, California.
- Kim, N.-H., Seo, Y.-J. & Lee, W.-S. 2006. Temperature effects of pad conditioning process on oxide CMP: Polishing pad, slurry characteristics, and surface reactions. *Microelectronic engineering*, 83, 362-370.
- Krishnan, M., Nalaskowski, J. W. & Cook, L. M. 2009. Chemical Mechanical Planarization: Slurry Chemistry, Materials, and Mechanisms. *Chemical Reviews*, 110, 178-204.
- Lai, J.-Y. 2001. *Mechanics, Mechanisms, and Modeling of the Chemical Mechanical Polishing Process*. Doctor of Philosophy Dissertation, Massachusetts Institute of Technology.
- Lee, D. H., Kwon, D. J., Hong, Y. K. & Park, J. G. 2004. A 3D numerical study of the polishing behavior during an oxide chemical mechanical planarization process. *Key Engineering Materials*, 257-258, 433-8.
- Lee, J. H. & Yoon, S. W. 2008. *Apparatus And Method For Conditioning Polishing Pad For Chemical Mechanical Polishing Apparatus*, WO Patent 2008001970.
- Lee, S., Jeong, S., Park, K., Kim, H. & Jeong, H. 2009. Kinematical modeling of pad profile variation during conditioning in chemical mechanical polishing. *Japanese Journal of Applied Physics*, 48.
- Li, M., Zhu, Y., Li, J. & Lin, K. Year. Modeling of polishing pad wear in chemical mechanical polishing. *In: 10th International Conference on Machining and Advanced Manufacturing Technology*, November 7, 2009 - November 9, 2009, 2010 Jinan, China. Trans Tech Publications Ltd, 318-321.
- Li, Y. 2007. *Microelectronic Applications of Chemical Mechanical Planarization*, John Wiley & Sons.
- Li, Y. 2008. *Microelectronic Applications Of Chemical Mechanical Planarization*, Hoboken, New Jersey, John Wiley & Sons, Inc.
- Li, Z., Lee, H., Borucki, L., Rogers, C., Kikuma, R., Rikita, N., Nagasawa, K. & Philipossian, A. 2006. Effects of disk design and kinematics of conditioners on process hydrodynamics during copper CMP. *Journal of The Electrochemical Society*, 153, 399-404.
- Liao, Y. S., Hong, P. W. & Yang, C. T. 2004. A study of the characteristics of the diamond dresser in the CMP process. *Key Engineering Materials*, 257-258, 371-6.

- Liao, Y. S. & Yang, C. T. 2009. Investigation of the wear of the pad conditioner in chemical mechanical polishing process. *Advanced Materials Research*, 76-78, 195-200.
- Lim, K. P. & Lee, K. E. 2007. *Real time monitoring of CMP pad conditioning process* US Patent 7300338.
- Lin, Y.-Y., Lo, S.-P., Lin, S.-L. & Chiu, J.-T. 2008. A hybrid model combining simulation and optimization in chemical mechanical polishing process. *Journal of materials processing technology*, 202, 156-64.
- Lu, G., Lu, G. Q. & Xiao, Z. M. 1999. Mechanical Properties of Porous Materials. *Journal of Porous Materials*, 6, 359-368.
- Lu, H., Fookes, B., Obeng, Y., Machinski, S. & Richardson, K. A. 2002. Quantitative analysis of physical and chemical changes in CMP polyurethane pad surfaces. *Materials Characterization*, 49, 35-44.
- Lujan, R. J. 2006. *Off-line tool for breaking in multiple pad conditioning disks used in a chemical mechanical polishing system*, US Patent 7371156.
- Machinski, S., Richardson, K. & Easter, W. 2001. Microstructural Characterization of CMP Polyurethane Polishing Pads. In: OPILA, R. L., REIDSEMA-SIMPSON, C., SUNDARAM, K. B. & SEAL, S. (eds.) *Chemical mechanical planarization IV*. Pennington, New Jersey: Electrochemical Society.
- Manocha, C., Kumar, A. & Gupta, V. K. 2010. Study of conditioner abrasives in chemical mechanical planarization. *2009 MRS Spring Meeting*. San Francisco, CA, United states: Materials Research Society.
- Mcgrath, J. & Davis, C. Year. Combining a finite element model and a removal model to evaluate the effect of wafer and pad shape on removal in CMP. In, 2003 Orlando, FL., United states. Electrochemical Society Inc., 305-312.
- Mudhivarthi, S., Gitis, N., Kuiry, S., Vinogradov, M. & Kumar, A. 2006. Effect of temperature on pad conditioning process during chemical-mechanical planarization. *11th International CMP-MIC Conference*. Fremont, California.
- Myoung, B. Y. & Yu, S. N. 2004. *Conditioner for polishing pad and method for manufacturing the same*, US Patent 6818029.
- Nanz, G. & Camilletti, L. E. 1995. Modeling of chemical-mechanical polishing: a review. *IEEE Transactions on Semiconductor Manufacturing*, 8, 382-9.

- Nishioka, T., Iwami, S., Kawakami, T., Tateyama, Y., Ohtani, H. & Miyashita, N. 2001. Modeling on mechanical properties of polishing pads in CMP process. *Chemical-Mechanical Polishing 2000 - Fundamentals and Materials Issues. Symposium*. Warrendale, PA, USA: Mater. Res. Soc.
- Ohi, T. 2004. Trends and future developments for diamond CMP pad conditioners. *Industrial Diamond Review*, 64, 14-17.
- Park, J. 2005. CMP Pad Conditioners. *Shinhan Diamond Presentation, Semiconductor TFT*.
- Pei-Lum, T. & Rick, H. 2007. Estimating chemical mechanical polishing pad wear with compressibility. *International Journal of Advanced Manufacturing Technology*, 32, 682-9.
- Pei-Lum, T., Zhe-Hao, H., Sheng-Wei, C. & Cheng-Yi, S. 2009. Study on the CMP pad life with its mechanical properties. *Key Engineering Materials*, 389-390, 481-6.
- Philipossian, A. & Olsen, S. 2003. Fundamental Tribological and Removal Rate Studies of Inter-Layer Dielectric Chemical Mechanical Planarization. *Japanese Journal of Applied Physics, Part 1: Regular Papers and Short Notes and Review Papers*, 42, 6371-6379.
- Pietsch, G. J. & Kerstan, M. 2005. Understanding simultaneous double-disk grinding: operation principle and material removal kinematics in silicon wafer planarization. *Precision Engineering*, 29, 189-196.
- Prasad, A. 2007. *Method for manufacturing microporous CMP materials having controlled pore size*, US Patent 7311862.
- Preston, F. W. 1927. The theory and design of plate glass polishing. *Society of Glass Technology -- Journal*, 11, 214-256.
- Pysher, D., Goers, B. & Zabasajja, J. Year. Design, characteristics and performance of diamond pad conditioners. *In: 2010 MRS Spring Meeting, April 5, 2010 - April 9, 2010, 2010 San Francisco, CA, United states. Materials Research Society*, 67-74.
- Qi, H. J., Joyce, K. & Boyce, M. C. 2003. Durometer Hardness and the Stress-Strain Behavior of Elastomeric Materials. *Rubber Chemistry and Technology*, 76, 419-435.
- Qin, N., Guo, D. M., Kang, R. K. & Huo, F. W. 2009. Effect of conditioning parameters on surface non-uniformity of polishing pad in chemical mechanical planarization. *Key Engineering Materials*, 389-390, 498-503.

- Reed, P., Minsker, B. & Goldberg, D. E. 2000. Designing a competent simple genetic algorithm for search and optimization. *Water Resour. Res.*, 36, 3757-3761.
- Renner, G. 2004. Genetic algorithms in computer-aided design. *Computer-Aided Design and Applications*, 1, 691-700.
- Ridha, M. 2007. *Mechanical and Failure Properties of Rigid Polyurethane Foam Under Tension*. Doctor of Philosophy Thesis, National University of Singapore.
- Rodel 2001. Rodel IC1400 CMP Pad Product Brochure.
- Rohm and Haas 2004. IC 1000 Polishing Pad Product Brochure.
- Seike, Y., Denardis, D., Sugiyama, M., Miyachi, K., Doi, T. & Philipossian, A. 2005. Development and analysis of a high-pressure micro jet pad conditioning system for interlayer dielectric chemical mechanical planarization. *Japanese Journal of Applied Physics, Part 1: Regular Papers and Short Notes and Review Papers*, 44, 1225-1231.
- Seike, Y., Lee, H.-S., Takaoka, M., Miyachi, K., Amari, M., Doi, T. & Philipossian, A. 2006. Development of a pad conditioning process for interlayer dielectric CMP using high-pressure micro jet technology. *Journal of The Electrochemical Society*, 153, 223-228.
- Seo, H.-D., Lee, S.-H. & Jeong, H.-D. 1999. Characterization Of The Composite Conditioning Aided By Ultrasonic Vibration. *Electrochemical Society Proceedings*, Vol 99-37, 445-451.
- Sexton, M. J. 2009. *Characterization of Chemical-Mechanical Planarization Pads with X-Ray Microtomography and Finite Element Modeling*. Master of Science Thesis, Drexel University.
- Shimizu, A. 2010. *CMP conditioner and method of manufacturing the same*, US Patent Application 20100273402.
- Shon-Roy, L. 2012. CMP Market Outlook and New Technology - Dynamic Slurry Metrology. *Electronic Materials Information*. Techcet Electronic Materials.
- Singh, R. K., Galpin, A., Smith, J. & Wargo, C. R. 2011. New Developments in the Characterization of CMP Pad Conditioners. *Levitronix CMP & Ultrapure Fluid Handling Conference*. Westin Park Central Dallas, TX.
- Skocypec, R., La Belle, A. & Whisler, W. 2007. *Method and apparatus for conditioning a polishing pad*, US Patent 7175510 B2.

- Sun, T., Borucki, L., Zhuang, Y. & Philipossian, A. 2010. Investigating the effect of diamond size and conditioning force on chemical mechanical planarization pad topography. *Microelectronic Engineering*, 87, 553-559.
- Sung, C.-M. 2007. Contoured CMP pad dresser and associated methods, US Patent Application 7201645.0
- Sung, J. C. 2005. The Next Generation Diamond Pad Conditioners for Chemical Mechanical Planarization. *Kinik-USA whitepaper*.
- Sung, J. C. 2006. PCD Planer for Dressing CMP Pads. *11th International CMP-MIC Conference*. Fremont, California.
- Sung, J. C., Chou, C.-S., Chen, Y.-T., Chou, C.-C., Pai, Y.-L., Hu, S.-C. & Sung, M. 2009. Polycrystalline Diamond (PCD) shaving dresser: The Ultimate Diamond Disk (UDD) for CMP pad conditioning. *ISTC/CSTIC 2009*. 1 PART 1 ed. Shanghai, China: Electrochemical Society Inc.
- Sung, J. C. & Kan, M.-C. 2006. The In-Situ Dressing of CMP Pad Conditioners with Novel Coating Protection. *11th International CMP-MIC Conference*. Fremont, California.
- Sung, J. C., Ming-Yi, T., Aoki, M., Cheng-Shiang, C. & Sung, M. 2008. PCD pad conditioners for low pressure chemical mechanical planarisation of semiconductors. *International Journal of Abrasive Technology*, 1, 327-55.
- Thear, E. & Kimock, F. 2004a. Chemical mechanical planarization (CMP)-Factors controlling the consistency of conditioning July 2010. Available: <http://www.azom.com/details.asp?ArticleID=3633> [Accessed July 2010].
- Thear, E. & Kimock, F. 2004b. Improving productivity through optimization of the CMP conditioning process. Available: http://www.morgantechnicalceramics.com/resources/technical_articles/improving-productivity-through-optimization-of-the-cmp-conditioning-process/?page_index=1.
- Tsai, M.-Y. 2010a. Polycrystalline diamond shaving conditioner for CMP pad conditioning. *Journal of materials processing technology*, 210, 1095-1102.
- Tsai, M.-Y., Chen, S.-T., Liao, Y.-S. & Sung, J. 2009. Novel diamond conditioner dressing characteristics of CMP polishing pad. *International Journal of Machine Tools and Manufacture*, 49, 722-729.
- Tsai, M. Y. Year. Blade diamond disk for conditioning CMP polishing pad. *In: 2009 International Conference on Manufacturing Science and Engineering, ICMSE*

- 2009, December 26, 2009 - December 28, 2009, 2010b Zhuhai, China. Trans Tech Publications, 3-6.
- Tsai, M. Y. & Sung, J. C. Year. Dressing behaviors of PCD conditioners on CMP polishing pads. *In: 12th International Symposium on Advances in Abrasive Technology, ISAAT2009, September 27, 2009 - September 30, 2009, 2009 Gold Coast, QLD, Australia.* Trans Tech Publications, 201-206.
- Tso, P. L. & Ho, S. Y. 2004. A study on the dressing rate in CMP pad conditioning. *Key Engineering Materials*, 257-258, 377-80.
- Tyan, F. 2007. Pad conditioning density distribution in CMP process with diamond dresser. *IEEE Transactions on Semiconductor Manufacturing*, 20, 464-75.
- Unknown 2009. Product Brochure for Norton AP360 Advanced CMP Pad Conditioner for Oxide and Metal Wafer Processing. Worcester, MA: Saint-Gobain Abrasives, Inc.
- Wang, C., Paul, E., Kobayashi, T. & Li, Y. 2008. Pads for IC CMP. *In: LI, Y. (ed.) Microelectronic Applications of Chemical Mechanical Planarization.* Hoboken, New Jersey: John Wiley & Sons, Inc.
- Wiegand, S. & Stoyan, D. 2006. Stochastic models for pad structure and pad conditioning used in chemical-mechanical polishing. *Journal of Engineering Mathematics*, 54, 333-43.
- Wielonski, R. F. & Peterman Jr., L. M. 2007. *CMP diamond conditioning disk* US Patent 7300338.
- Wilson, P. 2011. Maintaining US leadership in Semiconductors. *AAAS Annual Meeting.* Washington DC, USA: American Association for the Advancement of Science.
- Wolfgang, M. A. 2002. The International Technology Roadmap for Semiconductors— Perspectives and challenges for the next 15 years. *Current Opinion in Solid State and Materials Science*, 6, 371-377.
- Wright, A. 1991. Genetic Algorithms for Real Parameter Optimization. *In: RAWLINS, G. (ed.) Foundations of genetic algorithms.* Morgan Kaufmann.
- Yan, B., Zhang, X.-M. & Lu, X. 2004. Model of material removal rate during chemical mechanical planarization of microelectronic materials. *Gongcheng Lixue/Engineering Mechanics*, 21, 126-131.

- Yang, J., Oh, D., Kim, H. & Kim, T. 2010. Investigation on Surface Hardening of Polyurethane Pads During Chemical Mechanical Polishing (CMP). *Journal of Electronic Materials*, 39, 338-346.
- Yang, X.-S. 2012. Multiobjective firefly algorithm for continuous optimization. *Engineering with Computers*, 1-10.
- Yeh, H.-M. & Chen, K.-S. 2010. Development of a pad conditioning simulation module with a diamond dresser for CMP applications. *International Journal of Advanced Manufacturing Technology*, 50, 1-12.
- Zantye, P. B., Kumar, A. & Sikder, A. K. 2004. Chemical mechanical planarization for microelectronics applications. *Materials Science and Engineering R: Reports*, 45.
- Zhang, X., Wang, H., Huang, Q., Kumar, A. & Zhai, J. Year. Statistical and experimental analysis of correlated time-varying process variables for conditions diagnosis in chemicalmechanical planarization. *In*, 2009 445 Hoes Lane / P.O. Box 1331, Piscataway, NJ 08855-1331, United States. Institute of Electrical and Electronics Engineers Inc., 512-521.
- Zhang, X. H., Pei, Z. J. & Fisher, G. K. Year. Chemical mechanical polishing of silicon wafers: Finite element analysis of wafer flatness. *In*, 2005 New York, NY 10016-5990, United States. American Society of Mechanical Engineers, 893-900.
- Zhang, X. H., Pei, Z. J. & Fisher, G. R. Year. Measurement methods of pad properties for chemical mechanical polishing. *In*, 2008 New York, NY 10016-5990, United States. American Society of Mechanical Engineers, 517-522.
- Zhenyu, K., Oztekin, A., Beyca, O. F., Phatak, U., Bukkapatnam, S. & Komanduri, R. 2010. Process Performance Prediction for Chemical Mechanical Planarization (CMP) by Integration of Nonlinear Bayesian Analysis and Statistical Modeling. *IEEE Transactions on Semiconductor Manufacturing*, 23, 316-27.
- Zhou, Y.-Y. & Davis, E. C. 1999. Variation of polish pad shape during pad dressing. *Materials Science and Engineering B: Solid-State Materials for Advanced Technology*, 68, 91-98.
- Zhou, Z., Yuan, J., Lv, B. & Zheng, J. Year. Study on pad conditioning parameters in silicon wafer CMP process. *In*, 2008 Laubisrutistr.24, Stafa-Zuerich, CH-8712, Switzerland. Trans Tech Publications Ltd, 309-313.
- Zwicker, G., Borst, C., Economikos, L. & Philipossian, A. 2007. Advances and Challenges in Chemical Mechanical Planarization. *MRS Spring Meeting*. San Francisco, CA, United States: Materials Research Society.

APPENDIX I

SELECTED PAD CONDITIONING ANALYTICAL MODELS

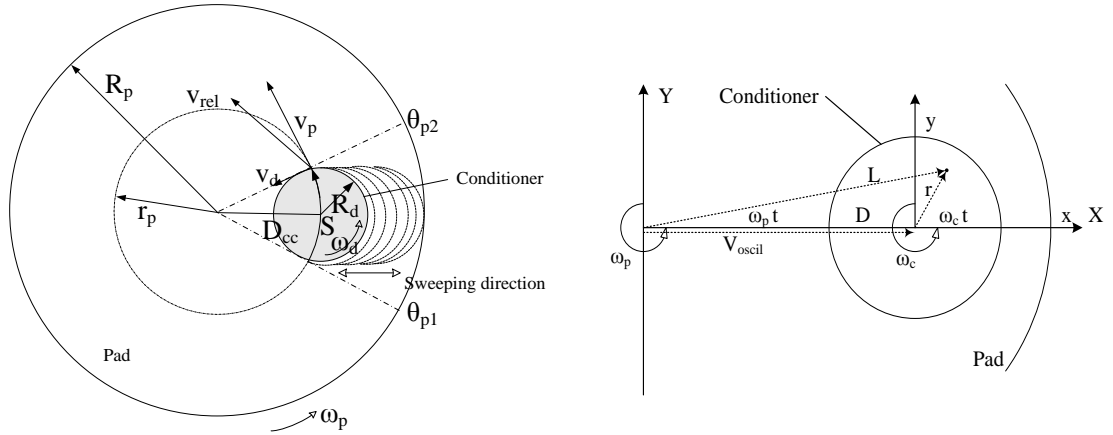


Figure I. Representative figure for Chen et al's model, 2000 **Figure II. Representative figure for Chang et al's model, 2007**

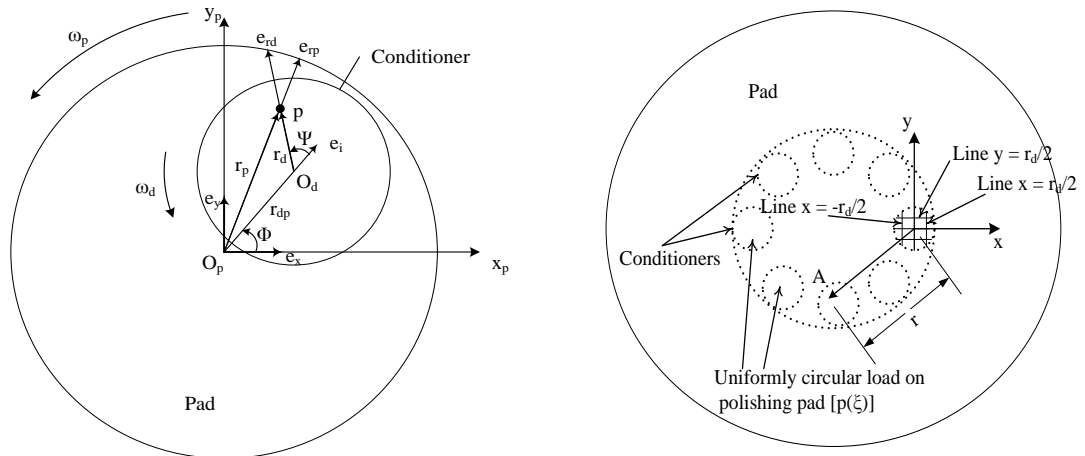


Figure III. Representative figure for Tyang's model, 2005 **Figure IV. Representative figure for Horng's model, 2003**

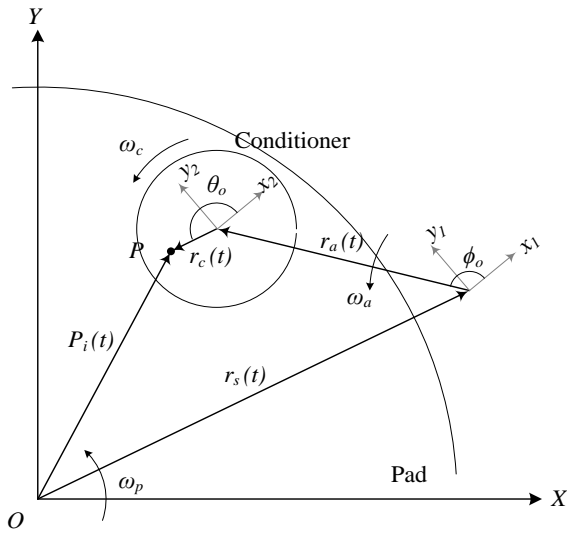


Figure V. Representative figure for Lee's model, 2009

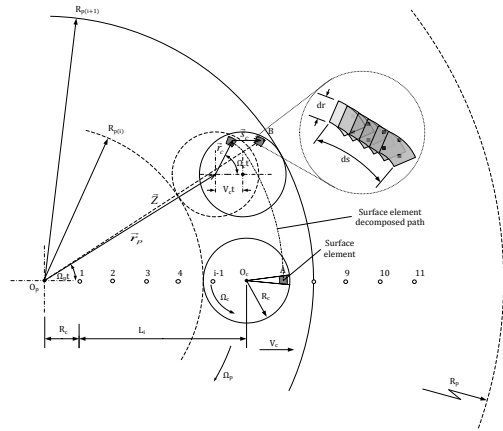


Figure VI. Representative figure for Baisie's model, 2010

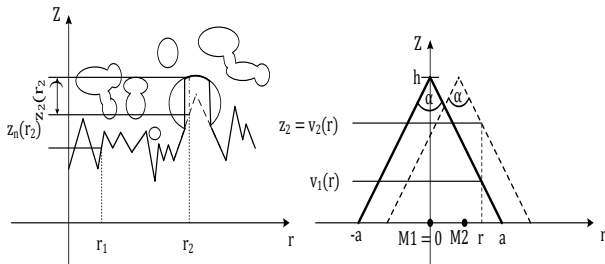


Figure VII. Representative figure for Wiegand and Stoyan's model, 2006

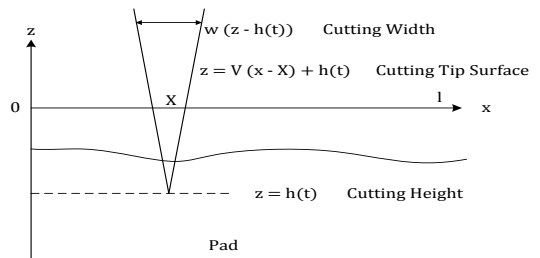


Figure VIII. Representative figure for Borucki's model, 2004

Table I Summary of selected pad conditioning analytical models

Liao et al's Model (2004)		
Assumptions:	Proposed Analytical Model:	Main Conclusions:
<ul style="list-style-type: none"> ▪ Conditioning is likened to metal cutting to derive power consumed to remove unit volume of pad. ▪ $P = \Delta P$ since P, the rate of total energy consumed in conditioning process is almost linearly proportional to ΔP, CMP machine power consumption. ▪ Grit size effect and hardness of pad are taken into account. 	$\Delta P = K \frac{D^a F^b}{N^c w^d} \quad (2)$ <p> <i>D</i> -dressing rate <i>F</i> - downforce <i>N</i> -total number of working diamonds <i>w</i> -average groove width scribed by the diamonds <i>K, a, b, c</i> and <i>d</i> are all constants </p>	<ol style="list-style-type: none"> 1. Dressing rate <i>D</i> is related to power consumption of the CMP machine. 2. Except down force, dressing rate model developed consists only of design parameters of a conditioner. 3. More practical since Preston equation used by others includes down force and pad speed which are usually fixed by CMP machine makers and difficult to adjust.
Tso and Ho's Model (2004)		
Assumptions:	Proposed Analytical model:	Main Conclusions:
<ul style="list-style-type: none"> ▪ Inference is made to the lapping model of ductile material. 	$\begin{aligned} & \text{Dressing Rate} \\ & = K_D \frac{V_D}{R \cdot A} \lambda d_0 \left(\frac{P}{H_p} \right)^{1.5} \end{aligned} \quad (3)$ <p> <i>K_D</i> - dressing rate constant <i>A</i> -dressing area <i>λ</i> - density of abrasive distribute <i>V_D</i> -conditioning velocity <i>R</i> -knife-edge of diamond grit <i>d₀</i> - size of abrasive diameter <i>λ d₀</i> -separation between diamonds <i>H_p</i> -hardness of polishing pad <i>P</i> -conditioning pressure </p>	<ol style="list-style-type: none"> 1. Since conditioning pressure and velocity directly influence the dressing rate of pad significantly, selection must be for lower conditioning pressure and velocity in a prerequisite of ideal conditioning effects to avoid the excessive pad removal. 2. Longer soaking time increases dressing rate. 3. pH value of slurry influences the intensity of the diamond grit on the diamond conditioner.
Lee et al's Model (2009)		
Assumptions:	Proposed Analytical Model:	Main Conclusions:
<ul style="list-style-type: none"> ▪ A Preston-type relationship is applied to analyze the pad wear. ▪ Conditioner induces uniform pressure on pad and there is constant contact between them. ▪ Pad properties are isotropic. ▪ Point diamond grits are distributed uniformly on conditioner. ▪ Dwell time at turning points of swing arm are negligible. 	$= k_c \cdot p_c \cdot \left[\frac{1}{a_j} \sum \int_{t_{j,in}}^{t_{j,out}} v_i(t) dt \right] \quad (4)$ <p> <i>q_j</i>- wear amount at minute circular pad area <i>k_c</i> - constant related to conditioning <i>p_c</i> - conditioning pressure <i>a_j</i> - <i>j</i>th minute circular pad area <i>v_i(t)</i> – velocity of point P relative to pad </p>	<ol style="list-style-type: none"> 1. There is close correlation among conditioner velocity profiles, sliding distance distribution and pad surface profile.

Chen et al's Model (2000)		
Assumptions:	Proposed Analytical Model:	Main Conclusions:
<ul style="list-style-type: none"> ▪ For a given position, relative velocity (V_{rel}) is a function of pad speed (V_p), conditioner speed (V_d) and the center to center distance (D_{cc}). ▪ For a given radial position pad is conditioned by a disc for a range of D_{cc} i.e. , $r_p - R_d \leq D_{cc} \leq r_p + R_d$ ▪ The generalized Preston equation is employed to describe pad wear rate. ▪ Local pressure $P(r_p)$ at radial position is inversely proportional to local wear thickness $\Delta h(r_p)$. ▪ \bar{P} is constant and $\Delta \bar{h}$ is known. 	$WR = \frac{\Delta h}{\Delta t} = K_p P^\alpha V_{avg,s}^\beta \quad (5)$ $\frac{\Delta h}{\Delta t} = K_p \left[\frac{\bar{P}}{\Delta h / \Delta \bar{h}} \right]^\alpha V_{avg,s}^\beta \quad (6)$ <p> WR -Wear Rate $V_{avg,s}$ - sweeping averaged velocity Δh - wear thickness of pad $\Delta \bar{h}$ - averaged wear thickness of pad across radial position Δt - actual conditioning time P - pressure \bar{P} - averaged pressure K_p - constant </p>	<ol style="list-style-type: none"> 1. The velocity term ($V_{avg,s}$) plays a relatively insignificant role. What is important is the actual conditioning time Δt therefore optimizing its distribution is essential to achieving uniformity 2. For pad profile optimization: <ul style="list-style-type: none"> • Set the angular velocity of disc and platen close while maintaining a small difference (eg make the disc-radius-to-pad-radius as small as possible. • Let the disc diameter be an integer multiple of the sweeping range. • Widen the sweeping range. • Increase the number of zones.
Baisie et al's Model (2010)		
Assumptions:	Proposed Analytical Model:	Main Conclusions:
<ul style="list-style-type: none"> ▪ For each cycle, conditioner sweeps once over the radius of the pad in a predetermined manner. ▪ Average conditioning pressure is constant. ▪ Wear thickness is directly proportional to swept area (sum of surface elements) and inversely proportional to pad surface area. 	$A_{swept(i)} = \int_0^{2\pi} \int_0^{R_c} \int_0^{t_i} \sqrt{\dot{\varphi}^2 r^2 + \dot{r}^2} dt dr_c d\varphi \quad (7)$ $\Delta h_i = k \cdot N \cdot \frac{A_{swept(i)}}{\pi \cdot (L_{i+1} + 2R_c)^2 - \pi \cdot L_i^2} \quad (8)$ <p> $A_{swept(i)}$ - area swept along conditioner trajectory during segment sweeping time t_i. R_c - conditioner radius (r, φ) - polar form representation of trajectory function Δh_i - pad sectional wear k - constant N - number of sweeping cycles L - initial position of conditioner center </p>	<ol style="list-style-type: none"> 1. When the total conditioning time remains constant, the segment sweeping time does not affect the pad surface shape. 2. The sweeping profile has a “mirroring” effect on the pad surface shape. Thus the flat sweeping profile gives the best pad shape. 3. Higher pad rotating speed generates more pad wear and makes the pad surface shape more concave. 4. The conditioner rotating speed exhibits a much weaker effect on the pad surface shape than the pad rotating speed. 5. The smaller the conditioner diameter, the flatter the pad surface shape.

Hornig's Model (2003)		
Assumptions:	Proposed Analytical Model:	Main Conclusions:
<ul style="list-style-type: none"> ▪ Contact surface between conditioner and polishing pad is regarded as a smooth plane. ▪ Conditioning model is simplified as plate subjected to multi-uniformly circular load. ▪ Several conditioners are working simultaneously. 	<p> ν - poisson ratio E - Young's modulus $P(\xi)$ - pressure applied on plate r_d - radius of circular load N_d - number of conditioners H - pad thickness </p> <p>Deformation of a point along line $y = 0$ due to the load on a line parallel to the x-axis with a length of $2\sqrt{r_d^2 - \xi^2}$ and a width of $d\xi$ is represented by $\omega(r, 0, z)$</p> <p>Deformation of pad subjected to single conditioner along the radial direction is calculated relative to the reference point ($r=0, z=H$) in the half space. Thus, the relative displacement between ($r, 0, 0$) and ($0, 0, H$), due to the uniform load from $\xi = -rd$ to $\xi = rd$ is given as</p> $u_i(r) = \int_{-r_d}^{r_d} (\omega(r, 0, 0) - \omega(0, 0, H)) d\xi, \quad i = 1, 2, \dots, N_d \quad (9)$ <p>Total deformation can be given as</p> $\delta_{total} = \sum_{i=1}^{N_d} u_i(r) \quad (10)$	<ol style="list-style-type: none"> 1. When the depth of pad, H increases, the deformation increase due to the decrease in pad stiffness. 2. For the line parallel to the y-axis, the deformation in negative direction of x-coordinate is always larger than those of positive direction because the circular load causes maximum deformation value in center, and this condition is also true for the line parallel to x-axis. 3. For the line parallel to the x-axis, when the distance measured from original point increases, the deformation decreases. 4. For the y-coordinates, the deformation in negative direction is always larger than those of positive direction because the effect of multi-circular load is stronger in negative y-coordinate.

Chang et al's Model (2007)		
Assumptions:	Proposed Analytical Model:	Main Conclusions:
<ul style="list-style-type: none"> ▪ A Preston-type relationship is applied to analyze the pad wear rate under constant pressure. ▪ The oscillation velocity of the conditioner is neglected to analyze the relative velocity distribution. ▪ Properties of all consumables such as slurry and pad, etc. are homogenous. ▪ The pad wear amount at a given point on the pad is the average value of the integration of the pad wear amount with respect to the time. 	<p> ω_c - angular velocity of conditioner wheel ω_p - angular velocity of pad, D - distance between pad rotation center and conditioner wheel rotation center r - radial distance between given point on the conditioner wheel and conditioner center V_{oscill} - oscillation velocity of the conditioner moving on pad. $v_{p/c}$ - relative velocity of point on pad with respect to conditioner </p> <p> $S = S(L)$ = Sliding distance on the pad is given as; </p> $S = \int_0^{t'} v_{p/c} dt$ $= 2D \cos^{-1} \left(\frac{D^2 + L^2 - r_c^2}{2DL} \right) \times \left\{ R + \frac{(\rho' \zeta')^2}{4R} \left(\frac{R-1}{R} \right) + \rho' \zeta' \right\}$ <p style="text-align: center;">(11)</p> <p> $H_{avg}(L_l)$, can be considered as the pad wear amount at radial distance, L_l. (calculated by using Simpson's Approximation Method with the MATLAB Program) is given as </p> $H_{avg}(L) = \frac{1}{2\pi L} \int_0^{t'} H dt = \frac{1}{2\pi L} \int_0^{t'} kps dt$ $= \frac{kp}{2\pi L} \int_0^{t'} S(D, R) dt$ <p style="text-align: center;">(12)</p> <p> $R(t)$ - rotation-velocity ratio (ω_c/ω_p) function $D(t)$ - distance between the rotation centers function t' - half of the oscillation period </p>	<ol style="list-style-type: none"> 1. The spatial distribution of the sliding distance on the pad is not uniform, but has a concave shape according to the rotation-velocity ratio, R. 2. Longer conditioning induces higher concavity of the polishing pad. 3. The profile of the pad wear amount can be controlled by combining the critical parameters, $D(t)$ and $R(t)$.

Tyan's Model (2007)		
Assumptions:	Proposed Analytical Model:	Main Conclusions:
<ul style="list-style-type: none"> ▪ The diamond grains are uniformly distributed. ▪ A slow sweeping motion is applied during dressing 	<p>The ensemble of the whole trajectories on the pad;</p> $\bigoplus_{j=1}^{N_d} \begin{bmatrix} \rho_{pj} \cos(\psi_{pj}) \\ \rho_{pj} \sin(\psi_{pj}) \end{bmatrix} =$ $R - (-\tau)R(\omega_{dn}\tau) \times \left\{ \bigoplus_{j=1}^{N_d} \begin{bmatrix} \rho_{dj} \cos(\psi_{dj}) \\ \rho_{dj} \sin(\psi_{dj}) \end{bmatrix} \right\} + R(-\tau) \begin{bmatrix} \rho_c(\tau) \\ 0 \end{bmatrix} \quad (13)$ <p>Where (ρ_{pj}, ψ_{pj}) - j^{th} polishing trajectory generated by the j^{th} single diamond grain located at (ρ_{dj}, ψ_{dj}) on a conditioner having N_d number of grains</p> <p>Wear experienced at a point is proportional to the conditioning density (CD) = (time) average of total segment length per unit area in the radial direction.</p> $CD(\rho_p) = \frac{1}{T} \int_0^T \lim_{d\rho_p \rightarrow 0} \frac{\sum_{j \in I(\rho_p)} \frac{dl_j}{d\tau} d\tau}{2\pi\rho_p d\rho_p} \quad (14)$ <p>ρ_p - assigned radius on polishing pad T - elapsed time in domain $= (2\pi/\omega_{sn})$ dl_j - length of trajectory segment caused by the grain 'j' located at (ρ_{dj}, ψ_{dj}) on conditioner $I(\rho_p) \triangleq [j \mid \rho_p \leq \rho_{pj} \leq \rho_p + d\rho_p, j = 1, \dots, N_d]$, which is the set of indexes for which the corresponding trajectories fall within the annular area $2\pi\rho_p d\rho_p$ on the pad (note that $I(\rho_p)$ is time varying in general)</p>	<ol style="list-style-type: none"> 1. To have flat distribution of pad wear rate, the ratio of disk-radius to pad-radius has to be made as small as possible. 2. The effect of the pattern of grain distribution on conditioning density function is insignificant. 3. A slow simple harmonic sweeping process cannot achieve a uniform profile in the CD.

Wiegand and Stoyan's Model (2006)		
Assumptions:	Proposed Analytical Model:	Main Conclusions:
<ul style="list-style-type: none"> ▪ The pad surface is modeled as a , piece of a homogeneous (stationary) and ergodic random field $[Zn(x)]$, ▪ x is given in polar coordinates $x = (r, \theta)$ with $0 \leq r \leq r_{pad}$ and $0 \leq \theta \leq 2\pi$. ▪ $Zn(x)$ is the surface depth of the pad at the point x at time n and is non-negative. ▪ The discretized time n depends on rotation speed ω of pad. ▪ The starting value of the pad surface depth is $Z_0(x) \equiv 0$. ▪ Since stationarity is assumed, the one-dimensional distribution function of the random field: ▪ $F_n(z) = P(Zn(x) \leq z)$ ▪ Conditioner stays at a fixed depth and the effect of a conditioner disk is approximated by the effect of a one-dimensional bar conditioner. The N cutting elements of the disk are assumed to be arranged on a line with mean spacing l, $l \leq r_{pad}$ 	<p>In the case of a solid pad the probability density function of surface depth after n cuts is;</p> $f_n(z) = \begin{cases} \frac{n}{h} \exp\left(\frac{n}{h}z - h\right) & \text{if } z \geq h \\ 0 & \text{if } z < 0 \end{cases} \quad (15)$ <p>Density function for random variable of additional depth at r caused by a cut pore is;</p> $g(z) = \begin{cases} p\delta(z) + (1-p)h_1(z) & \text{if } z \geq h \\ 0 & \text{if } z < 0 \end{cases} \quad (16)$ <p>Linear contact distribution function H_l in case of a Boolean model is;</p> $h_l(z) = \lambda_2 \exp(-\lambda_2 z) \quad (17)$ <p>For conditioning of a foamed pad, the probability density function of Z_n^* is obtained by convolution (*) as;</p> $f(z) = f_n(z) * g(z) = \begin{cases} \frac{\frac{n}{h}(1-p)\lambda_2}{\frac{n}{h} + \lambda_2} (\exp(\lambda_2(h-z)) - \exp(-n - \lambda_2 z)) & \text{if } z > h \\ p \frac{n}{h} \exp\left(\frac{n}{h}(z-h)\right) + \frac{\frac{n}{h}(1-p)\lambda_2}{\frac{n}{h} + \lambda_2} \left(\exp\left(\frac{n}{h_2}z - n\right) - \exp(-n - \lambda_2 z)\right) & \text{if } 0 \leq z \leq h \\ 0 & \text{if } z < 0 \end{cases} \quad (18)$	<ol style="list-style-type: none"> 1. Large h produce much pad removal; shortens pad lifetime therefore a small cutting depth h is intended in industry. 2. Conditioning has to be applied for longer times, n to remove irregularities on pad surface 3. For pad parameter λ_2, If pad is too smooth, pores are small with low variation, λ_2 is large, right function tail is short and steep), removal will be too small. 4. If pad is too rough (a high degree of variability, a long right tail), there is large removal variation and consequently a rough wafer surface.

Borucki's Model (2004)		
Assumptions:	Proposed Analytical Model:	Main Conclusions:
<ul style="list-style-type: none"> ▪ The cutting surface of tool has an array of identical diamond tips, which are assumed to be triangular with opening angle α, ▪ The theory uses the average furrow shape cut or plowed by conditioner diamonds on a solid pad. ▪ The conditioner rotates slowly enough that each diamond cuts a non self-intersecting furrow on each pad rotation. ▪ The average density of furrows (#/unit length) at each pad radius is independent of the conditioner rotation rate. ▪ A circular conditioner can be replaced by an equivalent bar conditioner that creates the same density of new furrows by the end of each half sweep. ▪ The ability of any diamond to cut the pad material is not dependent on the shape of the pad-surface it encounters. 	<p><i>For a moving conditioner on a solid pad:</i> Surface height probability density function , (PDF) - probability of finding a point between z and $z+dz$ is given as;</p> $\phi(z, t) = \frac{\frac{\Omega}{\pi cvl}(z - h_o + ct)}{1 - \exp\left[-\frac{\Omega}{2\pi cvl}(h_o - ct)^2\right]} \times \exp\left(-\frac{\Omega}{2\pi cvl}(z - h_o + ct)^2\right)$ <p>Average surface height is given as;</p> $\bar{s}(t) = \frac{1}{1 - e^{-\Lambda}} \left(1 - \frac{\sqrt{\pi} \operatorname{erf}(\sqrt{\Lambda})}{2\sqrt{\Lambda}}\right) (h_o - ct)$ <p>RMS(root mean square) roughness as measured by the standard deviation $\sigma(t_n)$ is given as;</p> $\sigma^2(t) \sim \frac{(4 - \pi)\pi cvl}{2\Omega} \quad t \rightarrow \infty$ <p><i>For foamed pad during simultaneous conditioning and wear:</i> Complementary Cumulative Density Function (CCDF) i.e. density of the remaining pad material at a given height z at time t is given as;</p> $q_f(z, t) = \int_z^0 q(\zeta, t) \Phi(z - \zeta) d\zeta$ <p>(foamed) (solid) (intrinsic)</p>	<ol style="list-style-type: none"> 1. Model relates the foamed pad CCDF to that of an identically conditioned virtual solid pad via a convolution involving the foamed pad intrinsic PDF. 2. Results agree with the corresponding Monte Carlo simulations. 3. Conditioning and wear of a foamed pad is modeled by combining the virtual solid pad evolution equation with the fundamental convolution that relates the solid and foamed pad CCDFs.

Borucki's Model (2006)		
Assumptions:	Proposed Analytical Model:	Main Conclusions:
<p>The theory consists of three main parts: a theory of conditioning, a theory of the coefficient of friction (COF), and a removal rate theory.</p>	<p>Measure of surface abruptness is given as;</p> $\lambda(L) = \frac{2\pi\Delta s}{\Omega w_{max}} \frac{c(L)}{a(L)} \quad (23)$ <p>ω - pad rotating speed in Radians/sec, L - Conditioner load c - cut rate Δs - center-to-center length of sweep a - total number of actively cutting diamonds.</p> <p>Viscous contribution to the COF from contacting asperities is approximately</p> $\mu_{visc} \approx 0.9(\mu_0 V(1 - v^2)/E)^{0.36} k_z^{0.19} \lambda^{-0.17} \quad (24)$ <p>K_s - mean asperity summit curvature V - sliding speed, μ_0 - fluid viscosity, E - pad Young's modulus, ν - Poisson ratio, μ_{visc}^1 - value of μ_{visc} when K_s and λ are both 1.</p> <p>Material removal rate includes chemical rate k_1 and mechanical rate k_2 given as;</p> $RR = \frac{M_w}{\rho_{ck}} \frac{k_1 k_2}{k_1 + k_2}$ $k_1 = A \exp\left(-\frac{E}{kT}\right), \quad k_2 = c_p \mu_k p V \quad (25)$ <p>A, c_p are empirical constants, E -activation energy of the rate limiting chemical step P - applied polishing pressure T - reaction temperature</p>	<p>1. A causal connection involving pad surface abruptness can be traced theoretically between a conditioner design feature (grit size) and operating mode (load) and the resulting removal rates and friction coefficients.</p>

APPENDIX II

PUBLISHED EXPERIMENTAL DATA

CHARACTERIZATION OF PAD CONDITIONING PROFILES

IN OXIDE CHEMICAL-MECHANICAL POLISHING

Peter W. Freeman
Rodel Inc., 451 Bellevue Dr., Newark, DE 19713

Lucia Markert
SEMATECH, 2706 Montopolis Dr., Austin, TX 78741

Abstract

The current joint development project between SEMATECH and Rodel focuses on the reduction of pad-related process variability in chemical mechanical polishing (CMP). An essential part of the initial phase of the project was the installation and qualification of an IPEC/Westech 372U polishing tool. The Westech 372U tool is unique in that it incorporates the APP1000 conditioner which is designed to allow the user to modify the length of time the conditioner takes to traverse across 10 different segments from the center of the pad to the outside of the pad. Theoretically this allows the user to modify the pad profile and as a result modify the relative polishing pressure across the wafer thus affecting polish uniformity across the wafer. This paper discusses the effect of using different time profiles on the resulting pad shape after a long duration of conditioning and correlates these shapes to polishing performance. In addition a simple computer model was developed that successfully predicts pad erosion profiles.

Introduction

Chemical Mechanical Polishing (CMP) is becoming a crucial step in fabricating integrated circuits, especially for linewidths of 0.5 μm or less. Planarization of dielectric layers is important on both the local scale (distances $< 100 \mu\text{m}$) and the global scale (distances $> 10 \text{mm}$) for increasing line density and for meeting depth of focus requirements in subsequent lithography steps. For metal films, CMP is gaining acceptance not only in forming tungsten plugs/studs for vertical interconnects, but also in defining vertical and horizontal interconnects for dual damascene architectures.

The objective of this work was to understand the effect of using different conditioning time profiles on the resulting pad shape (i.e., erosion profile) and to relate these shapes to oxide polishing performance. In addition, a computer simulation was written to predict the final pad shape using the conditioning time profile as input.

Experimental

The APP1000 conditioner on the Westech 372U is designed to allow the user to adjust the length of time the conditioner takes to traverse each of 10 discrete segments from the center of the pad to the outside edge. This is accomplished through the Pad Maintenance Panel and Conditioner Sweep Profile portions of the tool software. The length of the conditioner sweep is calculated as:

$$\text{sweep length} = \text{platen diameter} - \text{conditioner end effector diameter}$$

The sweep length is divided into ten equal segments and the user can set a time for each segment individually. The conditioner traverses the pad radius in a continuous sweep using the time profile specified.

All polishing and conditioning was done on Rodel® EX1400 polishing pads. The process parameters are summarized in Table 1. In each experiment, wafers were polished in groups of 20 until a total of 160 wafers had been polished. Each group was run as one thermal sheet oxide wafer followed by nineteen

dummy wafers. The thermal oxide wafer in the first group was polished before conditioning the pad. Approximately one minute of conditioning followed every wafer and the total conditioning time for each pad was approximately 160 minutes. The pad erosion profiles after conditioning were measured with a Mitutoyo® model IDC-112EB thickness measurement gauge. On each sheet wafer the oxide thickness was measured before and after polishing with a Prometrix® FT-500 Film Thickness Analyzer. The 9-point thickness measurements (center, 4 points mid-radius, and 4 points edge) had a 6 mm edge exclusion.

Three conditioning sweep profiles, as listed in Table 2, were tested. Flat1 and Flat2 were two different approaches to producing a constant erosion profile across the pad. Flat1 increased linearly in time from the center to the edge of the pad under the assumption that the conditioning time should increase linearly with radius to compensate for the linear increase in pad area conditioned per platen revolution with radius. Flat1 also has time added to the first and last segments to compensate for end effector placement and lift-off. Flat2 had a constant time profile under the assumption that the erosion rate would be independent of the pad area increase with radius. Bell was a modified Flat1 profile, designed to create a bell shape in the pad by increasing the conditioning times at the beginning and end of the sweep and reducing the conditioning time at the center of the sweep.

Table 1: Process Parameters

Polish Parameters		Conditioning Parameters	
Time	2 min	#sweeps	1 post-polish
Downforce	6 psi	Time	1 min (app.)
Pad temp	100 °F	Downforce	7 lbs
Platen RPM	36 rpm	End RPM	70 rpm
Carrier RPM	54 rpm	Platen speed	75 rpm
Back Pressure	0 psi	Slurry Flow	150 ml/min
Flow Rate	150 ml/min	Profile	variable
Oscillation	10 mm	End Effector	200 grit diamond

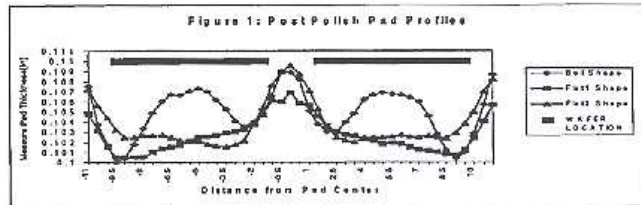
Table 2: Conditioning Sweep Profiles

Location on Pad Segment	Center									Edge
	1	2	3	4	5	6	7	8	9	
Flat1	4.1	4.0	4.4	4.8	5.2	5.6	6.0	6.4	6.8	7.2
Flat2	5.5	5.5	5.5	5.5	5.5	5.5	5.5	5.5	5.5	5.5
Bell	8.1	5.4	4.0	2.2	2.4	2.6	2.8	5.8	9.8	13

Results and Discussion

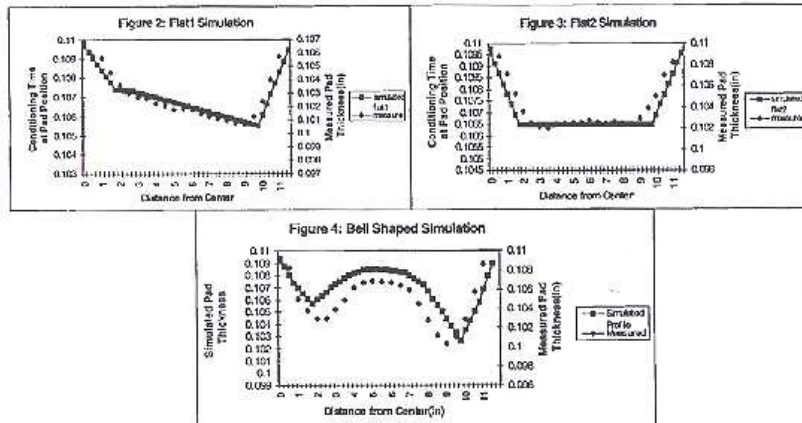
Figure 1 shows the post-conditioning pad profiles for the Flat1, Flat2 and Bell conditioning sweeps. The Flat1 profile shows that linearly increasing the sweep time from the center to the edge of the pad, proportionally increases the erosion from the center to the edge of the pad. The Flat2 profile shows that a constant time profile yields a constant pad removal rate across the radius. The Bell profile shows that less conditioning in the center of the sweep results in less erosion in this area relative to the center and edge of the pad. The Bell shape also includes the effect of linearly increasing time, as was seen in the Flat1 shape.

In each case, the placement and lift-off of the end effector at the beginning and end of the sweep produces a distinct transition region in the pad shape. The feature has a width corresponding to the end effector radius due to lack of a neighboring segment for overlap of the end effector sweep.

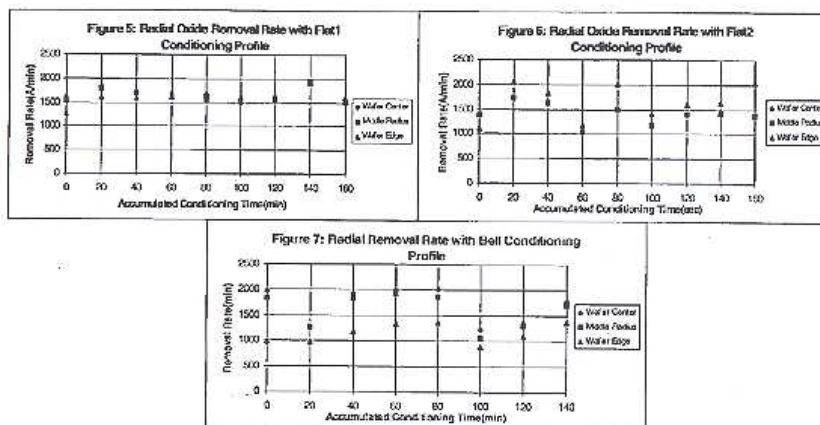


The results indicate that, for this tool configuration, the amount of pad erosion is proportional to the time the conditioner spends at a given point. This effect could be a result of pad erosion being proportional to linear velocity and inversely proportional to area conditioned, which could cause the radial pad erosion to appear as a function of time alone. The experiments in this report do not test whether this is the case. If, however, the velocity effect was dominant, one would expect Flat2 to have linearly increasing erosion like that of Flat1. If the pad area effect was dominant, the Flat1 erosion would be level and erosion in the Flat2 would be linearly decreasing.

In order to predict the pad shape for specific conditioning parameters, a simple model was developed. This model calculates the total time the end effector spends over a given radial section of the pad. With an infinitesimally small end effector each segment would have a discrete erosion rate. However the end effector is large (2" diameter). When the end effector enters a new segment and the sweep rate changes, half of the end effector is still in the previous segment. In the model, each of the standard segments is further divided into 4 smaller sections for calculating the total time the end effector spends over that section. Figures 2, 3 and 4 show the measured pad profiles overlaid with the predicted profile from the simulator. From these figures it is clear that the simple model accurately predicts the resulting erosion profile.



Figures 5, 6 and 7 show the radial removal rates at the center, mid-radius, and edge of the oxide wafers polished during the Flat1, Flat2 and Bell conditioning trials respectively. Figures 6 and 7 clearly show that the removal rate profile on the wafer can be changed from edge fast, with the Flat2 profile, to edge slow, with the Bell profile. All three figures show that the first wafer measured, which was run before conditioning, has a different removal rate profile than the last wafer measured.



When examining these results, it is important to recognize that for a 200mm wafer, the wafer edge extends into the initial (set-down) and final (lift-off) segments of the end effector sweep. As shown in Figure 1, the wafer edges are in the transition regions. When removal rate at a specific location on the wafer is considered with respect to the relative position on the pad during polishing, the results are consistent with a dependence on wafer contact with the pad. For the Bell profile, if the wafer placement in Figure 1 is compared with the removal rate pattern in Figure 7, one sees that the center of the wafer is over a high point in the pad shape and also has a higher removal rate than the wafer edge. The lower rate at the edge may be due to the measurement location being located over the trough at the edges of the pad profile. The same reasoning applies to the Flat2 removal rate results in Figure 6. Contact of the wafer edge with the steep trapezoidal sides of the profile reduces contact at the center of the wafer, resulting in edge fast polishing. The best results are evident in Figure 5 with the Flat1 profile. Near the center of the pad, profile has very little trough which may allow the mechanical gimbal on the wafer carrier to place the wafer in uniform contact with the pad. The lack of a trough at the beginning of the Flat1 profile results from the linearly increasing time profile and the additional time in segment 1 to compensate for end effector set-down.

Conclusions

In this work, we have shown that changing the conditioning time profile affects the pad erosion profile, as demonstrated for oxide polishing on a Rodel® EX1400 pad. The pad erosion profile can be predicted using a simple model with the conditioning time profile as input. The oxide removal rate at different sites on the wafer has been related to the pad erosion profile.

Acknowledgments

The authors would like to acknowledge Steve Carter, Dan Emerson, Ray Lavoie and Zhi Liu for polishing work at the Rodel Polishing Lab and Lee Cook and Brad Jones for technical discussions.

APPENDIX III

LIST OF PUBLICATION OUTCOMES FROM Ph.D. STUDY

Journal

1. **Baisie, E.A.**, Li, Z.C. and Zhang, X.H. "Diamond disc pad conditioning in chemical mechanical polishing: a conditioning density distribution model to predict pad surface shape" Accepted in International Journal of Manufacturing Research (IJMR).
2. Li, Z. C., **Baisie, E. A.**, and Zhang, X. H., 2012, "Diamond disc pad conditioning in chemical mechanical planarization (CMP): A surface element method to predict pad surface shape". Precision Engineering, 36(2), pp. 356-363.

Refereed Conference

1. **Baisie, E.A.**, Li, Z.C., Lin B. and Zhang, X.H. "Finite element modeling of pad deformation due to diamond disc conditioning in chemical mechanical polishing (CMP)". ASME International Manufacturing Science and Engineering Conference 2012, MSEC2012, June 4-8, 2012, (Notre Dame, IN, United States, 2012).
2. **Baisie, E.A.**, Li, Z.C. and Zhang, X.H. "Design optimization of grit arrangement and distribution for diamond disc pad conditioners". Industrial and Systems Engineering Research Conference, May 19-23, 2012, (Orlando, FL, United States, 2012).
3. **Baisie, E.A.**, Li, Z.C., Lin B. and Zhang, X.H. "A new image processing method to characterize pad foam morphology in chemical mechanical polishing". China Semiconductor Technology International Conference (CSTIC) 2012, March 18-19, 2012, (Shanghai, China, 2011).
4. Li, Z.C., **Baisie, E.A.**, and Zhang, X.H."Diamond disc pad conditioning in chemical mechanical planarization (CMP): A mathematical model to predict pad surface shape". ASME International Manufacturing Science and Engineering Conference 2011, MSEC2011, June 13-17, 2011, (Corvallis, OR, United States, 2011) (**Awarded Best Paper**)
5. **Baisie, E.A.**, Li, Z.C., Lin B. and Zhang, X.H. "Finite element analysis (FEA) of pad deformation due to diamond disc conditioning in chemical mechanical polishing (CMP)". China Semiconductor Technology International Conference (CSTIC) 2011, March 13-14, 2011, (Shanghai, China, 2011).

6. **Baisie, E.A.**, Li, Z.C. and Zhang, X.H. “Simulation of diamond disc conditioning in chemical mechanical polishing: effects of conditioning parameters on pad surface shape”. ASME International Manufacturing Science and Engineering Conference 2010, MSEC2010, October 12- 15, 2010, (Erie, PA, United States, 2010).
7. **Baisie, E.A.**, Li, Z.C. and Zhang, X.H. “Diamond disc pad conditioning in chemical mechanical polishing: A literature review of process modeling”. ASME International Manufacturing Science and Engineering Conference 2009, MSEC2009, October 4- 7, 2009, pp. 661-670, (West Lafayette, IN, United states, 2009).
8. **Baisie, E.A.**, Yang, M., Kaware, R., Hooker, M., Li, Z.C., Sun, W. and Zhang, X.H. “An economic study on chemical mechanical polishing of silicon wafers”. ASME International Manufacturing Science and Engineering Conference 2009, MSEC2009, October 4- 7, 2009, pp. 691-696, (West Lafayette, IN, United States, 2009).

Poster

1. **Baisie, E.A.**, Li, Z.C. and Zhang, X.H. “Pad conditioning in chemical mechanical polishing: A conditioning density distribution model to predict pad surface shape”. Poster presentation at 2011 NSF CMMI Engineering Research and Innovation Conference, January 4-7, 2011, (Atlanta, GA, United States, 2011).
2. **Baisie, E.A.**, Li, Z.C. and Zhang, X.H. “Modeling and simulation of pad surface shape due to diamond disc conditioning in chemical mechanical planarization”. Poster presentation at 1st Annual COE Graduate Student Research Poster Competition, April 26, 2012, (Greensboro, NC, United States, 2011).

Submitted/In preparation

1. **Baisie, E.A.**, Li, Z.C. and Zhang, X.H. “Design optimization of diamond disc pad conditioners”. Submitted to International Journal of Manufacturing, Materials and Mechanical Engineering (IJMMME).
2. **Baisie, E.A.**, Li, Z.C. and Zhang, X.H. “A review of diamond disc pad conditioning in chemical mechanical polishing”. For International Journal of Manufacturing, Materials and Mechanical Engineering (IJMMME).
3. **Baisie, E.A.**, Li, Z.C. Zhang, X.H., and Wangping Sun “Creative design and optimization of diamond discs”. For Wear (International Journal on the Science and Technology of Friction, Lubrication and Wear).

4. **Baisie, E.A.**, Li, Z.C. and Zhang, X.H. “A comparison of two simulation models for pad wear due to conditioning in chemical mechanical polishing”. For Wear (International Journal on the Science and Technology of Friction, Lubrication and Wear).